CONTROLLED POLYMER NANOSTRUCTURES

by

ALTERNATIVE LITHOGRAPHY

This research has been supported by the MESA$^+$ Institute for Nanotechnology (SRO Nanofabrication).

Controlled Polymer Nanostructures by Alternative Lithography

Canet Acikgoz

Ph. D. Thesis
University of Twente, Enschede, The Netherlands
ISBN: 978-90-365-2976-1

Publisher: Ipskamp Drukkers B. V., Josink Maatweg 43, 7545 PS, Enschede,
The Netherlends, http://www.ipskampdrukkers.nl

Cover graphics: www.filminthefridge.com

CONTROLLED POLYMER NANOSTRUCTURES BY ALTERNATIVE LITHOGRAPHY

PROEFSCHRIFT

ter verkrijging van
de graad van doctor aan de Universiteit Twente,
op gezag van de rector magnificus,
prof. dr. H. Brinksma,
volgens besluit van het College voor Promoties
in het openbaar te verdedigen
op vrijdag 12 februari 2010 om 15.00 uur

door

Canet Acikgoz

geboren op 10 januari 1980
te Iskenderun, Turkije

Dit proefschrift is goedgekeurd door:

Promotoren:	Prof. dr. ir. Jurriaan Huskens
	Prof. dr. G. Julius Vancso
Assistent Promotor:	Dr. Mark A. Hempenius

This thesis is dedicated to my family

Table of Contents

Chapter 1

General introduction

One of the main objectives of nanotechnology is to manipulate matter at the nanoscale and to directly control structure at this lengthscale. Depending on the structural features to be controlled, on the material used, and on the ultimate properties targeted, several fabrication approaches have been employed.[1] For example by scaling down lithographic techniques, thereby miniaturizing patterns and creating nanostructures which are essential in fields of future electronic devices,[2, 3] high density data storage,[4] and analytical and synthetic chemistry have been developed.[5, 6] The objectives of nanoscale fabrication of functional systems and devices are presently being pursued using two approaches: top-down and bottom-up techniques. Methods that are used in top-down approaches encompass mostly lithographic techniques such as (extreme) UV lithography, nanoimprint lithography, e-beam lithography, soft lithography and scanning probe lithography.[7] The challenges for these techniques lie in enhancing the resolution, reliability, speed, and overlay accuracy. In bottom-up nanofabrication, self-assembly of molecules or nanoparticles is used to create nanostructures or nanopatterns. The most important concern in bottom-up nanotechnology is the control over the spatial position of the molecules or nanoparticles.[8] For the fabrication of devices, a combination with top-down techniques is required.

In both approaches, polymers play an important role owing to their lengthscale, their processability, low cost, tunable properties, diverse functionalities and (if block copolymers are used) microphase separation. These features make polymers versatile materials for nanoscale UV lithography[9] and imprint lithography[10] as examples of existing top-down techniques where these materials are utilized either as a resist layer or as a substrate. Polymers have been widely used in patterning of surfaces by top-down “soft lithography”, which, according to Nuzzo et al., refers to a group of techniques using “elastomeric stamps, molds, and conformable photomasks” for pattern replication.[11, 12] Regarding the use of polymers in top-down techniques, each specific technique has its own merits, challenges and limitations.

Self-organizing materials, including liquid crystals, block co-polymers, hydrogen- and π-bonded complexes, and biopolymers, could form hierarchical structures which are extensively used in bottom-up approaches. Without doubt, the primary reason for using polymeric systems in these techniques is that they can form ordered nanoscale structures in bulk or in solution.[13] These ordered nanostructures, represented typically by block co-polymers, microemulsions, and many natural macromolecules, are tunable over a broad variety of morphologies ranging from discrete micelles to symmetric continuous network structures. Controlled functional polymer nanostructures can offer enhanced performance for various applications, such as organic photovoltaics, light emitting diodes, biosensors, and nanomedicine.[13]

Polymers containing inorganic elements or organometallic units in the main chain are interesting materials. In addition to their processibility typical to polymers, they also show potentially useful chemical, electrochemical, optical, and other interesting characteristics which can not be found in organic molecules.[14-17] Poly(ferrocenylsilane)s (PFSs), composed of alternating ferrocene and silane units in the main chain, belong to the class of organometallic polymers.[18, 19] The discovery of the anionic ring-opening polymerization of silicon-bridged ferrocenophanes by Manners et al. gave rise to well-defined, monodisperse PFS homo and block copolymers.[20] The presence of iron and silicon in the PFS backbone adds a distinctive functionality to this class of materials. PFSs are effective resists in reactive ion etching processes due to the formation of an etch-resistant iron/silicon oxide layer in oxygen plasmas, resulting in several lithographic applications.[14, 21, 22] PFS was used as ink in different lithographic techniques to generate patterns on micron and sub-micron scales[21] and block copolymer lithography was performed for nanopatterning since upon phase separation block copolymers of PFS blocks form well defined nanostructures.[23] These nanostructures can either be transferred into silicon substrates in a one-step etching process[24] or used as a template in the fabrication of nanometer-sized cobalt magnetic dots by a sequential process.[25]

Many polymers have been successfully patterned and they are also employed as synthetic templates for the fabrication of nanostructured materials. The variety in structures and the dimensions provided with polymers by using different techniques are presented in this thesis. The principal goal of this work is to enhance the use of polymers in bottom-up and top-down micro-and nanofabrication techniques providing patterned platforms. There is a need for further development in macromolecule-based lithography resists and polymer patterning, as currently available approaches show insufficient etch resistivity, adhesion to

the substrate, proper mold release properties, etc. PFS homo and block copolymers were applied as resists in lithographic applications such as NIL, UV-NIL and nanosphere lithography (NSL). UV-NIL was also employed to prepare polymer brush patterns which serve as platforms for protein immobilization.

Chapter 2 provides a literature review on existing lithography techniques and materials used by these techniques. It gives an overview of both conventional and unconventional lithography approaches and discusses the use of PFSs as resists in lithography.

In Chapter 3, the NSL technique is described to fabricate patterns at a silicon substrate with controlled shape by the use of PFS as an etch resist. Silica nanoparticles of different sizes were used as starting materials, and poly(ferrocenylmethylphenylsilane) (PFMPS) as an etch-resistant polymer, to produce a negative replica of the nanoparticle array. The size and shape of the pores were controlled by changing the etching time. The patterned silicon substrate was then employed as a mold for NIL.

Chapter 4 illustrates a new method to fabricate free-standing porous polyethersulfone (PES) membranes using NSL with colloidal silica, which yields highly ordered membranes with well-defined pore sizes using PFS as an etch resist. These membranes were utilized as a platform for the size-selective filtration of particles.

In Chapter 5, the application of PFS as a new type of imprint resist is reported. Thermal imprinting of PFMPS is demonstrated and the patterns are shown to be transferred into silicon substrates by reactive ion etching. The parameters for imprinting such as polymer molar mass and initial film thickness are investigated.

Chapter 6 describes the fabrication of PFS patterns by step-and-flash imprint lithography (S-FIL), which is a variant of UV-NIL, for use as high-contrast etch masks in dry etch processes. The possibility of creating etch resistant patterns of PFMPS with sizes down to the nm range is shown and plasma compositions leading to different etch profiles is demonstrated.

Chapter 7 introduces the fabrication of patterned polymer brush layers by S-FIL. “Grafting from” polymerization was performed on patterned surface-attached initiator surfaces. These substrates were subsequently used as a platform for protein immobilization.

Symmetry, pattern quality and correlation as a function of the primary structure of polystyrene-*block*-poly(ferrocenyldimethylsilane) (PS-*b*-PFS) is discussed in Chapter 8. A set of PS-*b*-PFS block copolymers were synthesized and the effects of volume fraction, molecular weight, and polydispersity index (PDI) on microdomain size distribution, period

and correlation length of thin films of spherical-morphology PS-*b*-PFS block copolymers are studied.

REFERENCES

[1] Z. Cui, *Nanofabrication Principles, Capabilities and Limits* Springer, United Kingdom, **2008**.

[2] D. I. Gittins, D. Bethell, D. J. Schiffrin, R. J. Nichols, *Nature* **2000**, *408*, 67.

[3] C. P. Collier, G. Mattersteig, E. W. Wong, Y. Luo, K. Beverly, J. Sampaio, F. M. Raymo, J. F. Stoddart, J. R. Heath, *Science* **2000**, *289*, 1172.

[4] M. I. Lutwyche, M. Despont, U. Drechsler, U. Durig, W. Haberle, H. Rothuizen, R. Stutz, R. Widmer, G. K. Binnig, P. Vettiger, *Appl. Phys. Lett.* **2000**, *77*, 3299.

[5] R. E. Service, *Science* **1995**, *268*, 1698.

[6] A. Manz, *Chimia* **1996**, *50*, 140.

[7] Y. N. Xia, J. A. Rogers, K. E. Paul, G. M. Whitesides, *Chem. Rev.* **1999**, *99*, 1823.

[8] B. D. Gates, Q. B. Xu, M. Stewart, D. Ryan, C. G. Willson, G. M. Whitesides, *Chem. Rev.* **2005**, *105*, 1171.

[9] J. Haisma, M. Verheijen, K. van den Heuvel, J. van den Berg, *J. Vac. Sci. Technol. B* **1996**, *14*, 4124.

[10] S. Y. Chou, P. R. Krauss, P. J. Renstrom, *Appl. Phys. Lett.* **1995**, *67*, 3114.

[11] J. A. Rogers, R. G. Nuzzo, *Mater. Today* **2005**, 50.

[12] Y. N. Xia, G. M. Whitesides, *Annu. Rev. Mater. Sci.* **1998**, *28*, 153.

[13] T. Liu, C. Burger, B. Chu, *Prog. Polym. Sci.* **2003**, *28*, 5.

[14] I. Korczagin, R. G. H. Lammertink, M. A. Hempenius, S. Golze, G. J. Vancso, *Adv. Polym. Sci.* **2006**, *200*, 91.

[15] A. C. Arsenault, V. Kitaev, I. Manners, G. A. Ozin, A. Mihi, H. Miguez, *J. Mater. Chem.* **2005**, *15*, 133.

[16] F. Fleischhaker, A. C. Arsenault, Z. Wang, V. Kitaev, F. C. Peiris, G. von Freymann, I. Manners, R. Zentel, G. A. Ozin, *Adv. Mater.* **2005**, *17*, 2455.

[17] K. Kulbaba, I. Manners, *Macromol. Rapid Commun.* **2001**, *22*, 711.

[18] I. Manners, *Synthetic Metal-Containing Polymers*, Wiley-VCH, Weinheim Germany, **2004**.

[19] I. Manners, *J. Polym. Sci. Part A: Polym. Chem.* **2002**, *40*, 179.

[20] Y. Z. Ni, R. Rulkens, I. Manners, *J. Am. Chem. Soc.* **1996**, *118*, 4102.

[21] I. Korczagin, S. Golze, M. A. Hempenius, G. J. Vancso, *Chem. Mater.* **2003**, *15*, 3663.

[22] I. Korczagin, H. Xu, M. A. Hempenius, G. J. Vancso, *Eur. Polym. J.* **2008**, *44*, 2523.

[23] R. G. H. Lammertink, M. A. Hempenius, E. L. Thomas, G. J. Vancso, *J. Polym. Sci. Part B: Polym. Phys.* **1999**, *37*, 1009.

[24] R. G. H. Lammertink, M. A. Hempenius, J. E. van den Enk, V. Z. H. Chan, E. L. Thomas, G. J. Vancso, *Adv. Mater.* **2000**, *12*, 98.

[25] J. Y. Cheng, C. A. Ross, V. Z. H. Chan, E. L. Thomas, R. G. H. Lammertink, G. J. Vancso, *Adv. Mater.* **2001**, *13*, 1174.

Chapter 2

Conventional and Alternative Lithography Techniques for the Fabrication of Nanostructures

ABSTRACT. This chapter gives an overview on lithography techniques and materials used by these techniques that are relevant for the subject of the thesis. The first part focuses on the conventional lithography techniques used to fabricate complex micro- and nanostructured surfaces. In the second part, the focus lies on patterning with unconventional lithography techniques such as printing, molding, and embossing, to fabricate nanostructures which are central to the development of a number of existing and emerging technologies. In the last part, an overview of organometallic polymers used as resists in nanolithography is given.

2.1 INTRODUCTION

Nanofabrication is the process of making functional structures with patterns having minimum dimensions of approximately <100 nm. Methods used to fabricate nanoscale structures and nanostructured materials are labelled as 'top-down' and 'bottom-up'. Photolithography and scanning beam lithography for the creation of patterns in the micrometer and nanometer range are so called top-down approaches, in which the structure is imposed on the substrate by a mask or by direct writing. When the surface is structured by self-assembly of small building blocks such as copolymers, vesicles, micelles, or particles, 'bottom-up' term is generally used.[1] Similarly, direct 'one-to-one' manipulation of atoms, molecules and nanoscale molecular objects is also referred to as 'bottom-up' assembly.

The top-down techniques including photolithography[2, 3] and scanning beam lithography[4] are known as conventional lithography. These techniques have relatively high cost and/or expose substrates to high energy radiation and relatively high temperatures. Alternative techniques have emerged to pattern relatively fragile materials, such as organic materials other than photoresists. These techniques are often employed in research and allow fast prototyping of nanostructures. Unconventional nanofabrication techniques explored are molding,[5] embossing,[6, 7] printing,[8, 9] scanning probe lithography,[10-12] edge lithography,[13-16] and self-assembly.[17, 18] The first three techniques are top-down approaches whereas scanning probe lithography, edge lithography and self-assembly bridge 'top-down' and 'bottom up' strategies for nanofabrication,

Critical issues such as resolution, reliability, speed, and overlay accuracy need to be considered in developing new lithography techniques. Unconventional nanofabrication techniques offer alternatives to photolithography and create opportunities for fabrication on nonplanar surfaces and over large areas. Moreover, they have the potential to be low-cost for manufacturing and they are easier to operate and are applicable to biological materials.

This chapter gives an overview on lithography techniques and materials used in these lithographic techniques. Herein, the first part focuses on the conventional lithography techniques used to fabricate complex micro- and nanostructured surfaces. In the second part, the focus lies on patterning with unconventional lithography techniques such as printing, molding, and embossing to fabricate nanostructures which are central to the development of a number of existing and emerging technologies. A brief introduction to organometallic polymers is provided in the last part and their use in nanolithography is shown, as they play a pivotal role in the nanofabrication schemes developed in this thesis.

2.2 CONVENTIONAL LITHOGRAPHY

Conventional techniques for nanofabrication are commercially available and widely implemented in manufacturing. These conventional approaches have their limitations such as high cost and the difficulty in accessing the facilities to use them. There are two dominant methods for conventional lithography: photolithography and particle beam lithography such as electron beam lithography and ion beam lithography.

2.2.1 Photolithography

Photolithographic methods all share the same operational principle: exposure of an appropriate material to electromagnetic radiation to modify the solubility of the material as a result of chemical changes in its molecular structure, followed by developing of the material (Figure 2.1a). The exposed photoresist is immersed in solvents that dissolve the exposed (positive photoresist) or unexposed (negative photoresist) regions to provide access to the surface of the substrate. Pattern transfer is achieved by an etching process.[19]

Most efforts in lithography have been directed at shrinking the lateral dimensions of the features, and different resolution enhancement approaches (projection and immersion optics, phase-shifting masks) have been developed.[3, 20] In current semiconductor nanofabrication, photolithography can pattern 37 nm-wide features with 193-nm wavelength.[21]

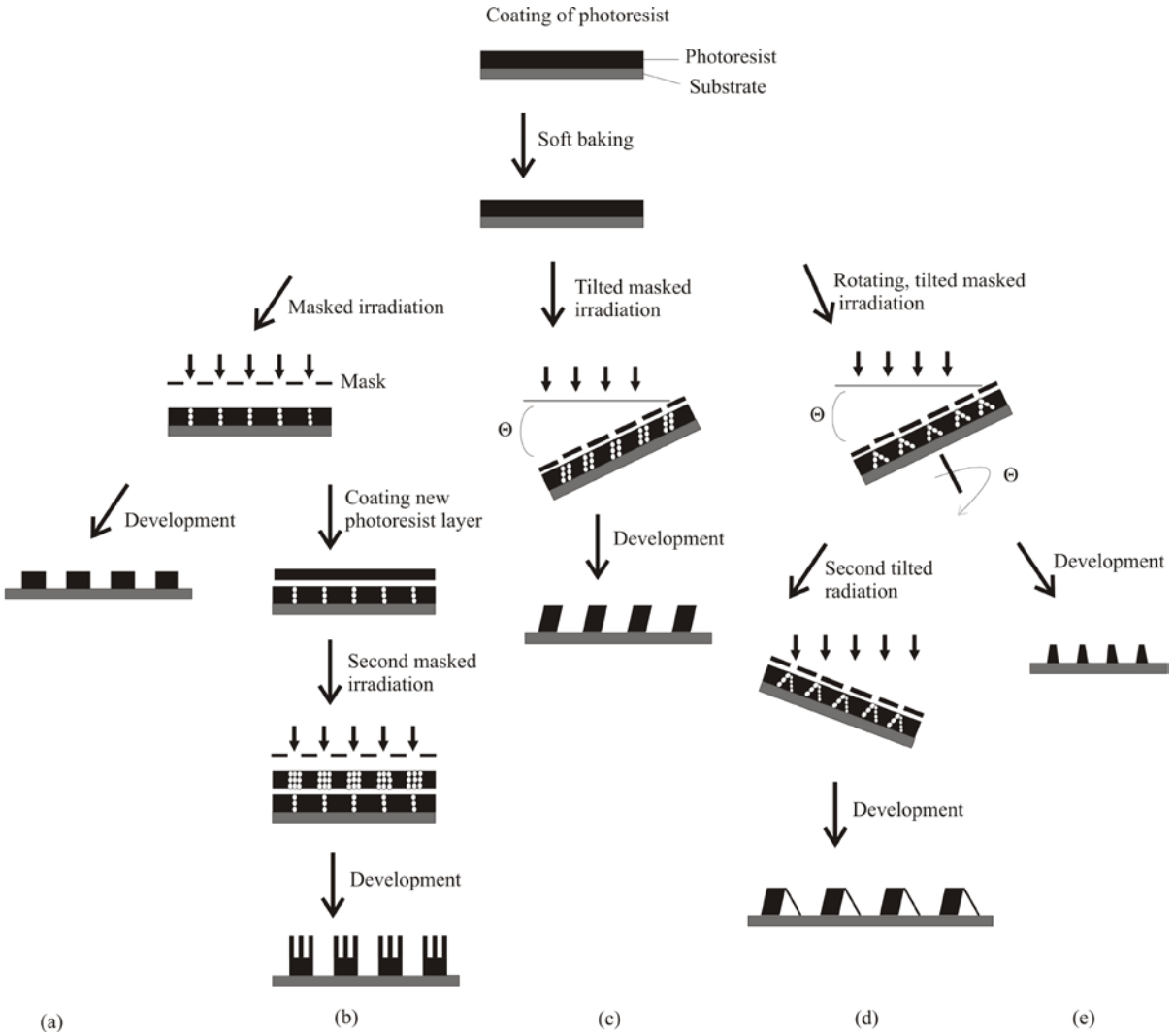

Figure 2.1 Photolithographic methods using masked irradiation and a negative photoresist material: (a) Patterning by single exposure, (b) patterning by layer-by-layer coating and exposure, (c) tilted patterning by single inclined exposure, (d) patterning by double inclined exposure, (e) tapered patterns by rotating tilted exposure. [22]

Recently, photolithographic approaches have been extended to generate more complex structures including high aspect ratio, tilted, suspended, or curved geometries (Figure 2.1).[22] In conventional lithography, the mask and resist film are perpendicularly aligned with respect to the irradiation source. By tilting the mask and resist film with respect to the beam using a tilting stage, inclined structures can be fabricated (Figure 2.1c). Han *et al*. showed the generation of bridges, embedded channels, and V-grooves with aspect ratios >4 using SU-8 (epoxy-based negative photoresist) and a conventional UV mask aligner (Figure 2.2a).[23] More complex 3D structures can be fabricated with three or four times inclined UV exposures along different axes (Figure 2.1d).[24, 25] Inclined micro-pillars with an aspect ratio

of 20 (Figure 2.2b) were fabricated using a two-axes exposure method with four backside exposures but the multi-exposure process can generate heavy UV dose domains which could cause distortions. Tapered structures with nonvertical sidewalls can be also obtained if the photomask and substrate with photoresist are tilted and rotated simultaneously during irradiation as shown in Figure 2.1d and the SEM image in Figure 2.2c.[23]

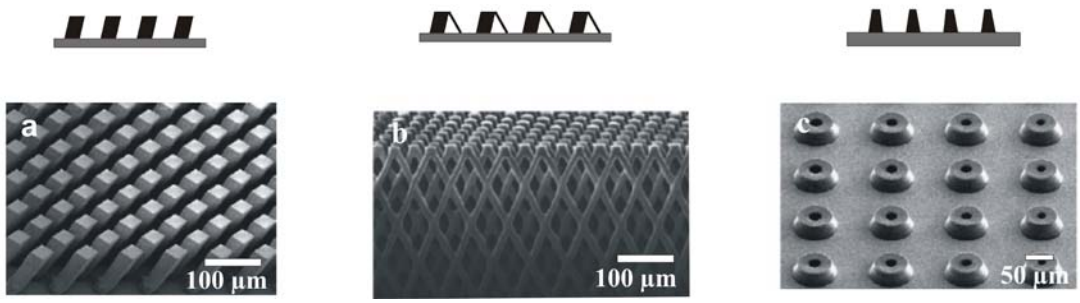

Figure 2.2 SEM images of (a) tilted SU-8 patterns,[23] (b) patterns by double inclined exposure,[24] (c) tapered patterns by rotating tilted exposure.[23]

2.2.2 Serial Writing with Charged Particles

Serial writing with electrons or ions is a lithographic technique with low throughput, high cost and only suited for small area fabrication. These techniques provide, however, flexibility in feature design making them attractive in academic research.

2.2.2.1 Electron Beam Lithography

In typical e-beam lithography, a beam of electrons is used to expose an electron sensitive resist. The electrons generate secondary electrons with relatively low energy to form free radicals and radical cations, which interact with the surface of a layer of resist, such as poly(methyl methacrylate) (PMMA). Interaction of the electron beam with the resist causes local changes in its solubility, and in the case of PMMA, the electrons will locally induce chain scissions that makes the polymer soluble in a developer. PMMA was one of the first polymers recognized to exhibit sensitivity to electron beam radiation and is nowadays the most frequently used polymer in e-beam lithography.[22]

The resolution is limited because of the electron scattering of primary and secondary electrons in the resist even though electron wavelengths on the order of 1Å can be achieved. Patterns with features as small as ~50 nm can be generated by this technique.[26]

E-beam lithography is impractical for mass production because of long writing times. Therefore, it is mainly used to produce photomasks in optical lithography or to produce small

numbers of nanostructures for research purposes. It is also used in the areas where optical lithography fails such as for the fabrication of high frequency GaAs field-effect transistor (FET) devices that require a resolution down to ~100 nm.[27]

2.2.2.2 Ion Beam Lithography

This method includes a variation of the electron beam lithography technique, using a focused ion beam (FIB) instead of an electron beam. High energy ions, such as Ga^+, H^+, or He^+ are able to penetrate a resist material with well defined paths. The penetration depth depends on the ion energy. Ion-electron interactions do not result in significant deviation of the trajectory of the ion from the straight line path. Therefore high aspect ratio structures with vertical side walls can be fabricated. Similar to e-beam writing, the low energy secondary electrons initiate chemical reactions.[22]

The utilization of a focused mega-electron-volt (MeV) proton beam to write accurate high-aspect-ratio walls of 30 nm width with sub-3 nm edge smoothness has been reported.[28] Typically, a MeV proton beam is focused to a sub-100 nm spot size and scanned over a suitable resist material. When the proton beam interacts with matter it follows an almost straight path. The secondary electrons induced by the primary proton beam have low energy and therefore limited range, resulting in minimal proximity effects. These features enable smooth three-dimensional structures to be directly written into resist materials. The technique is named *p-beam writing*.[28]

2.3 ALTERNATIVE LITHOGRAPHIES

Photolithography has circumvented many limitations during its development and is widely used to fabricate nanostructures.[29, 30] However, the limitations based on the physics of diffraction and interactions of high energy photons are hard to overcome. This technique cannot easily be performed on polymeric or curved substrates and cannot pattern large areas with high resolution in a single step. It also has the disadvantage of high capital and operational cost. Hence in order to accomplish smaller features at a lower cost, new patterning techniques are being explored and developed. Some of the oldest and conceptually simplest forms of plastics macroscale processing (embossing, molding, stamping, or printing are now being re-examined for their potential adaptation to nanofabrication. In the molding technique, the surface relief of a hard stamp or mold is transferred into a soft material. Several methods have been developed in the past decade to obtain micro- and nanostructured polymer surfaces using molding or related strategies. Some of them are i) temperature-based

processing (hot embossing or nanoimprint lithography (NIL) and thermal injection molding of thermoplastic polymers), (ii) light-initiated polymerization (UV-NIL and step-and-flash NIL), (iii) soft lithography, (iv) solvent-based processing, and (v) nanosphere lithography. Figure 2.3 gives an overview of the processing steps involved.

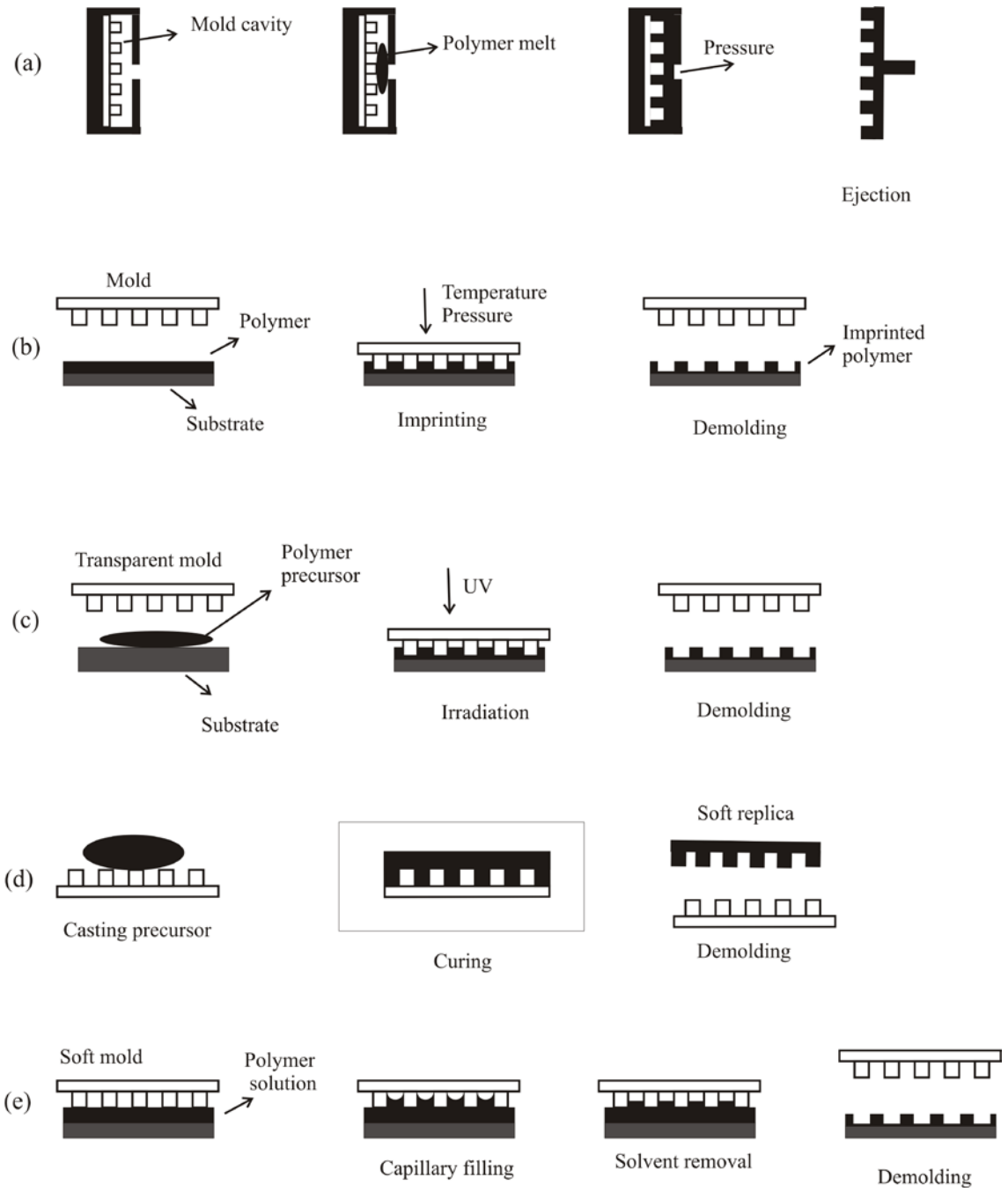

Figure 2.3 Different alternative lithographic processes. (a) Injection molding, (b) hot embossing (thermal NIL), (c) UV-NIL, (d) soft lithography, (e) solvent-assisted molding. [22]

2.3.1 Mold Fabrication

Mold fabrication is the most time- and cost-consuming step and one of the largest limitations in industrial application.[31] For this reason, a master is fabricated and copies of the master in other hard materials are preferentially used as molds for imprinting. High resolution 3D stamps are fabricated by e-beam lithography and dry etching, while shallow stamps by e-beam lithography and metal lift-off can be obtained.[32] A widespread choice of stamp material is Si with an oxide layer on top.[33, 34] Masters of Si are fabricated by reactive ion etching techniques [35] or deposition of nickel and other metals on patterned resist substrates. Small features with sub-20 nm dimensions have been achieved by electron beam lithography and lift off.[36] An optimized double-layer resist system allowed the formation of a Cr etching mask of 15-20 nm in diameter. However, the metal roughness was found to be a problem for sizes below 10 nm due to the crystal grain structure of the evaporated metal.[37] Selecting the mold material should be carefully done and issues such as hardness, compatibility with other microfabrication processing and thermal expansion coefficients must be considered. Diamond[38] and lithium[39] have been investigated as potential mold materials for NIL by some groups. Taniguchi et al. used a spin-on-glass (SOG) material, which is almost the same as quartz in composition, as a material for hard stamps.[40] The SOG acted as a positive-tone electron beam resist and nanopatterns were fabricated by using e-beam lithography (EBL). The obtained pattern was directly usable as a nanoimprint mold without the risk of etching.

EBL has been established as a useful method for production of masters but so far lacks the commercial viability due to the high cost related to the exposure procedure. Etching of poly(tetrafluoroethylene) (PTFE) using synchrotron radiation has also been shown to perform 3D fabrication of masters.[41] Owing to its thermostability, resistance to chemicals and its very low adhesion, PTFE may be one of the most suitable materials for molding polymers, however PTFE is notoriously difficult to process. Processing of 1000 µm height structures by synchrotron radiation takes about 10 min, much shorter than achieved by X-ray lithography. Due to the directional emission of synchrotron radiation, high aspect ratio structures can be easily created.

In order to facilitate mold release, antisticking surface coatings are being used. These layers lower the surface tension of the mold surface and reduce adhesion. Different strategies can be employed: (i) use of fluoropolymer films deposited (noncovalently bonded) on the stamps with the help of a plasma treatment; (ii) treatment of silicon masters with perfluorosilanes, e.g., 1*H*,1*H*,2*H*,2*H*-perfluorodecyltrichlorosilane;[42] and (iii) treatment of

Ni or alumina stamps with fluorinated alkyl phosphoric acid derivatives.[43] Alternatively, molds made of fluoropolymers, such as PTFE, can be used. These molds are fabricated by casting a fluoropolymer solution on the master followed by drying, or imprinting the fluoropolymer melt.

One of the many advantages of molding is that it does not use light energy beams, and therefore, its resolution is not limited by the effects of wave diffraction, scattering, or back scattering from the substrate.[30] The same mold can be used several times to fabricate nanostructures which makes it a low cost technique. The availability of a suitable mold and the possibility of removing the molded material from it without damage are the prerequisites for molding.

2.3.2 Nanoimprint Lithography: Embossing Thermoplastic Materials

The principle of nanoimprint lithography[7, 33, 34] (hot embossing) and thermal injection is that a hard mold containing nanoscale features on its surface is used to deform a thermoplastic polymer deposited on the wafer substrate under controlled temperature and pressure (Figure 2.3b).[44] Increase of the temperature of the polymer reduces the viscosity of the material so that pressure application causes the polymer melt to flow into the cavities of the mold. The subsequent cooling of the system freezes the pattern on the target surface, thus providing a negative copy of the master.

Injection molding and hot embossing differ in their applications and process conditions. In injection molding, a polymer melt is injected at high pressure into a cavity where it cools and hardens (Figure 2.3a). In NIL, polymer sheets are compressed between the plates of an embossing press against the mold. Since imprint lithography makes a replica of surface patterns, the resist materials used in imprinting should be deformable under the applied pressure.[33, 45] In NIL, typically a thermoplastic material is used as the imprinting resist and a suitable imprint temperature is chosen which is above the glass transition temperature of the material. It has been shown that an optimal imprinting temperature is 70-80 ^{o}C above the T_g of the material used,[46] to ensure the polymer has a sufficiently reduced viscosity so that imprinting can be performed at a reasonable pressure. Raising the temperature above the T_g of the polymer causes a significant drop in both Young's modulus and the viscosity. The viscosity of a polymer material not only depends on the temperature, but also strongly on the polymer molar mass. In practice, low-molecular weight polymers can be imprinted at lower temperatures, lower pressures, or within shorter times.[47] A high imprint pressure is needed for resist viscosities of 1000 Pa s and more to provide conformal

contact between substrate and stamp over large areas. Thin polymer layer can be chosen where cavities are only partially filled, and thick layers can be used for the integration of lenses and microfluidic channels.[48-50] A good choice of process parameters such as height, pressure, thickness and temperature is always required to imprint polymers.

The availability of polymers such as PMMA and PS with a range of molar masses M_w and different polydispersities is an advantage for thermal NIL, and rheological characterization of the thermoplastic materials is available.[51] These materials are, however, not fully optimized for the special requirements of the NIL process. One of the most important requirements of the polymers used for NIL is that they should provide excellent mold releasing properties during the demolding process. Commercially available polymers can hardly satisfy this requirement. During imprinting of high aspect ratio patterns, the imprinted polymer tends to adhere to the mold, creating pattern defects although the mould surface is treated with an antisticking layer. In addition, a higher dry etching resistance is desirable if the imprinted polymer pattern is to be used as a mask for further pattern transfer. Adding a Si-containing material can address this problem.[52]

NIL can be used to mold a variety of polymeric materials and pattern features as small as ~5 nm[53] and aspect ratios of up to ~20.[54] Arrays of 10 nm diameter and 40 nm period holes in PMMA on either silicon or gold substrates, and 6 nm diameter and 65 nm period holes in PMMA on silicon substrates have been fabricated by NIL (Figure 2.4a).[53] NIL was used together with optical lithography to fabricate silicon quantum dot wires, which showed the same behavior as those fabricated using conventional electron-beam lithography. In addition, nanoimprint lithography was used to fabricate nanocompact disks with 10 nm features and 400 Gbits/in^2 data density—nearly three orders of magnitude higher than current CDs (Figure 2.4b).[53] Materials that have been patterned succesfully include biomolecules,[55] block copolymers,[56] and conducting polymers.[57] This process has been extended to pattern components for a range of microelectronics, optical, and optoelectronic devices.[58] The fabrication of 60-nm channel metal–oxide–semiconductor field-effect transistors on whole 4-in wafers using NIL was presented. The nanotransistors exhibit excellent operational characteristics across the wafer.[59]

Nanoimprint lithography has made great progress in a relatively short time but there are still some challenges related to this technique, one of which is the lifetime of the mold. Nanoimprint molds have to be replaced after ~50 consecutive imprints. High pressures and heating and cooling cycles cause stress and wear on the nanoimprint mold. Room temperature nanoimprint lithography[60] has been developed to overcome this problem. Spin-on-glass[61]

or hydrogen silsequioxane[62] have been used as resist materials at room temperature nanoimprint lithography. Some different approaches have also been developed targeting the problems mentioned above. One of the approaches is reverse nanoimprint lithography[52] which employs a polymer film spin-coated onto the mold rather than on the substrate. The produced film can be transferred from the mold to the substrate by NIL (Figure 2.4c). This technique was performed by using PMMA and Figure 2.4c shows imprinted PMMA patterns with 350 nm line spacing. This technique can also be used to transfer patterns onto substrates that are not suitable for spin-coating or have surface topographies, which have been a long-standing problem in imprint-based lithography.[63] Multilayer resist approaches with a thick planarization layer on top of the non-flat substrate have been used to solve this problem but these approaches require complex processes with multiple steps and need deep etching through the thick planarization layer.[64] Reverse imprinting has solved this problem very efficiently. Figure 2.4d shows polycarbonate grating structures reverse imprinted over etched features on a Si substrate which could have potential application in chemical and biological analysis.[63] This technique also offers the fabrication of three-dimensional structures by a layer-by-layer approach. Figure 2.4e demonstrates the imprinted three-layer nanostructure, using three different polymers. The imprinting results depend on several parameters such as T_g of the polymers, film thickness, width and height of the features on the substrate, and mechanical properties of the polymers.[63]

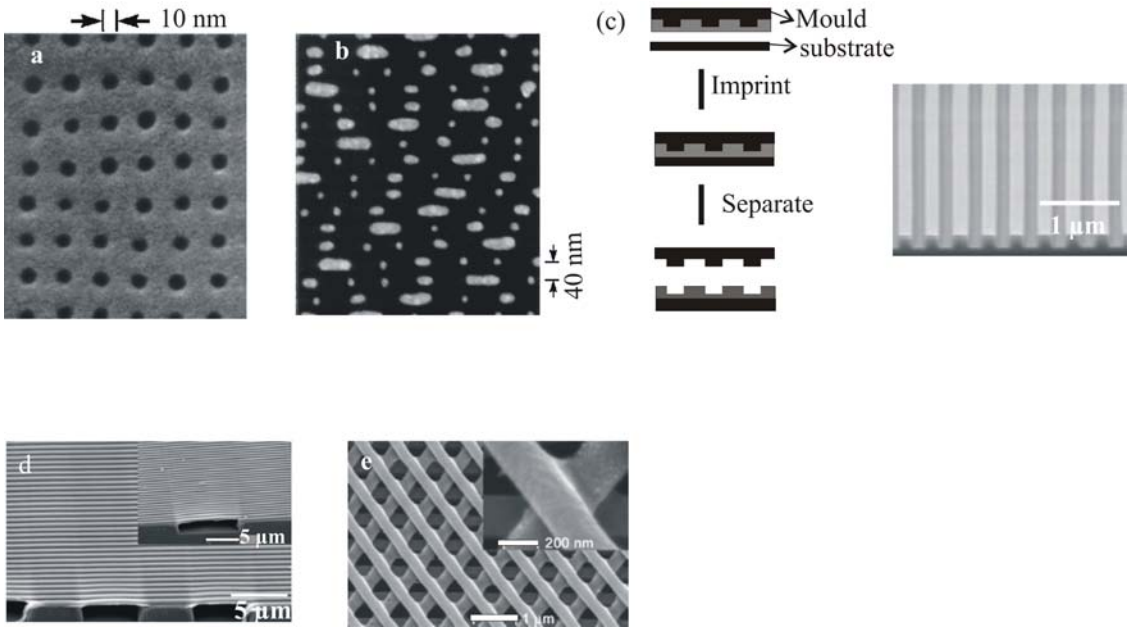

Figure 2.4 (a) SEM image of holes imprinted into PMMA.[53] (b) SEM image of a 40 nm track of a nano-CD fabricated by NIL and metal lift-off.[53] (c) Schematic of reverse nanoimprint and SEM of reverse imprinted PMMA gratings with 350 nm line width/spacing.[63] (d) SEM image of polycarbonate grating structures imprinted with reverse imprinting.[63] (e) SEM image of an imprinted three-layer nanostructure, using three different polymers.[63]

A high viscosity of the polymer film presents another challenge for nanofabrication using NIL. An optimal pattern size and feature density should be provided for NIL.[65] Embossing micrometer–scale features can be more challenging than nano-scale features since filling large areas within the mold requires more lateral displacement of the polymer than smaller features and thus the processing time increases. The thickness of the residual layer can also vary across the imprinted region depending on the pattern density or layout of the patterns. Residual layer non-uniformities present a challenge for transferring the pattern uniformly into the underlying substrate.[1]

During imprinting, the resist is displaced by squeeze flow and capillary forces.[66] The flow phenomena have been investigated by use of specific test patterns, for example negative and positive stamps or stamps with different pattern sizes. It was found that large patterns are much harder to be filled completely than small patterns. This is due to the polymer having to be transferred over large distances in the case of micrometer sized structures.

Combination of NIL with other patterning techniques allows the fabrication of 3D structures.[67] It has been shown that performing a step of imprinting into a PMMA film and

utilizing that prepatterned polymer layer as a resist for X-ray lithography provides a flexible method to fabricate a wide class of complex small-scale 3D structures (Figure 2.5).

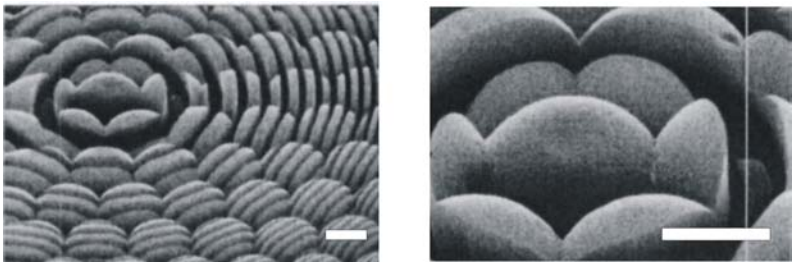

Figure 2.5 3D patterns obtained by combining X-ray lithography with NIL. The scale bar represents 10 μm.[67]

NIL has also been combined with photolithography to replicate structures in negative tone resists by introducing a hybrid mask concept which is made of UV transparent material and acts both as a NIL mold and as a photolithography mask.[52] A further improvement has been made by placing a metal layer on top of the mold so that exposure of the resist layer underneath could be prevented while unexposed residual layer can be removed easily in a developer solution. This can eliminate the residual layer removal step in NIL completely and could simultaneously solve the problem associated with the non-uniformity of the residual layer.

2.3.3 Ultraviolet-assisted Nanoimprint Lithography (UV-NIL)

UV-NIL[68] makes use of UV-curable polymeric materials for imprinting. In this technique, the mold (made of quartz, indium tin oxide or hydrogen silsesquioxane)[69-71] is pressed into the UV-curable solution at room temperature after which the solution is photopolymerized by UV-irradiation (Figure 2.3c). Due to the low viscosity of the resist, only low pressure is needed to press the mold into the resist. After the detachment of the mold, a replica of the mold's topography remains in the resist layer.

There are some advantages of UV-NIL over thermal NIL: i) UV curing is rapid, therefore, high-throughput can be achieved; ii) it can be performed at room temperature and low pressure; iii) the low viscosity of the polymeric precursors facilitates filling of high aspect ratio cavities; iv) since thermal cycling is not required in UV-NIL, accurate shape transfer can be obtained. A thin residual layer remains which is different from conventional lithography.

Acrylates are most often used in UV-NIL formulations, because of their commercial availability, low viscosity, and rapid photopolymerization via radical propagation.[22] However, the application of acrylates requires an inert atmosphere since oxygen is a strong radical inhibitor for this process. Vinyl ethers have been proposed to replace acrylates since their polymerization proceeds via a cationic mechanism which is insensitive to oxygen.[72] The limitation of vinyl ether formulations is that they adhere to the substrate more strongly so that double force is required for mold release. This is overcome by the higher tensile strength of vinyl formulations. Figure 2.6 shows some UV-curable resists used for imprinting.

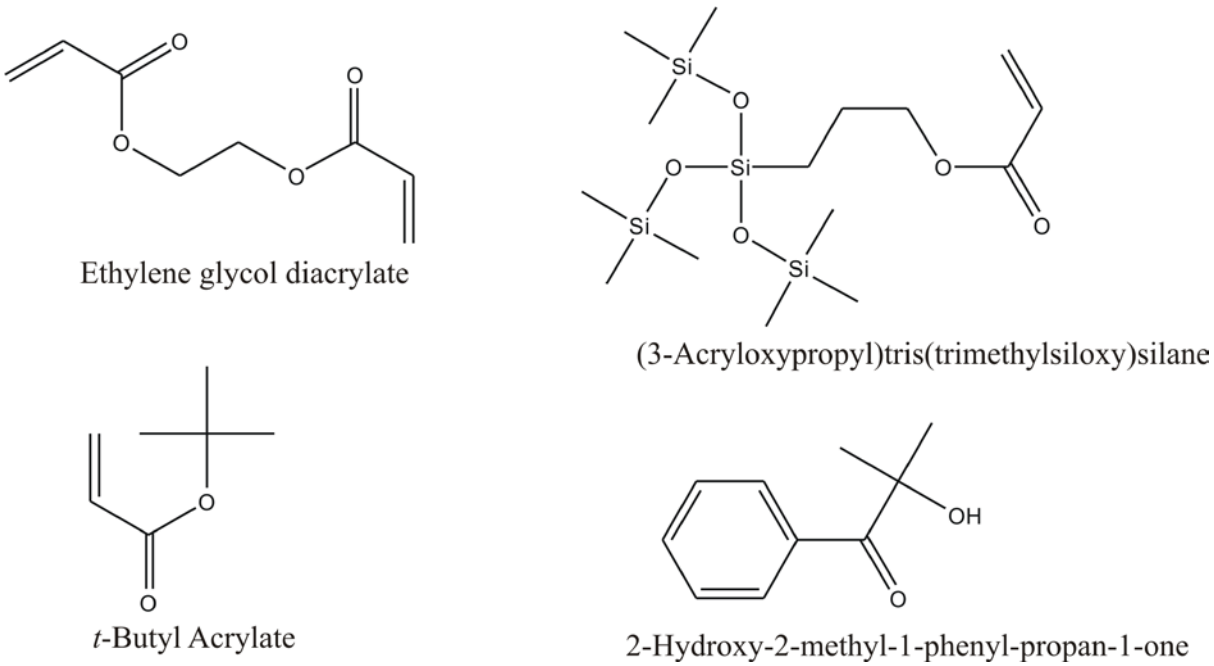

Figure 2.6 UV-curable resist components.

Shrinkage is an important parameter to be optimized to avoid rupture of the embossed structures during demolding. During UV curing, the material shrinks by a value between 3-15% and this facilitates demolding. However this makes pattern design and control difficult. In order to obtain high aspect ratio structures the UV irradiation should be controlled. Excessive UV curing causes excessive shrinkage and brittleness of the resist which also results in cracking and breaking during demolding. Insufficient UV curing leads to low cohesive strength of the polymer and causes distortion and collapse of the structures.[73] A profound analysis of the factors such as UV polymerization time, vertical walls and surface energy of the mould, surface roughness, and resin transparency affecting replication and demolding during UV-NIL have been reported.[73, 74]

Jung et al. have developed a UV-NIL process to fabricate 34×34 crossbar circuits with a half-pitch of 50 nm.[75] In this process, a new resist formulation including benzyl methacrylate monomer and irgacure (photoinitiator) was used to overcome the shrinkage problem during curing and to minimize the residual layer thickness. The problem of trapped air during contact with the mold was solved by changing the surface energy of the substrate.

Step-and-flash imprint lithography (SFIL),[76, 77] a UV-NIL variant, uses a photocurable prepolymer solution as a material to replicate the topography of a mold. In SFIL, a low viscosity, photocurable liquid or solution is not spin-coated but dispensed in the form of small droplets onto the substrate to fill the voids of the quartz mold. The solution contains a low-molecular-molar mass monomer and a photoinitiator. Exposing this solution to UV light cures the photopolymer to make a solidified replica while in contact with the mold. Removing the mold leaves the inverse replica on the substrate. Because of the ability to pattern at room temperature and at low pressure, the template can be stepped to pattern the whole wafer area as in a stepper lithography tool. Examples of imprinted features by SFIL are shown in Figure 2.7a-d.

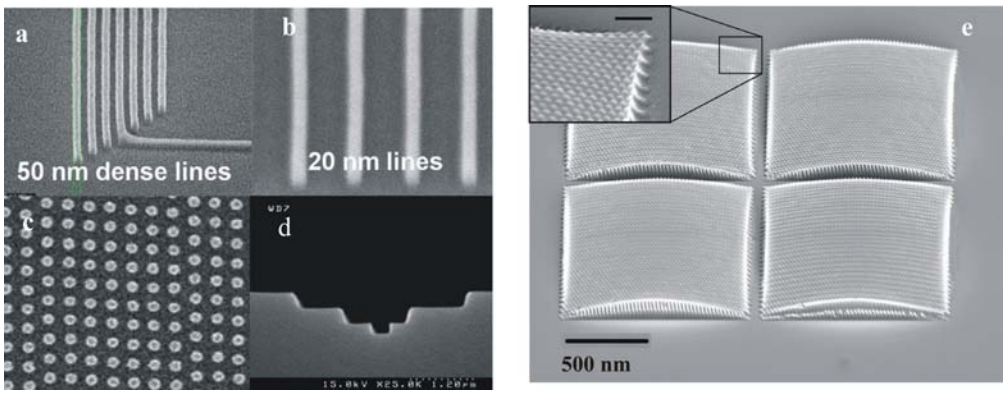

Figure 2.7 SEM images of imprinted images by the S-FIL process: (a) 50 nm dense lines, (b) 20 nm semidense lines, (c) 60 nm posts, and (d) three-tiered structures. (e) SEM image of an S-FIL replicated structure (the inset scale bar shows 80 nm lenses on the surface).[77, 78]

SFIL avoids incomplete mold filling by using monomeric fluids with a low viscosity. However, complete displacement of the fluid by the mold is prevented by hydrodynamic forces resulting in a residual layer of cured material between patterned features.[1, 78] The substrate and the mold should be parallel and flat enough to obtain a uniform residual layer over the entire imprinted area. The residual layer can be removed via etching.

Fluid dynamics is an important issue in the SFIL process.[79] There are several parameters that govern fluid flow of the liquid monomer between the substrate and the template. Parameters governing the fluid flow include the number of initial monomer drops and the relative volume of drops dispensed, flow front arrest at edges of high aspect ratio features and template edges, air entrapment during feature filling, template velocity and force used for imprint, and imprint time.

Pattern density is not a problem for this technique in contrast to thermal NIL.[66, 80] The imprint quality for thermal NIL is limited by the differences in pattern size which is not the case for SFIL since a low viscosity fluid is used. However, shrinkage as a result of polymerization must be controlled since this could affect the size, shape and the placement of the replicated structures.

By using an SFIL multilayer method, PMMA lines of 60 nm with an aspect ratio of 6 and 80 nm lines with an aspect ratio of 14 were reported in early publications.[30] Multilayer device fabrication is possible since distortions caused by differential thermal expansion are not an issue. This process can pattern dielectric gates for the fabrication of a metal oxide semiconducter field-effect transistor (MOSFET) and is also being developed to pattern curved surfaces and topographies in a single step. The fabrication of contact holes of 80 nm was demonstrated which is a significant advance in high density semiconducter devices.[78]

The ultimate resolution of replication by SFIL is unknown but it has been limited by the size of the structures created on the template. Different methods have been employed to fabricate templates, one of which is the use of EBL which requires several processing steps: application of resist onto a fused silica substrate, electron beam exposure, resist development, oxygen plasma etching, chrome etching, resist stripping and fused silica dry etching.[70, 76] In another process, a conductive and transparent layer of indium tin oxide on the glass substrate was incorporated to suppress charging for SEM inspection, and the UV characteristics of the final template were affected minimally which resulted in features as small as 30 nm.[78] In another template fabrication process, to eliminate the etching process, a film of hydrogen silsesquioxane (HSQ) was spin-coated on the ITO layer and then directly written with e-beam lithography. The use of HSQ for direct patterning of SFIL template structures is very convenient since it becomes a durable oxide in its cured state.[71] The use of Focused Ion Beam (FIB) writing as an alternative process to EBL has been demonstrated for the fabrication of 3D structures for SFIL templates which reduces the number of aforementioned lithography steps.[81] As an example, Figure 2.7e shows a fabricated array of concave Motheye lenses employing FIB and then replicated through SFIL imprinting.

2.3.4 Soft Lithography

Soft lithography refers to a collection of pattern replication methods that rely on an elastomeric mold.[8] The process can be separated into two parts: fabrication of elastomeric elements by casting and thermal curing of a liquid prepolymer on a master and the use of these elements as a mold or stamp in a subsequent patterning process (Figure 2.3d). A number of polymers can be used for molding. Elastomers such as poly(dimethylsiloxane) or PDMS (for example, Sylgard 184, Dow Corning) are a versatile class of polymers for replication of the master.[82] PDMS has a number of useful properties for nanofabrication as it is durable, inert to most of the materials being patterned or molded and chemically resistant to many solvents. Despite the advantages of PDMS, the material also suffers from high compressibility which causes shallow relief features of a stamp to deform, buckle, or collaps, in addition, these relief structures tend to deform upon release from the master because of surface tension.[83-86] Other elastomers tested as pattern transfer elements are polyurethane, polyimide, and cross-linked Novolac resins. A new class of fluoropolymers called perfluoropolyethers (PFPE) are used to replace PDMS owing to their excellent release properties and resistance to swelling by organic solvents and monomers. A microfluidic device based on PFPE was fabricated and tested by using different solvents, thus proving its potential in the field of microfluidics.[87]

Microcontact printing (μCP), a soft lithography technique,[88, 89] transfers molecules from a patterned PDMS stamp to a substrate by the formation of covalent bonds.[90-92] It was mainly developed for self-assembled monolayers (SAMs) of alkanethiols on gold and silver. In this process, an elastomeric PDMS stamp inked with an appropriate solution of an alkanethiol, is brought into contact with the surface of a substrate to transfer the ink molecules to those regions of the substrate that contact the stamp. The flexibility of the PDMS stamp and the conformal contact between the stamp and the surface of the substrate are both advantageous for printing over large areas and on curved surfaces. The patterned SAMs can be used either as resists in selective wet etching[92] or as templates[93, 94] in selective deposition to form patterned structures of a variety of materials: metals, silicon, organic polymers.[9, 95]

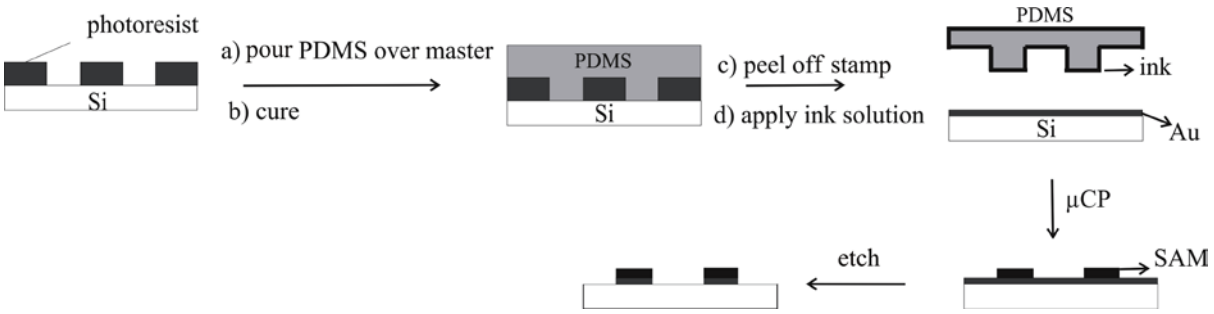

Figure 2.9 Schematic illustration of the μCP procedure.

High aspect ratio (HAR) patterns were obtained by direct casting of PDMS onto a mold prepared by using excimer laser perforating into wax films coated on glass or metal. Micro-hairs of PDMS (post dimensions of 30 μm) were manufactured with aspect ratios of up to 20 (Figure 2.8a).[96] However, thinner size posts obtained were curved in spirals due to the capillary effects and air being trapped in the holes. X-ray LIGA (a German acronym for lithography, electroplating, and molding) molds have also been used to fabricate HAR structures from PDMS with an aspect ratio of 15.[97] The low Young's modulus of PDMS limits its use in HAR patterning of submicrometer structures. Soft elastomeric features are affected by gravity, adhesion, and capillary forces and may collapse, generating defects in the pattern formed.[9] To improve the mechanical stability of elastomeric stamps, alternative materials have been proposed such as composite PDMS,[98] UV-curable PDMS[99] and photocurable fluorinated organic-inorganic hybrids.[100]

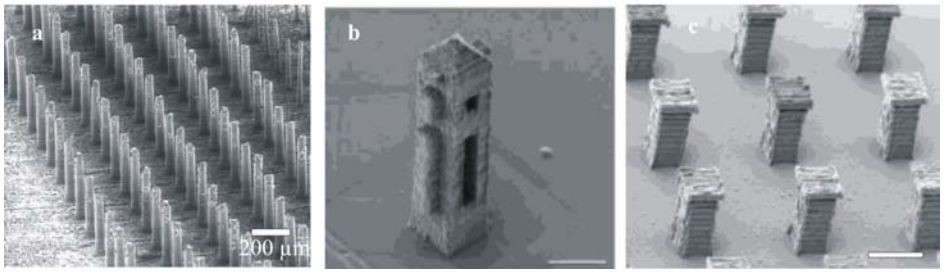

Figure 2.8 SEM images of (a) an array of microposts in PDMS, (b) and (c) replicas in acrylic resin obtained after soft molding with PDMS (the scale bars in (b) and (c) represent 10 μm).[96]

Soft molding includes the patterning techniques based on flexible PDMS stamps and has some advantages over molding with hard masters. The demolding step is facilitated by the elasticity and low surface energy of PDMS which also gives the possibility to replicate

the size and shape of the features present on the mold by mechanical deformation. Multiple PDMS molds can be inexpensively fabricated from a single master.[101]

There are different molding processes depending on the material to be molded by PDMS and the hardening mechanism. One of these is solvent-assisted micro-molding where the polymer solution is drawn into the cavities of the PDMS mold by capillary forces (Figure 2.3e). The others are mainly UV molding of polymer films and micromolding in capillaries (MIMIC).[1, 101]

Soft lithography is relatively cheap and flexible and allows one to control surface chemistry which can be modified by plasma treatment and reaction with organosilanes. This makes the technique very useful when complex organic functional groups are needed in chemistry, biology or biochemistry. Replication of 3D structures is possible because of the softness and elasticity of PDMS. Structures created with an acrylic polymer using multiphoton absorption polymerization (MAP) were replicated by microtransfer molding using a PDMS stamp (Figure 2.8b and c). It is not possible to use microtransfer molding to replicate every structure generated by the MAP technique but careful study of the effects of peeling rate and angle of PDMS stamp removal could increase the reproducibility.[102]

2.3.5 Colloidal Lithography

Colloidal lithography uses particles which are an attractive tool for nanofabrication due to their ability to self-organize. The self-assembled particles have been used in the fabrication of nanopatterns and lithographic masks. Colloidal lithography is inexpensive, inherently parallel, high-throughput, and has a high materials versatility. It is capable of producing well-ordered, 2D-3D periodic arrays of nanoparticles from a variety of materials on many substrates. Three dimensional layers are of interest for photonic applications, whereas two-dimensional layers are used as etch or lithographic masks.[103]

2.3.5.1 Synthetic Methods to Prepare Colloidal Particles

Various polymerization methods such as emulsion, dispersion, precipitation and suspension polymerization can be used to synthesize polymer colloidal particles.[104] Polymer particles such as polystyrene (PS) and poly(methyl methacrylate) (PMMA) are commonly synthesized by emulsion and dispersion polymerization. The particle sizes vary in the range of 0.05 to 10 μm depending on the reaction conditions. For emulsifier-free emulsion polymerization,[105] the reaction temperature and the monomer concentration are the most important factors that control the size of the particles. Increase of the temperature and a

decrease of the monomer concentration give rise to a decrease of the particle size since the solubility of the monomer in the aqueous phase depends on the temperature, and the depletion time of the monomer varies with the monomer concentration. The seed polymerization method[106] can be used for monodisperse polymeric spheres larger than 1 μm in diameter. Larger polymer particles are produced by additional repeated polymerization onto the seed polymer latexes which broadens the polydispersity due to the repeated addition of the raw materials. A single-step dispersion polymerization is generally used as an alternative to produce larger particles. In dispersion polymerization, the reaction site is a monomer droplet stabilized by a smaller amount of surfactants and an initiator, which is soluble in oil and diffuses to the monomer droplets which act as a bulk polymerization reactor.[103, 107]

Stöber et al.[107] developed a technique to prepare inorganic oxide particles, for example silica particles, by using sol-gel chemistry. It is based on the hydrolysis and condensation of tetraethylorthosilicate (TEOS) in a mixture of alcohol, water and ammonia. Synthesis of inorganic particles is achieved following two steps which are nucleation and subsequent growth. To obtain monodisperse particles, these two steps should be separated such that the nuclei can be homogeneously generated without simultaneous growth. In general, the size and polydispersity of particles are related to many factors such as pH, the concentration of the catalyst, the composition of reagents, the type of solvent, and the reaction temperature, which all affect the rates of hydrolysis and condensation.[108]

The principles involved in the preparation of particles have been described[109] and it is now possible to obtain uniform metal oxides, halides, sulfides, selenides, phosphates, carbonates, etc. in different morphologies. Properties of these powders can be modified either by producing solids of internally mixed composition or by coating cores with shells of a different compound.[109]

2.3.5.2 Methods of Colloidal Crystal Assembly

Dispersion stability and the crystallization of the colloidal dispersion are governed by interactions including Van der Waals forces, steric repulsion, and Coulombic repulsion. During the fabrication of colloidal templates or masks, the evaporation of solvent may induce self-assembly of the colloidal particles which makes capillary forces important in the arrangement of the particles.[103, 110] Figure 2.10 shows the strategies for fabricating 2D colloidal arrays including dip-coating, floating on an interface, electrophoretic deposition, physical and chemical template-guided self-assembly, and spin-casting.

In dip-coating,[111] capillary forces and controlled evaporation induce self-organization of particles (Figure 2.10a). The quality of the self-organization is determined by the evaporation rate, which can be controlled by a step motor which helps to lift up the substrate from the colloidal suspension at a controlled rate such that the entire surface can be covered by domains.

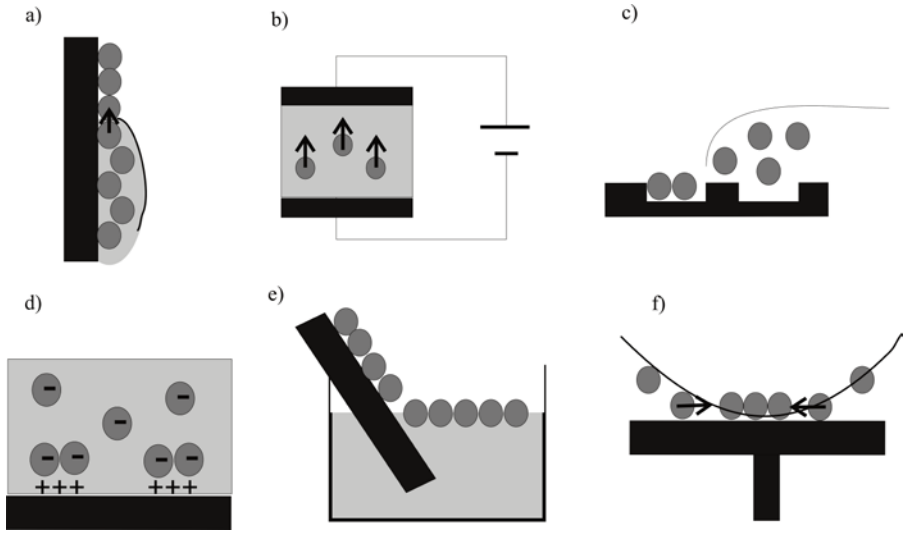

Figure 2.10 Self-assembly strategies to create ordered colloidal arrays: a) dip-coating, b) electrophoretic deposition of colloids, c) template-guided self-organization, d) chemical or electrochemical self-organization of colloidal particles, e) lifting up a colloidal array from an interface using a substrate, f) spin-coating of assembled colloidal particles.

Electrophoretic deposition[112, 113] of the particles employs electric fields to move the particles as shown in Figure 2.10b. Particle assembly takes place inside a thin layer of a colloidal suspension sandwiched between conducting substrates such as indium tin oxide coated glass substrates followed by applying the electric field across the electrodes.[35] Electrophoretic movement not only accelerates the sedimentation speed of small colloidal particles but also guides the growth of a colloidal crystal over a large area in a controlled manner. The combination of patterned electrode templates with electric field driven assembly was shown to control crystal packing and lattice orientation control. Hexagonal and square type packing symmetries of 2D colloidal monolayers were obtained over large surfaces by uisng this so called graphoepitaxy method.[113]

Defect formation can be suppressed by template-assisted self-assembly of colloidal particles.[114] A chemically[115, 116] (Figure 2.10d) or topographically[117] (Figure 2.10c) patterned substrate can be used for the selective deposition of colloidal particles. Physical

templates based on relief structures patterned on the surfaces of solid substrates have been used by Xia et al. to produce a variety of structures including polygonal, polyhedral, spiral, and hybrid aggregates of spherical particles that are difficult to fabricate with other methods.[117] The structure of the aggregates was controlled by changing the shape and the dimensions of the template using conventional photolithography, which also prevented the production of templates with feature sizes smaller than 100 nm.

Figure 2.10e shows the assembly of a colloidal array floating on an interface. The quality and packing of the array at the interface can be controlled by changing the concentration of the particles or electrolytes, the particle size, the surface charge and the hydrophobicity of the particles.[118, 119] For example, silica colloids modified by silanizing the surface to enhance the hydrophobicity were self-assembled at an octane/water interface. A monolayer without variation in the layer thickness could be obtained which is not possible for evaporation-induced self-assembly.[120] The Langmuir-Blodgett film technique can also be used to obtain such a uniform layer. [121]

Another way of preparing a colloidal array is by using spin-coating.[122] The colloidal particles organize themselves into a hexagonal array more rapidly due to the centrifugal forces (Figure 2.10f). The thickness of the particle layer is controlled by adjusting the particle loading and the spin speed. Spin-coating provides advantages for both scaling up and mass production since the process is rapid and compatible with wafer processing.

2.3.5.3 Nanopatterning with Colloidal Masks

Colloidal particles in a hexagonally packed array can be used as a mask so that deposition or etching proceeds through the interstices between the colloidal particles. Evaporation and sputtering into these interstices has been used to produce very thin films (< 30 nm) of metals and inorganic oxides. The sputtered material can be chosen without any limitation, and the size, height, and number density of the metal dots can be controlled by simply adjusting the particle size and the sputtering conditions.

The use of colloidal particle arrays as masks for metal sputtering or etching substrates was pioneered by Fischer et al. and Deckman et al.[123, 124] Duyne et al.[125] used single- or double-layered PS particles on various substrates as a mask for metal deposition as illustrated in Figure 2.11. As seen in Figure 2.11a and b, a hexagonally ordered triangular array of metal dots formed from a single layer colloidal mask, and a spherical dot array with different unit lattices was fabricated from the double-layer mask (Figure 2.11c, d). The reason for the formation of a spherical dot array is that when a second layer of nanospheres assembles onto

the first, every other three-fold hole is blocked, and a smaller density of six-fold interstices results as shown in Figure 2.11c and d.

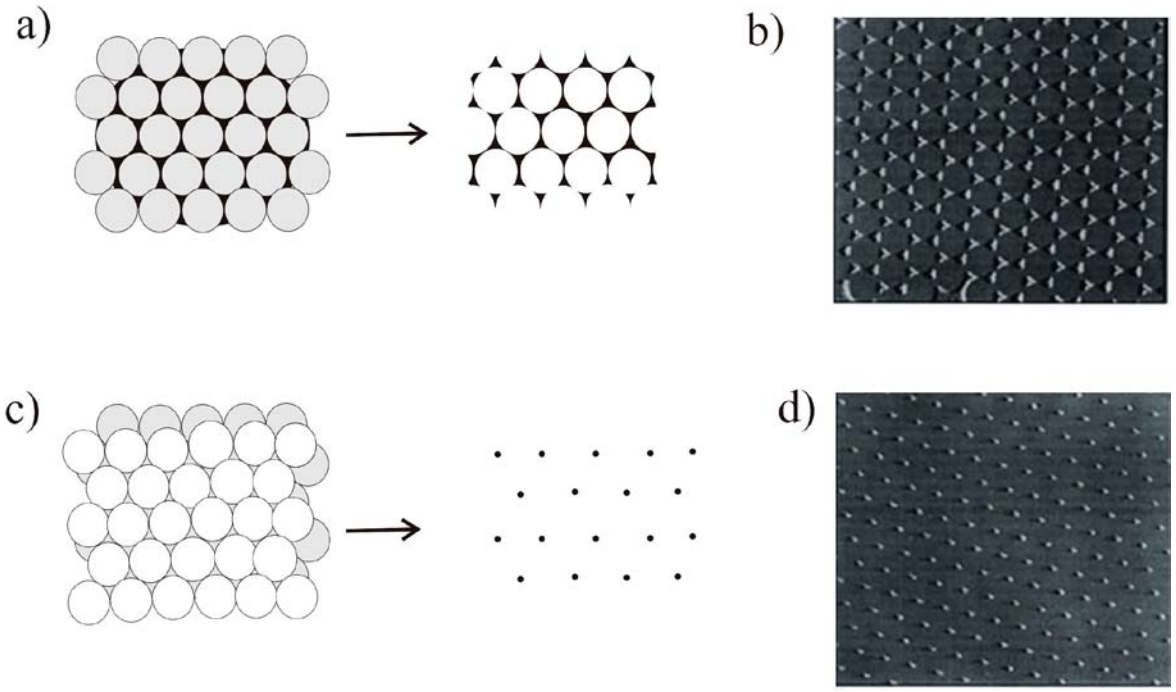

Figure 2.11 (a) Schematic diagram of a single layer nanosphere mask and (b) a hexagonally ordered triangular array of metal dots after removal of the template. (c) Schematic diagram of a double layer nanosphere mask and (d) spherical dot arrays after removal of the template.[125]

Colloidal arrays as masks have also been used for the nanofabrication of various organic and inorganic materials. The deposited materials, in some cases, can be used as seeds for the growth of other functional materials. For instance, carbon nanotubes were grown on nickel nanodots that were pre-deposited through a colloidal mask by using plasma-enhanced chemical vapor deposition (PECVD) (Figure 2.12a).[126] Zinc oxide nanorod arrays were also prepared using PS particles as a template for patterning gold catalyst particles and subsequent bottom-up growth in a tube furnace using chemical vapor deposition (Figure 2.12b).[127] Similarly, an organic light-emiting nanodiode (OLED) array was fabricated by deposition of multilayers through the interstices of the particle array without causing etching damage which is the case for conventional masking processes.[128] Patterning of ferromagnetic arrays was demonstrated over an area greater than 1 cm^2 without agglomeration of particles after metal evaporation which gave control over the diameter, aspect ratio, and pitch of the fabricated elements.

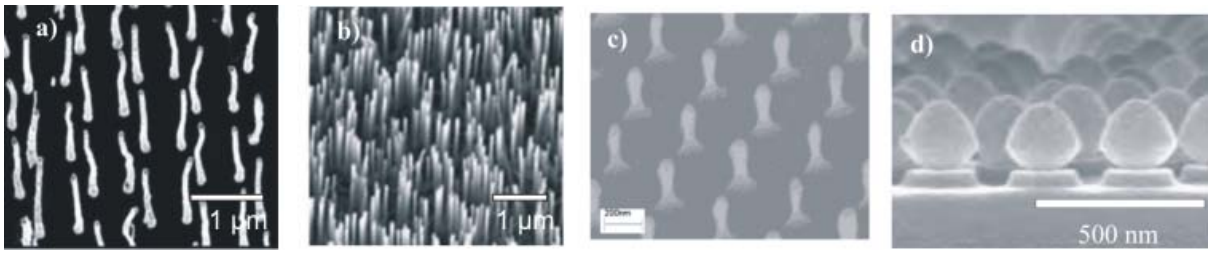

Figure 2.12 (a) Vertically aligned carbon nanotube array by using plasma-enhanced chemical vapor deposition (PECVD).[126] (b) ZnO nanorod arrays prepared using gold catalyst particles and subsequent bottom-up growth in a tube furnace using chemical vapor deposition[127] (c) SEM image of silicon nanopillars fabricated by means of an aluminum etch mask obtained using a PS particle array.[129] The scale bar indicates 200 nm. (d) Cross-sectional image of the Si nanopillars after etching.

Sputtered metal arrays can be used as etching masks to create surface topography. Silicon nanopillars with diameters as small as 40 nm and aspect ratios of up to 7 were fabricated by preparing an aluminum etch mask using a PS particle array (Figure 2.12c).[129] Large-area periodic silicon nanopillar arrays have been obtained after metal deposition, lift-off, and etching processes. By varying the etching parameters, such as mask materials and etching recipes, the size and the shape of silicon nanopillars can be modified, thus size and shape control of nanostructures can be achieved.[129]

The combination of colloidal lithography (CL) and alkanethiol self-assembly was used to create substrates with controlled surface topography and chemical composition. Patterns exhibiting also chemical contrast allow one to investigate the interfacial interactions or adsorption behavior of biomolecules and nanoparticles. For example, Michel et al. created topographical contrast via colloidal patterning to design platforms for the attachment of targeted proteins.[130] Nanopillars of TiO_2 (50-90 nm in diameter, 20 nm in height) on oxidized silicon were fabricated by using colloidal lithography and were then rendered hydrophobic by the selective self-assembly of an organophosphate, whereas a poly(ethylene glycol)-grafted copolymer was adsorbed onto the surrounding SiO_2, rendering it protein resistant. Further binding of streptavidin onto the organophosphate and immobilization of biotinylated liposomes to the streptavidin was accomplished successfully.[130]

Tan et al.[131] used particle arrays as a mask to fabricate a dome structure by reactive ion etching [35] which converts the spheres into nonspherical particles. Single and double layers of packed colloidal polystyrene microspheres of uniform size (diameter 1.2 μm) were spin-coated onto cleaned Si substrates, which were then exposed to CF_4 and O_2 plasma

mixtures. Due to preferential etching in the direction normal to the surface of the substrate, the microspheres were reduced to a nonspherical form resembling a biconvex microlense (Figure 2.12d).

Spherical colloidal particles can be utilized for preparing various types of porous materials that exhibit precisely controlled pore sizes and highly ordered 3D porous structures. After drying the colloidal array, the voids between the colloidal spheres are fully infiltrated with a liquid precursor such as an ultraviolet [132] or thermally curable organic prepolymer,[109] or an ordinary organic monomer (plus an initiator).[133] Subsequent solidification of the precursor and removal of the colloidal spheres gives a 3D porous structure. Johnson et al.[133] prepared ordered mesoporous polymers by filling the pores in the colloidal crystals (silica spheres of 35 nm in diameter) with divinylbenzene (DVB), ethyleneglycol dimethacrylate (EDMA), or a mixture of the two. Polymerization and subsequent dissolution of the silica template left a polycrystalline network of interconnected pores. When mixtures of DVB and EDMA were used, the pore size of the polymer replicas varied continuously between 35 and 15 nm because the polymer shrinks when the silica template is removed.[133] Initiated chemical vapor deposition (iCVD) has also been used to produce grafted polymeric layers (Figure 2.13).[134] Patterns were generated for a broad range of materials including organic polymers (pBA, pHEMA), fluoropolymers (pPFDA, pPFM) and organosilicones. Since iCVD is a solvent-free process, it has many advantages compared to solution polymerization.[134]

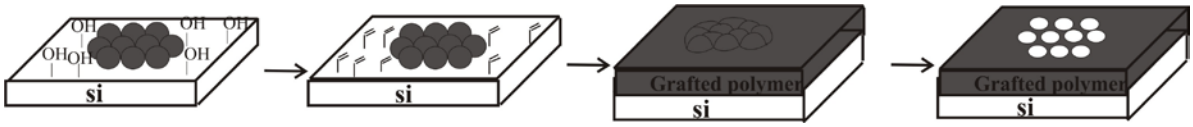

Figure 2.13 Schematic process to produce polymeric nanostructures using CL. A hydroxylated substrate was treated with a vapor-phase silane coupling agent, which covalently attaches the vinyl groups to the substrate in the exposed regions of the colloidal mask. The polymer was grafted and the grafted film was sonicated to remove the colloidal template, leaving an array of bowl-shaped nanostructures.

2.3.5.4 Modification of Colloidal Masks

One of the disadvantages of the CL method is the limited control over the shape of the patterns, which is triangular or spherical. Adjustment of the deposition method and modification of the colloidal masks have been suggested to overcome this limitation.[103] The

deposition method can be modified by tilted or rotated deposition through the as prepared colloidal mask. The angle between the deposition flow and the substrate normal can be controlled and a variety of structures (elongated triangles or double triangles) has been obtained by varying this angle. However, the shapes obtained are restricted by the mask shape.[103]

A more effective approach is to modify the colloidal particles by suitable post-treatment such as RIE, ion milling, or annealing. The deformation of polymeric beads such as PS and PMMA occurs above the glass transition temparature and this has been utilized to modify the colloidal mask for fabricating a gold disk array via CL. The size of the disk was adjusted by changing the annealing time, since polymeric particles spread over a wider distance with the annealing time (Figure 2.14a-f). Microwave heating can also be used to anneal the polymer particles which gives more precise control over the degree of annealing.[135] Kosiorek et al. produced particles with morphologies such as rings, rods, and dots by changing the mask morphology by temperature processing and varying the evaporation conditions.[135] The technique was shown to scale down the size of metallic nanoparticles from 200 to 30 nm, while preserving the original nanospheres pacing and order. It was shown that by temperature treatment it is easy to control the spaces between the spheres, and therefore the size of the particles deposited through the PS mask.

Meanwhile, RIE has been used to modify the colloidal mask by changing the size and the shape of the particles.[136] RIE has been employed to control the surface morphology and roughness and to enhance the surface hydrophilicity in polymeric and biological applications. RIE was used to fabricate polymeric nanofibrillar surfaces and patterned structures using colloidal single layers and double layers. Choi et al. have created well organized layers of nonspherical colloidal particles by using anisotropic RIE of the spherical polymer latexes that were stacked layer-by-layer, with the top layer acting as a mask.[137] The shadowing effect from the upper layer of particles to the layers beneath resulted in nonspherically etched polymeric structures (Figure 2.14g). The resulting patterns and particle shapes were dependent on the crystal orientation relative to the substrate (Figure 2.14h), the number of colloidal layers, and the RIE conditions.

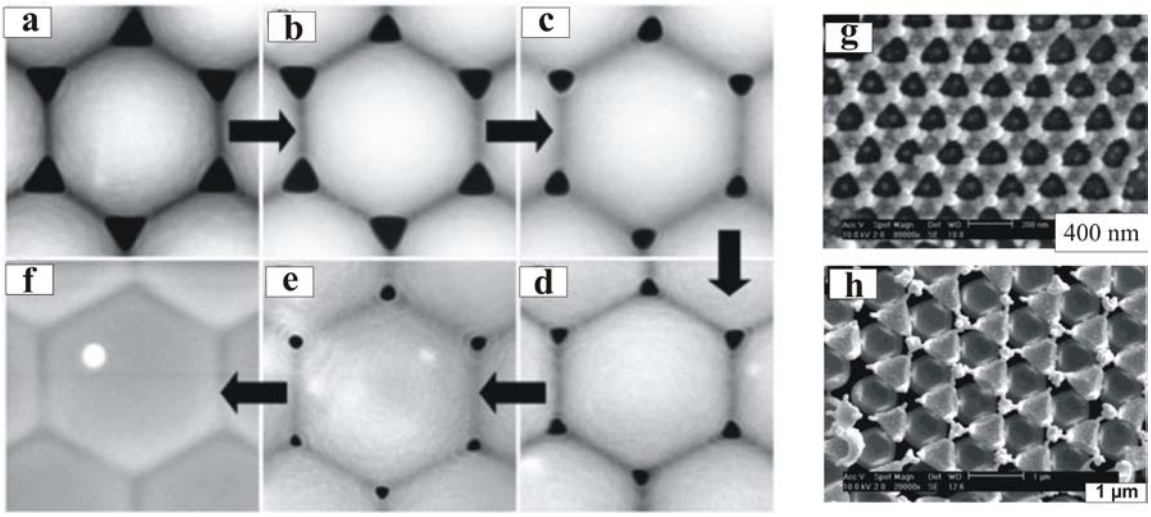

Figure 2.14 A 540-nm PS latex mask annealed in 25 mL of a water/EtOH/ acetone mixture by a) 1, b) 2, c) 4, d) 6, e) 7, and f) 10 microwave pulses.[135] g) Binary particle arrays and 2-D nanopatterns produced from a double layer of small PS beads (200 nm). h) Ternary particle arrays produced after partial RIE etching of PS beads in fcc symmetry.[137]

2.4 SURFACE STRUCTURING with ORGANOMETALLIC POLYMERS

Poly(ferrocenylsilane)s (PFSs) composed of alternating ferrocene and silane units in the main chain, belong to the class of organometallic polymers. High molar mass poly(ferrocenylsilane) macromolecules were discovered in the early 1990s by Manners et al.[138] by thermal-ring opening polymerization of highly strained, silicon-bridged [1]ferrocenophanes. There are several ways to polymerize silicon-bridged [1]ferrocenophanes such as by use of anionic initiators,[139] transition metal catalysts[140, 141] or in the solid state using a ^{60}C γ-ray source[142] (Figure 2.15). The physical properties of PFS depend on the substituents at silicon. Symmetrically substitued PFSs are often semicrystalline,[143] whereas asymmetrically substitued PFSs are, in general, amorphous.[144] Several types of PFSs bearing alkyl, alkoxy, aryloxy, and amino groups have been synthesized.[145]

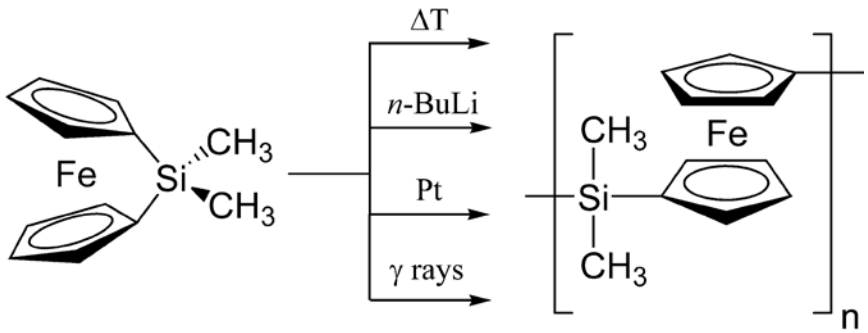

Figure 2.15 Ring opening polymerization of strained dimethylsila[1]ferrocenophane.

The presence of alternating ferrocene and silane units in the backbone renders this organometallic polymer highly useful for applications in optics, semiconductors, nanopatterned catalysis for carbon nanotube growth, electrochemically responsive substrates or media, etc.[138, 145-147] One of the unique applications is their use as resists in "maskless" lithography due to the presence of Fe and Si in the backbone which makes PFSs highly etch resistant in reactive ion etching environments in comparison with organic polymers.[148] Pattern transfer into various substrates by using these organometallic homopolymers as inks in soft lithography owing to their etch resistance has been already demonstrated[149] and silicon nanopillars with aspect ratios of 10 have also been fabricated.[149] One of the most spectacular applications included the use of a PFS-*b*-PS diblock copolymer work to transfer spherical patterns into magnetic cobalt films via stepwise etching using plasma etching and ion sputtering steps.[150]

Organometallic compounds are known to act as an etch barrier in oxygen and oxygen containing plasmas since the products of chemical etching with oxygen plasmas are non-volatile and do not desorb from the surface.[148] When PFS films are exposed to oxygen plasma, a thin Fe/Si-oxide layer forms on top of the film, as proven by XPS.[151] The XPS spectra of poly(ferrocenyldimethylsilane) gave information regarding the atoms present at the surface after treatment with oxygen plasma. It was shown that the carbon concentration was reduced at the surface, while the oxygen, iron and silicon concentration increased and aromaticity was destroyed.

Two soft lithography approaches, solvent-assisted dewetting and capillary force lithography (Figure 2.16a), were employed to pattern PFS.[149] The use of poly(ferrocenyldimethylsilane) as an ink in microcontact printing was not successful because of the poor wettability of the PDMS stamp. Although the wettability of the PDMS stamps was improved by treating the stamp with with an oxygen plasma prior to inking, PFS patterns did not replicate fully the stamp pattern which proves that the polymer solution dewets between the stamp and Si surface, forming continuous lines in the middle of the protruding stamp. A chemically patterned substrate, prepared by microcontact printing, was also used as a template to spin-coat poly(ferrocenyldimethylsilane) which directed the dewetting of the polymer film.[148]

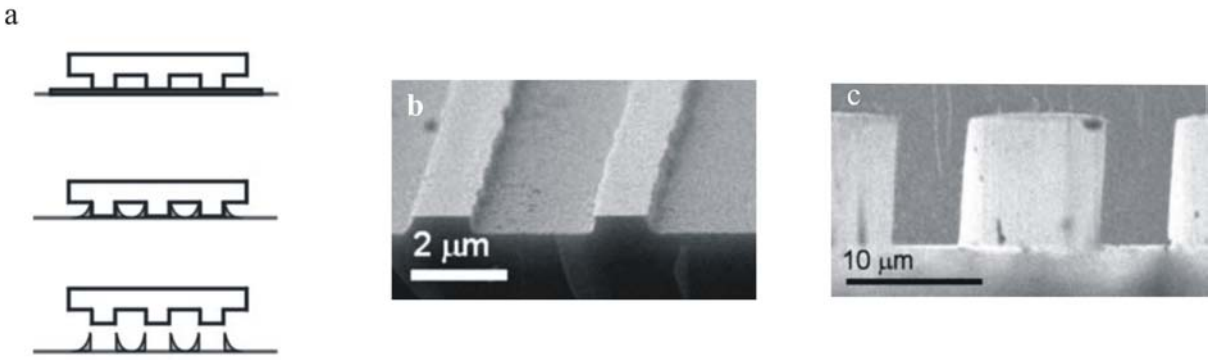

Figure 2.16 a) The scheme for capillary force lithography. b) SEM image of a substrate patterned with capillary force lithography. c) SEM image of a substrate patterned with MIMIC.[148]

Capillary force lithography (CFL) was also employed to pattern PFS.[148] Polymer structures of 110 nm high and 500 nm wide were fabricated and subsequently developed by CF_4/O_2 RIE. In addition, the influence of processing conditions and polymer architecture on the pattern transfer in CFL using PFS etch resists was investigated. The patterns in CFL experiments were fabricated by placing the PDMS mold in contact with the 20 nm thin polymer films and keeping it for 4 h at temperatures ranging from 30 to 140 ^{o}C, under vacuum. Polymers with low molar mass and corresponding low viscosities showed signs of polymer dewetting, on the other hand polymers with too high viscosity did not yield patterns. Most of the good quality patterns were prepared with polymer viscosities which fall into the range between 50 and 1500 Pa·s.[152]

Thin films of organic-organometallic block copolymers self-assemble to form regions that have a significantly different etching behavior. This property of PFS was used in block copolymer lithography where structures down to 20 nm could be etched into the substrate. PFS block copolymers were also employed to pattern thin films, as was shown by the use of ferrocenylsilane-styrene block copolymers as templates in the fabrication of cobalt magnetic dot arrays.[150] The organic-rich phase is quickly removed whereas the organometallic-rich phase shows high resistance against oxygen and fluorocarbon plasmas which opens up the possibility of transferring the patterns generated by block copolymer self-assembly in a one-step etching process into the underlying substrate.[150]

Phase-separated thin films of PS-*b*-PFS were used to synthesize carbon nanotubes which show catalytic activity.[153] Substrates for nanotube growth were prepared by spin coating. After spin-coating, the substrates were annealed in vacuum and subsequently treated in oxygen plasma in order to remove the PS matrix and to form iron oxide-containing nanoparticles. Carbon nanotube growth was then performed on the substrates using acetylene as the carbon source.

Combining block copolymer self-assembly with long-range ordering methods would allow nanostructures to be lithographically fabricated in precise positions on a substrate.[154] Graphoepitaxy is a method that allows the formation of nanostructures by spin-coating a block copolymer over surfaces already patterned with shallow grooves.[155] The effect of the width of the grooves on pattern order has been shown and within a 300-nm-wide groove, about nine rows of close-packed PFS features were aligned.[156] Figure 2.17a shows a top view and cross section of a sphere array after spin-coating, annealing and etching. The top surface shows a square symmetry in the sphere packing, and the cross section shows 11 rows of spheres parallel to the surface of the substrate as shown 2.17b. For the smallest V grooves with the thinnest films, a single of row spheres was formed. The commensurability between the thickness of the layer and the plane spacing determines the packing and the size of domains.[155] Ross et al. have also studied the locations and long range order of the PFS microdomains by using templates of different sizes.[156]

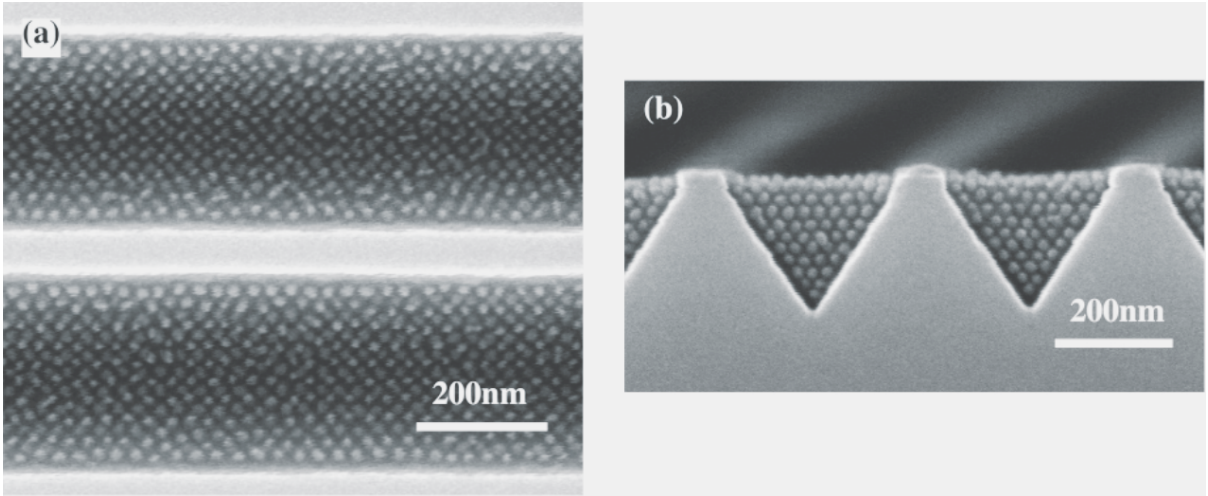

Figure 2.17 SEM images of PS-PFS films in V grooves after 72 h annealing and etching (a) square packing of spheres is visible in the top view, (b) the same sample as that in part a in a cross sectional view showing a sphere array with 11 rows.[155]

Well controlled 1D arrays were formed by templating a spherical-morphology block copolymer within a narrow groove. made from a hydrogen silsesquioxane resist layer patterned using electron-beam lithography. A single row of PFS domains forms when $0.6 < W/d_0 < 1.5$. where d_0 is domain spacing and W is the confinement width of the channel. It was shown in Figure 2.18 that the domains were distorted into ellipses with aspect ratio and major axis orientation controlled by the groove width.

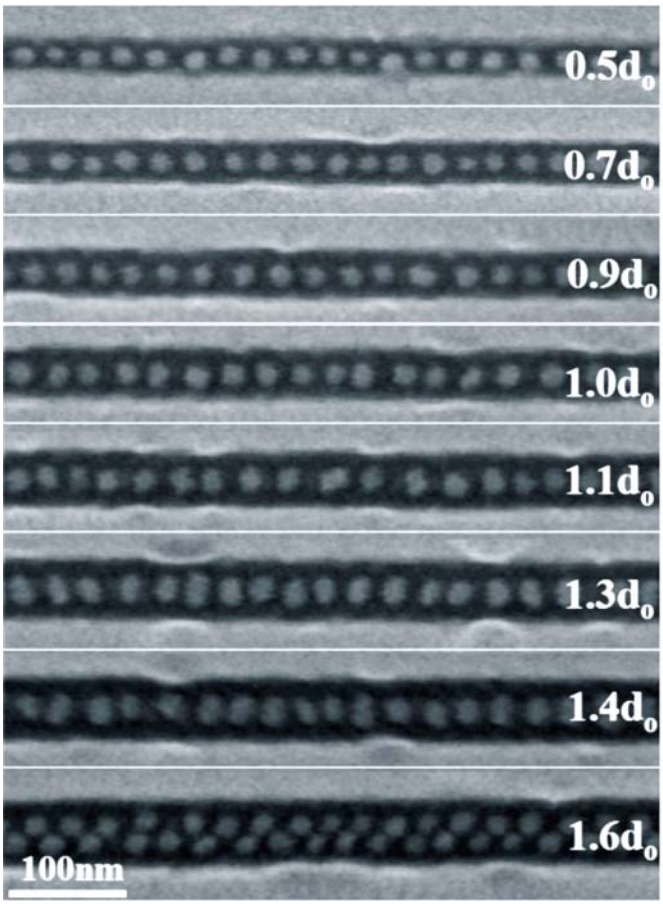

Figure 2.18 SEM image of PFS block copolymer domains within channels of different confinement widths *W*. A single row of spheres forms for $0.6 < W/d_0 < 1.5$, where d_0 is the equilibrium row spacing of this block copolymer.[157]

CONCLUSIONS

Conventional and unconvential techniques have enabled fabrication of 2D and 3D structures ranging from several tens of nanometers to micrometer scales. Historically, photolithography has been the dominant technique for replication despite of its resolution limit. Photolithography continues to overcome obstacles to achieve new resolution limits which, however, increases the cost. The high cost of conventional equipment for nanofabrication pave the way to unconventional techniques. Unconventinal techniques for nanofabrication are being widely accepted and they are extensively explored for research purposes. Molding, embossing, and printing techniques provide higher resolution patterning with high througput at a lower cost. Despite all recent progress in patterning, each patterning method has its own specific strengths and advantages and can not meet the requirements of all fabrication needs. In addition, the large-scale fabrication of surfaces by using reported methods still remains a big challenge. Combining of different fabrication methods could help the future development of devices and their performances.

2.5 REFERENCES

[1] B. D. Gates, Q. B. Xu, M. Stewart, D. Ryan, C. G. Willson, G. M. Whitesides, *Chem. Rev.* **2005**, *105*, 1171.

[2] T. Ito, S. Okazaki, *Nature* **2000**, *406*, 1027.

[3] G. M. Wallraff, W. D. Hinsberg, *Chem. Rev.* **1999**, *99*, 1801.

[4] K. Gamo, *Microelectron. Eng.* **1996**, *32*, 159.

[5] Y. N. Xia, E. Kim, X. M. Zhao, J. A. Rogers, M. Prentiss, G. M. Whitesides, *Science* **1996**, *273*, 347.

[6] S. Y. Chou, S. J. Schablitsky, L. Zhuang, *J. Vac. Sci. Technol. B* **1997**, *15*, 2864.

[7] S. Y. Chou, P. R. Krauss, P. J. Renstrom, *Science* **1996**, *272*, 85.

[8] Y. N. Xia, G. M. Whitesides, *Ange. Chem. Int. Ed.* **1998**, *37*, 551.

[9] Y. N. Xia, G. M. Whitesides, *Annu. Rev. Mater. Sci.* **1998**, *28*, 153.

[10] D. M. Eigler, E. K. Schweizer, *Nature* **1990**, *344*, 524.

[11] R. D. Piner, J. Zhu, F. Xu, S. H. Hong, C. A. Mirkin, *Science* **1999**, *283*, 661.

[12] D. Wouters, U. S. Schubert, *Angew. Chem. Int. Ed.* **2004**, *43*, 2480.

[13] J. A. Rogers, K. E. Paul, R. J. Jackman, G. M. Whitesides, *Appl. Phys. Lett.* **1997**, *70*, 2658.

[14] J. A. Rogers, K. E. Paul, R. J. Jackman, G. M. Whitesides, *J. Vac. Sci. Technol. B* **1998**, *16*, 59.

[15] N. A. Melosh, A. Boukai, F. Diana, B. Gerardot, A. Badolato, P. M. Petroff, J. R. Heath, *Science* **2003**, *300*, 112.

[16] Q. B. Xu, B. D. Gates, G. M. Whitesides, *J. Am. Chem. Soc.* **2004**, *126*, 1332.

[17] G. M. Whitesides, P. E. Laibinis, *Langmuir* **1990**, *6*, 87.

[18] G. M. Whitesides, J. P. Mathias, C. T. Seto, *Science* **1991**, *254*, 1312.

[19] W. M. Moreau, *Semiconductor Lithography: Principles and Materials*, Plenum, New York, **1988**.

[20] M. Rothschild, T. M. Bloomstein, R. R. Kunz, V. Liberman, M. Switkes, S. T. Palmacci, J. H. C. Sedlacek, D. Hardy, A. Grenville, *J. Vac. Sci. Technol. B* **2004**, *22*, 2877.

[21] M. Rothschild, *Mater. Today* **2005**, *18*.

[22] A. del Campo, E. Arzt, *Chem. Rev.* **2008**, *108*, 911.

[23] M. Han, W. Lee, S. K. Lee, S. S. Lee, *Sens Actuators A: Phys.* **2004**, *111*, 14.

[24] H. Sato, Y. Houshi, S. Shoji, *Microsystem Technologies* **2004**, *10*, 440.

[25] F. Romanato, M. Tormen, L. Businaro, L. Vaccari, T. Stomeo, A. Passaseo, E. Di Fabrizio, *Microelectron. Eng.* **2004**, *73-4*, 870.

[26] H. Elsner, H. G. Meyer, *Microelectron. Eng.* **2001**, *57-8*, 291.

[27] Y. N. Xia, J. A. Rogers, K. E. Paul, G. M. Whitesides, *Chem. Rev.* **1999**, *99*, 1823.

[28] J. A. van Kan, A. A. Bettiol, F. Watt, *Appl. Phys. Lett.* **2003**, *83*, 1629.

[29] S. Okazaki, *J. Vac. Sci. Technol. B* **1991**, *9*, 2829.

[30] M. Colburn, A. Grot, B. J. Choi, M. Amistoso, T. Bailey, S. V. Sreenivasan, J. G. Ekerdt, C. G. Willson, *J. Vac. Sci. Technol. B* **2001**, *19*, 2162.

[31] I. Junarsa, P. F. Nealeya, *J. Vac. Sci. Technol. B* **2004**, *22*, 2685.

[32] K. Ansari, P. G. Shao, J. A. van Kan, A. A. Bettiol, F. Watt, *Nuclear Instruments and Methods in Physics Research Section B: Beam Interactions with Materials and Atoms* **2005**, *231*, 407.

[33] S. Y. Chou, P. R. Krauss, P. J. Renstrom, *Applied Physics Letters* **1995**, *67*, 3114.

[34] S. Y. Chou, P. R. Krauss, P. J. Renstrom, *J. Vac. Sci. Technol. B* **1996**, *14*, 4129.

[35] A. E. Larsen, D. G. Grier, *Phys. Rev. Lett.* **1996**, *76*, 3862.

[36] I. Maximov, E. L. Sarwe, M. Beck, K. Deppert, M. Graczyk, M. H. Magnusson, L. Montelius, *Microelectron. Eng.* **2002**, *61-2*, 449.

[37] C. M. Sotomayor Torres, S. Zankovych, J. Seekamp, A. P. Kam, C. Clavijo Cedeño, T. Hoffmann, J. Ahopelto, F. Reuther, K. Pfeiffer, G. Bleidiessel, G. Gruetzner, M. V. Maximov, B. Heidari, *Mater. Sci. Eng. C* **2003**, *23*, 23.

[38] J. Taniguchi, Y. Tokano, I. Miyamoto, M. Komuro, H. Hiroshima, *Nanotechnology* **2002**, *13*, 592.

[39] M. T. Li, Princeton University, **2003**.

[40] J. Taniguchi, K. Koga, Y. Kogo, I. Miyamoto, *Microelectron. Eng.*, *83*, 940.

[41] T. Katoh, N. Nishi, M. Fukagawa, H. Ueno, S. Sugiyama, *Sens. Actuators, A: Phys.* **2001**, *89*, 10.

[42] R. W. Jaszewski, H. Schift, P. Gröning, G. Margaritondo, *Microelectron. Eng.* **1997**, *35*, 381.

[43] M. Keil, M. Beck, G. Frennesson, E. Theander, E. Bolmsjo, L. Montelius, B. Heidari, *J. Vac. Sci. Technol. B* **2004**, *22*, 3283.

[44] A. Fuchs, B. Vratzov, T. Wahlbrink, Y. Georgiev, H. Kurz, *J. Vac. Sci. Technol. B.* **2004**, *22*, 3242.

[45] C. M. Sotomayor Torres, *Alternative Lithography*, Kluwer Academic, New York, **2003**.

[46] H. Schift, S. Bellini, J. Gobrecht, F. Reuther, M. Kubenz, M. B. Mikkelsen, K. Vogelsang, *Microelectron. Eng.* **2007**, *84*, 932.

[47] L. J. Guo, *Adv. Mater.* **2007**, *19*, 495.

[48] N. Bogdanski, M. Wissen, S. Mollenbeck, H. C. Scheer, *J. Vac. Sci. Technol. B* **2006**, *24*, 2998.

[49] N. Bogdanski, M. Wissen, A. Ziegler, H. C. Scheer, *Microelectron. Eng.* **2005**, *78-79*, 598.

[50] V. Studer, A. Pepin, Y. Chen, *Appl. Phys. Lett.* **2002**, *80*, 3614.

[51] H. Schift, *J. Vac. Sci. Technol. B* **2008**, *26*, 458.

[52] L. J. Guo, *J. Phys. D-Appl. Phys.* **2004**, *37*, R123.

[53] S. Y. Chou, P. R. Krauss, W. Zhang, L. J. Guo, L. Zhuang, *J. Vac. Sci. Technol. B* **1997**, *15*, 2897.

[54] K. Ansari, J. A. van Kan, A. A. Bettiol, F. Watt, *Appl. Phys. Lett.* **2004**, *85*, 476.

[55] J. D. Hoff, L. J. Cheng, E. Meyhofer, L. J. Guo, A. J. Hunt, *Nano Lett.* **2004**, *4*, 853.

[56] H. W. Li, W. T. S. Huck, *Nano Lett.* **2004**, *4*, 1633.

[57] M. Behl, J. Seekamp, S. Zankovych, C. M. S. Torres, R. Zentel, J. Ahopelto, *Adv. Mater.* **2002**, *14*, 588.

[58] M. T. Li, J. A. Wang, L. Zhuang, S. Y. Chou, *Appl. Phys. Lett.* **2000**, *76*, 673.

[59] W. Zhang, S. Y. Chou, *Appl. Phys. Lett.* **2003**, *83*, 1632.

[60] D. Y. Khang, H. Yoon, H. H. Lee, *Adv. Mater.* **2001**, *13*, 749.

[61] S. Matsui, Y. Igaku, H. Ishigaki, J. Fujita, M. Ishida, Y. Ochiai, M. Komuro, H. Hiroshima, *J. Vac. Sci. Technol. B* **2001**, *19*, 2801.

[62] S. Matsui, Y. Igaku, H. Ishigaki, J. Fujita, M. Ishida, Y. Ochiai, H. Namatsu, M. Komuro, *J. Vac. Sci. Technol. B* **2003**, *21*, 688.

[63] L. R. Bao, X. Cheng, X. D. Huang, L. J. Guo, S. W. Pang, A. F. Yee, *J. Vac. Sci. Technol. B* **2002**, *20*, 2881.

[64] N. Kehagias, V. Reboud, G. Chansin, M. Zelsmann, C. Jeppesen, C. Schuster, M. Kubenz, F. Reuther, G. Gruetzner, C. M. S. Torres, *Nanotechnology* **2007**, *18*.

[65] K. Pfeiffer, F. Reuther, M. Fink, G. Gruetzner, P. Carlberg, I. Maximov, L. Montelius, J. Seekamp, S. Zankovych, C. M. Sotomayor-Torres, H. Schulz, H. C. Scheer, *Microelectron. Eng.* **2003**, *67-8*, 266.

[66] H. C. Scheer, H. Schulz, *Microelectron. Eng.* **2001**, *56*, 311.

[67] M. Tormen, F. Romanato, M. Altissimo, L. Businaro, P. Candeloro, E. M. Di Fabrizio, *J. Vac. Sci. Technol. B* **2004**, *22*, 766.

[68] M. Bender, M. Otto, B. Hadam, B. Vratzov, B. Spangenberg, H. Kurz, *Microelectron. Eng.* **2000**, *53*, 233.

[69] W. J. Dauksher, K. J. Nordquist, D. P. Mancini, D. J. Resnick, J. H. Baker, A. E. Hooper, A. A. Talin, T. C. Bailey, A. M. Lemonds, S. V. Sreenivasan, J. G. Ekerdt, C. G. Willson, *J. Vac. Sci. Technol. B* **2002**, *20*, 2857.

[70] T. C. Bailey, D. J. Resnick, D. Mancini, K. J. Nordquist, W. J. Dauksher, E. Ainley, A. Talin, K. Gehoski, J. H. Baker, B. J. Choi, S. Johnson, M. Colburn, M. Meissl, S. V. Sreenivasan, J. G. Ekerdt, C. G. Willson, *Microelectron. Eng.* **2002**, *61-2*, 461.

[71] D. P. Mancini, K. A. Gehoski, E. Ainley, K. J. Nordquist, D. J. Resnick, T. C. Bailey, S. V. Sreenivasan, J. G. Ekerdt, C. G. Willson, *J. Vac. Sci. Technol. B* **2002**, *20*, 2896.

[72] E. K. Kim, N. A. Stacey, B. J. Smith, M. D. Dickey, S. C. Johnson, B. C. Trinque, C. G. Willson, *J. Vac. Sci. Technol. B* **2004**, *22*, 131.

[73] M. B. Chan-Park, Y. C. Lam, P. Laulia, S. C. Joshi, *Langmuir* **2005**, *21*, 2000.

[74] M. B. Chan-Park, Y. H. Yan, W. K. Neo, W. X. Zhou, J. Zhang, C. Y. Yue, *Langmuir* **2003**, *19*, 4371.

[75] G. Y. Jung, S. Ganapathiappan, D. A. A. Ohlberg, D. L. Olynick, Y. Chen, W. M. Tong, R. S. Williams, *Nano Lett.* **2004**, *4*, 1225.

[76] T. C. Bailey, S. C. Johnson, S. V. Sreenivasan, J. G. Ekerdt, C. G. Willson, D. J. Resnick, *J. Photopolym. Sci. Technol.* **2002**, *15*, 481.

[77] M. D. Stewart, S. C. Johnson, S. V. Sreenivasan, D. J. Resnick, C. G. Willson, *J. Microlith. Microfab. Microsys.* **2005**, *4*.

[78] D. J. Resnick, S. V. Sreenivasan, C. G. Willson, *Mater. Today* **2005**, *8*, 34.

[79] S. Reddy, R. T. Bonnecaze, *Microelectron. Eng.* **2005**, *82*, 60.

[80] H. C. Scheer, H. Schulz, T. Hoffmann, C. M. S. Torres, *J. Vac. Sci. Technol. B* **1998**, *16*, 3917.

[81] J. Kettle, R. T. Hoyle, S. Dimov, R. M. Perks, *Microelectron. Eng.* **2008**, *85*, 853.

[82] J. A. Ragers, R. G. Nuzzo, *Mater. Today* **2005**, 50.

[83] J. N. Lee, C. Park, G. M. Whitesides, *Anal. Chem.* **2003**, *75*, 6544.

[84] E. Delamarche, H. Schmid, B. Michel, H. Biebuyck, *Adv. Mater.* **1997**, *9*, 741.

[85] A. Bietsch, B. Michel, *J. Appl. Phys.* **2000**, *88*, 4310.

[86] C. Y. Hui, A. Jagota, Y. Y. Lin, E. J. Kramer, *Langmuir* **2002**, *18*, 1394.

[87] J. P. Rolland, R. M. Van Dam, D. A. Schorzman, S. R. Quake, J. M. DeSimone, *J. Am. Chem. Soc.* **2004**, *126*, 2322.

[88] Y. N. Xia, X. M. Zhao, G. M. Whitesides, *Microelectron. Eng.* **1996**, *32*, 255.

[89] Y. Xia, E. Kim, G. M. Whitesides, *J. Electrochem. Soc.* **1996**, *143*, 1070.

[90] A. Kumar, G. M. Whitesides, *Appl. Phys. Lett.* **1993**, *63*, 2002.

[91] A. Kumar, H. A. Biebuyck, G. M. Whitesides, *Langmuir* **1994**, *10*, 1498.

[92] Y. N. Xia, X. M. Zhao, E. Kim, G. M. Whitesides, *Chem. Mater.* **1995**, *7*, 2332.

[93] N. L. Jeon, P. G. Clem, D. A. Payne, R. G. Nuzzo, *Langmuir* **1996**, *12*, 5350.

[94] N. L. Jeon, K. Finnie, K. Branshaw, R. G. Nuzzo, *Langmuir* **1997**, *13*, 3382.

[95] N. L. Jeon, I. S. Choi, G. M. Whitesides, N. Y. Kim, P. E. Laibinis, Y. Harada, K. R. Finnie, G. S. Girolami, R. G. Nuzzo, *Appl. Phys. Lett.* **1999**, *75*, 4201.

[96] G. J. Schmitz, C. Brucker, P. Jacobs, *J. Micromech. Microeng.* **2005**, *15*, 1904.

[97] K. Kim, S. Park, J. B. Lee, H. Manohara, Y. Desta, M. Murphy, C. H. Ahn, *Microsyst. Technol.* **2002**, *9*, 5.

[98] T. W. Odom, J. C. Love, D. B. Wolfe, K. E. Paul, G. M. Whitesides, *Langmuir* **2002**, *18*, 5314.

[99] K. M. Choi, J. A. Rogers, *J. Am. Chem. Soc.* **2003**, *125*, 4060.

[100] D. G. Choi, J. H. Jeong, Y. S. Sim, E. S. Lee, W. S. Kim, B. S. Bae, *Langmuir* **2005**, *21*, 9390.

[101] B. D. Gates, Q. B. Xu, J. C. Love, D. B. Wolfe, G. M. Whitesides, *Annu. Rev. Mater. Res.* **2004**, *34*, 339.

[102] C. N. LaFratta, T. Baldacchini, R. A. Farrer, J. T. Fourkas, M. C. Teich, B. E. A. Saleh, M. J. Naughton, *J. Phys. Chem. B* **2004**, *108*, 11256.

[103] S. M. Yang, S. G. Jang, D. G. Choi, S. Kim, H. K. Yu, *Small* **2006**, *2*, 458.

[104] R. Arshady, *Colloid Polym. Sci.* **1992**, *270*, 717.

[105] R. H. Ottewill, J. N. Shaw, *Kolloid-Zeitschrift and Zeitschrift Fur Polymere* **1967**, *218*, 34.

[106] D. Z. Zou, L. Q. Sun, J. J. Aklonis, R. Salovey, *J. Polym. Sci., Part A: Polym. Chem* **1992**, *30*, 1463.

[107] W. Stober, A. Fink, E. Bohn, *J. Colloid and Interface Sci.* **1968**, *26*, 62.

[108] A. K. Van Helden, J. W. Jansen, A. Vrij, *J. Colloid Interface Sci.* **1981**, *81*, 354.

[109] Y. N. Xia, B. Gates, Y. D. Yin, Y. Lu, *Adv. Mater.* **2000**, *12*, 693.

[110] N. V. Dziomkina, G. J. Vancso, *Soft Matter* **2005**, *1*, 265.

[111] N. D. Denkov, O. D. Velev, P. A. Kralchevsky, I. B. Ivanov, H. Yoshimura, K. Nagayama, *Langmuir* **1992**, *8*, 3183.

[112] M. Trau, S. Sankaran, D. A. Saville, I. A. Aksay, *Nature* **1995**, *374*, 437.

[113] N. V. Dziomkina, M. A. Hempenius, G. J. Vancso, *Adv. Mater.* **2005**, *17*, 237.

[114] B. Gates, D. Qin, Y. N. Xia, *Adv. Mater.* **1999**, *11*, 466.

[115] J. Aizenberg, P. V. Braun, P. Wiltzius, *Phys. Rev. Lett.* **2000**, *84*, 2997.

[116] H. P. Zheng, I. Lee, M. F. Rubner, P. T. Hammond, *Adv. Mater.* **2002**, *14*, 569.

[117] Y. N. Xia, Y. D. Yin, Y. Lu, J. McLellan, *Adv. Funct. Mater.* **2003**, *13*, 907.

[118] M. Kondo, K. Shinozaki, L. Bergstrom, N. Mizutani, *Langmuir* **1995**, *11*, 394.

[119] H. H. Wickman, J. N. Korley, *Nature* **1998**, *393*, 445.

[120] R. Aveyard, J. H. Clint, D. Nees, V. N. Paunov, *Langmuir* **2000**, *16*, 1969.

[121] K. U. Fulda, B. Tieke, *Adv. Mater.* **1994**, *6*, 288.

[122] D. Y. Wang, H. Mohwald, *Adv. Mater.* **2004**, *16*, 244.

[123] H. W. Deckman, J. H. Dunsmuir, *Appl. Phys. Lett.* **1982**, *41*, 377.

[124] U. C. Fischer, H. P. Zingsheim, *J. Vac. Sci. Technol. A* **1981**, *19*, 881.

[125] J. C. Hulteen, R. P. Vanduyne, *J. Vac. Sci. Technol. A* **1995**, *13*, 1553.

[126] K. Kempa, B. Kimball, J. Rybczynski, Z. P. Huang, P. F. Wu, D. Steeves, M. Sennett, M. Giersig, D. Rao, D. L. Carnahan, D. Z. Wang, J. Y. Lao, W. Z. Li, Z. F. Ren, *Nano Lett.* **2003**, *3*, 13.

[127] X. D. Wang, C. J. Summers, Z. L. Wang, *Nano Lett.* **2004**, *4*, 423.

[128] J. G. C. Veinot, H. Yan, S. M. Smith, J. Cui, Q. L. Huang, T. J. Marks, *Nano Lett.* **2002**, *2*, 333.

[129] C. W. Kuo, J. Y. Shiu, P. L. Chen, *Chem. Mater.* **2003**, *15*, 2917.

[130] R. Michel, I. Reviakine, D. Sutherland, C. Fokas, G. Csucs, G. Danuser, N. D. Spencer, M. Textor, *Langmuir* **2002**, *18*, 8580.

[131] B. J. Y. Tan, C. H. Sow, K. Y. Lim, F. C. Cheong, G. L. Chong, A. T. S. Wee, C. K. Ong, *J. Phys. Chem. B* **2004**, *108*, 18575.

[132] J. Haisma, M. Verheijen, K. vandenHeuvel, J. vandenBerg, *J. Vac. Sci. Technol. B* **1996**, *14*, 4124.

[133] S. A. Johnson, P. J. Ollivier, T. E. Mallouk, *Science* **1999**, *283*, 963.

[134] N. J. Trujillo, S. H. Baxamusa, K. K. Gleason, *Chem. Mater.* **2009**, *21*, 742.

[135] A. Kosiorek, W. Kandulski, H. Glaczynska, M. Giersig, *Small* **2005**, *1*, 439.

[136] C. Haginoya, M. Ishibashi, K. Koike, *Appl. Phys. Lett.* **1997**, *71*, 2934.

[137] D. G. Choi, H. K. Yu, S. G. Jang, S. M. Yang, *J. Am. Chem. Soc.* **2004**, *126*, 7019.

[138] I. Manners, *Synthetic metal-containing polymers*, New York, **2004**.

[139] R. Rulkens, Y. Z. Ni, I. Manners, *J. Am. Chem. Soc.* **1994**, *116*, 12121.

[140] Y. Z. Ni, R. Rulkens, J. K. Pudelski, I. Manners, *Macromol. Rapid Commun.* **1995**, *16*, 637.

[141] P. GomezElipe, P. M. Macdonald, I. Manners, *Angew. Chem. Int. Ed.* **1997**, *36*, 762.

[142] J. Rasburn, R. Petersen, T. Jahr, R. Rulkens, I. Manners, G. J. Vancso, *Chem. Mater.* **1995**, *7*, 871.

[143] D. A. Foucher, R. Ziembinski, B. Z. Tang, P. M. Macdonald, J. Massey, C. R. Jaeger, G. J. Vancso, I. Manners, *Macromolecules* **1993**, *26*, 2878.

[144] D. Foucher, R. Ziembinski, R. Petersen, J. Pudelski, M. Edwards, Y. Z. Ni, J. Massey, C. R. Jaeger, G. J. Vancso, I. Manners, *Macromolecules* **1994**, *27*, 3992.

[145] K. Kulbaba, I. Manners, *Macromol. Rapid Commun.* **2001**, *22*, 711.

[146] J. Q. Lu, T. E. Kopley, N. Moll, D. Roitman, D. Chamberlin, Q. Fu, J. Liu, T. P. Russell, D. A. Rider, I. Manners, M. A. Winnik, *Chem. Mater.* **2005**, *17*, 2227.

[147] A. C. Arsenault, H. Miguez, V. Kitaev, G. A. Ozin, I. Manners, *Adv. Mater.* **2003**, *15*, 503.

[148] I. Korczagin, R. G. H. Lammertink, M. A. Hempenius, S. Golze, G. J. Vancso, *Adv. Polym. Sci.* **2006**, *200*, 91.

[149] I. Korczagin, S. Golze, M. A. Hempenius, G. J. Vancso, *Chem. Mater.* **2003**, *15*, 3663.

[150] J. Y. Cheng, C. A. Ross, V. Z. H. Chan, E. L. Thomas, R. G. H. Lammertink, G. J. Vancso, *Adv. Mater.* **2001**, *13*, 1174.

[151] R. G. H. Lammertink, M. A. Hempenius, V. Z. H. Chan, E. L. Thomas, G. J. Vancso, *Chem. Mater*. **2001**, *13*, 429.

[152] I. Korczagin, H. Xu, M. A. Hempenius, G. J. Vancso, *Eur. Polym. J.* **2008**, *44*, 2523.

[153] M. Roerdink, J. Pragt, I. Korczagin, M. A. Hempenius, T. Stockli, Y. Keles, H. F. Knapp, C. Hinderling, G. J. Vancso, *J. Nanosci. Nanotechnol.* **2007**, *7*, 1052.

[154] M. Roerdink, M. A. Hempenius, U. Gunst, H. F. Arlinghaus, G. J. Vancso, *Small* **2007**, *3*, 1415.

[155] V. P. Chuang, J. Y. Cheng, T. A. Savas, C. A. Ross, *Nano Lett.* **2006**, *6*, 2332.

[156] J. Y. Cheng, C. A. Ross, H. I. Smith, E. L. Thomas, *Adv. Mater.* **2006**, *18*, 2505.

[157] J. Y. Cheng, F. Zhang, V. P. Chuang, A. M. Mayes, C. A. Ross, *Nano Lett.* **2006**, *6*, 2099.

Chapter 3

3D Ordered Nanostructures Fabricated by Nanosphere Lithography Using an Organometallic Etch Mask

ABSTRACT. In this chapter a new approach for fabricating porous structures on silicon substrates is demonstrated by using colloidal particle arrays with a polymer mask of a highly etch-resistant organometallic polymer. Monolayers of silica particles, with diameters of 60 nm, 150 nm, 300 nm, and 1 μm, were formed on a silicon substrate and the voids of the arrays were filled with poly(ferrocenylmethylphenylsilane) (PFMPS). Argon ion sputtering removed the excess PFMPS on the particles which enabled removal of the particles with HF. Further pattern transfer steps with reactive ion etching for different time intervals provided structures in silicon. The resulting pores obtained after etching on silicon substrates were used as molds for nanoimprint lithography (NIL). The combination of the techniques of nanosphere lithography (NSL) and NIL resulted in 3D nanostructures with a hemispherical shape (inherited from the nanoparticles) which were obtained both in silicon and in PMMA

This work has been submitted to Nanoscale by C.Acikgoz, X. Y. Ling, I. Y. Phang, M. A. Hempenius, D. N. Reinhoudt, G. J. Vancso, and J. Huskens.

3.1 INTRODUCTION

Nanotechnology requires approaches to control the structure of matter down to the nm length scale for the fabrication of the future generations of optical, electronic and biological devices.[1] In particular, nanofabrication opens the door for the increasing demand of miniaturization owing to its ability to design and manufacture structures at the nanometer length scale.

Conventional lithographies, *e.g.* photolithography, e-beam lithography, X-ray lithography, and ion-beam lithography, although suitable for the fabrication of nanometer-sized structures, are often expensive with high capital and running costs.[2] As a result, alternative and unconventional techniques, *e.g.* soft lithography, nanoimprint lithography, scanning probe lithography and self-assembly have been developed in recent years to fulfill the needs for cheap and user-friendly fabrication techniques and in particular for use in research environments where rapid prototyping and versatility are crucial. Microcontact printing[3] has been demonstrated to produce self-assembled structures with high yield. However, because of the elastomeric properties of the PDMS stamp, it is difficult to fabricate structures with sub-micron dimensions.[3] Nanoimprint lithography, pioneered by Chou *et al.* has emerged as a good candidate for the fabrication of structures with nanometer scale dimensions.[4, 5] By applying a prefabricated master (or mold) onto a thin film of polymer above the glass transition temperature and at high pressure, structures are replicated by flow of the polymer into the mold features. For nanostructures, the fabrication of the mold is usually the bottleneck of this technique.

Nanosphere lithography (NSL) employs self-assembled single or double layers of particles as lithographic masks or templates to produce nanosized features of polymers and metals in a low cost and simple manner.[6-8] Complex equipment is not required to create patterns on the nanometer scale and the assembly of the particles is achieved readily by spin-coating or dip-coating. In most examples of NSL, particles are assembled into arrays in order to serve as templates, the voids of which are infiltrated by a material that solidifies therein. To fill the voids, a range of materials can be used using various routes such as chemical vapor deposition, liquid-phase reactions, deposition of small particles and sol-gel chemistry. [9-11] Long-range periodic structures such as honeycomb lattices,[12] hexagonally packed nanoparticle arrays and nano-triangles[13] have been obtained on diverse substrates such as graphite and diamond,[14] and polymers[15] after subsequent removal of the particles. Various ordered 1D nanostructure arrays, consisting of carbon nanotubes,[16] ZnO nanorods[17] and Si nanorods[18] have been produced by using nanoparticle arrays as the template. The use of

such nanoparticle arrays as masks for silicon etching has resulted in silicon pillars which are important for semiconductor technology.[19]

Spherical colloidal particles can be utilized also for preparing various types of porous materials that exhibit precisely controlled pore sizes and highly ordered 3D porous structures. After drying the colloidal array, the void spaces among the colloidal spheres are fully infiltrated with a liquid precursor such as an ultraviolet (UV)[20] or thermally curable organic prepolymer,[21] or an ordinary organic monomer (plus an initiator).[22] Poly(ferrocenylsilanes) (PFS)[23, 24] owe many of their useful and unique characteristics to the presence of ferrocene and silane units in the main chain which, upon exposure to oxygen plasma, lead to the formation of a silicon/iron oxide layer at the surface since inorganic components are converted into nonvolatile oxides which are inert to further etching.[25, 26] In this chapter, we show a simple and versatile approach to pattern silicon substrates by using NSL-prepared patterned PFMPS layers as an etch mask. The fabrication of 3D patterns into a silicon substrate with controlled shape is accomplished owing to the etch resistivity of PFMPS. The size of the pores is tuned by varying the etching time. Large-scale periodic structures with hemispherical shape are fabricated and these are used as a mold for NIL to imprint PMMA.

3.2 RESULTS & DISCUSSION

3.2.1 Assembly of Particles on Silicon Surfaces

The assembly of particles on a silicon substrate was achieved by convective self assembly.[27] Convective assembly has been defined as the mechanism of assembly of colloidal particle suspensions in thin evaporating films: the flow of water caused by solvent evaporation leads the particles to assemble onto a substrate in an ordered way. Figure 3.1 illustrates the experimental setup used for the particle assembly. A droplet of 0.2 wt % of particle suspension was added into the gap between a mobile substrate and a fixed glass slide while the temperature was controlled between 4 - 20℃. The substrate was then shifted to the left at a constant velocity (0.1 – 1 μm/s).[28] As seen in Figure 3.1, the substrates were considered into two zones, the assembly and bulk suspension zones. In the assembly zone, the particles assemble as a result of convective flow of particles induced by the evaporation of solvent. Between the glass slide and the substrate is the suspension zone (B). Convective flow allows the particles move from the suspension zone to the assembly zone. Using convective assembly, it is possible to generate large scale, highly ordered particle films on a substrate.

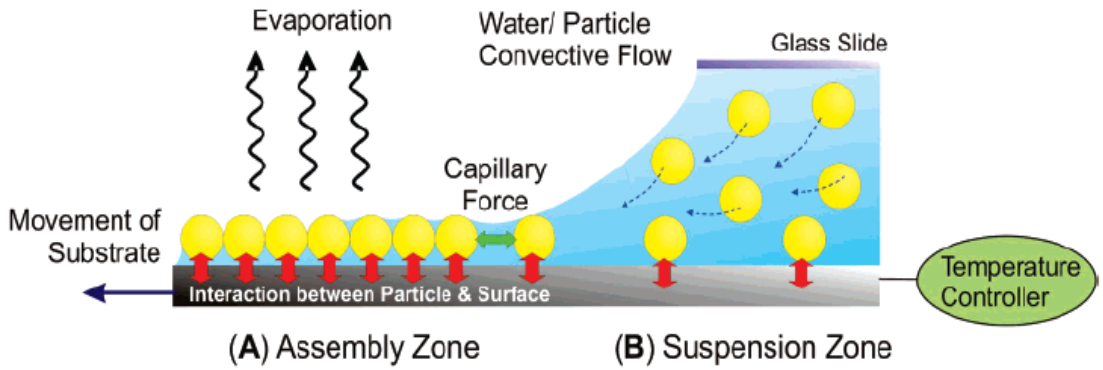

Figure 3.1 Schematic illustration of the assembly of particles on a substrate.[28]

3.2.2 Fabrication of Nanostructures

Figure 3.2 describes the fabrication procedure that is used to prepare 3D hemispherical nanostructures on a silicon substrate. Assembly of a particle array on a silicon substrate is followed by spin-coating of PFMPS, and by argon sputtering to open the surface of the nanoparticle array. The particles are etched away by aqueous HF before the sample is exposed to plasma etching into the underlying Si substrate and to nitric acid to remove the oxidized PFMPS. To fabricate a positive replica of the nanoparticle array into a polymer layer, the fabricated structure was used as a mold for NIL.

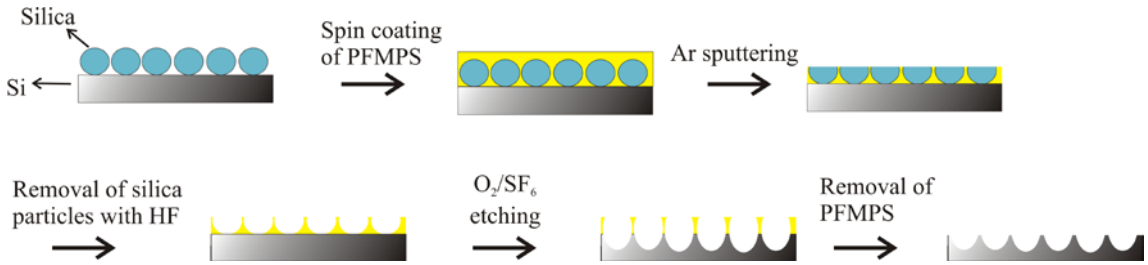

Figure 3.2 Fabrication scheme for patterned silicon substrates by the convective assembly of nanoparticles onto a substrate followed by spin coating of PFMPS, followed by etch steps for transferring the patterns into the Si substrate.

The initial nanoparticle array assembled from 300-nm SiO_2 nanoparticles was imaged by SEM and AFM. As shown in Figure 3.3 (A-C), the array is highly hexagonally close-packed (hcp), with occasional domain boundaries observed, which is common for a convectively assembled nanoparticle crystals.[29] The height profile of the array, as determined by atomic force microscopy (AFM), indicates that the array is uniform in curvature, as a result of the spherical nature of the particles.

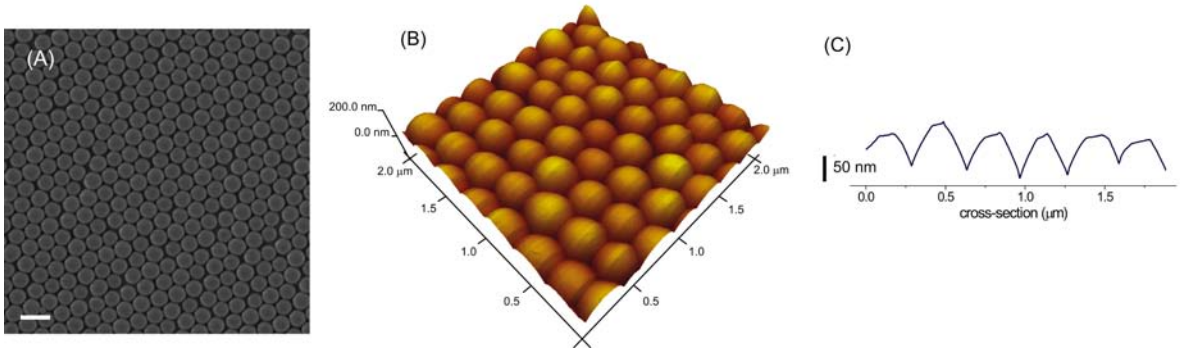

Figure 3.3 SEM (A) and AFM (B) images and AFM height profile (C) of a 300-nm particle array. The scale bar is 500 nm.

The spin-coating of PFMPS resulted in complete coverage of the nanoparticle array, with an excess layer of PFMPS formed on top of the array. Argon sputtering was applied to etch away the excess of PFMPS,[30] exposing the top surface of the nanoparticles (Figure 3.4 A-C). The 3D view of the surface showed that the particles remained in hcp-order and were interconnected by PFMPS. At this point, due to the infiltration of PFMPS, the roughness of the array had been diminished (Figure 3.4C), however, the array still maintained some degree of curvature.

The silica nanoparticles were etched by aqueous HF, leaving a porous PFMPS layer on the surface, which resembles a negative replica of the nanoparticle array (Figure 3.4D-F). High-resolution SEM (inset of Figure 3.4D) revealed that the spherical porous PFMPS mask layer exhibits a bowl-like shape with the top side open. The porous PFMPS mask layer is interconnected in the array, with a height of approximately 200 nm. The height profile reveals that the PFMPS mask layer separates the pores with a PFMPS wall of at least 60 nm wide.

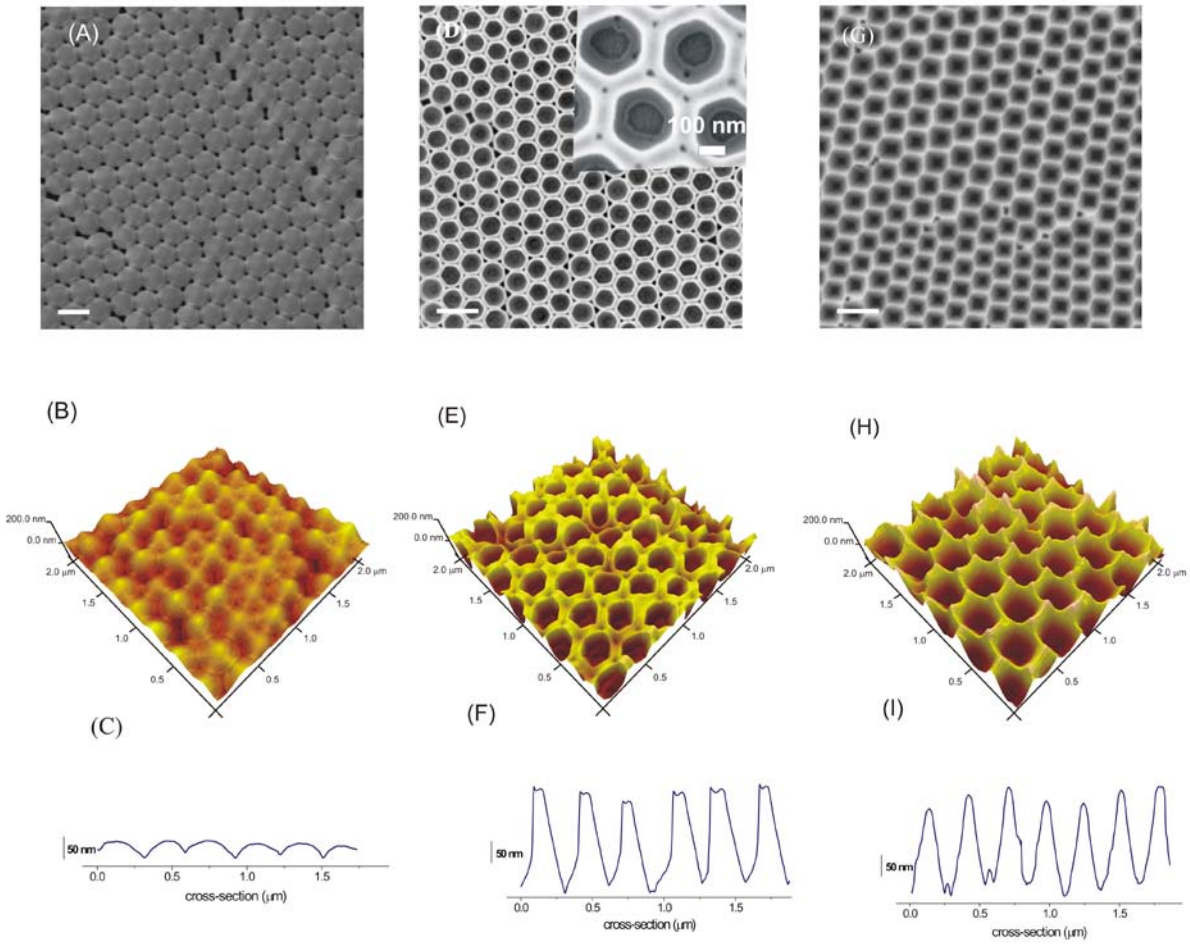

Figure 3.4 SEM and AFM images and AFM height profiles of samples made from a preformed particle array followed by spin-coating of PFMPS and argon sputtering (A-C), HF etching (D-F) and RIE and HNO_3 wet-etching (G-I). The scale bars indicate 500 nm.

PFMPS, owing to the presence of ferrocene and silicon, is known to be highly resistant to reactive ion etching (RIE).[26] While exposing the nanoparticle array infiltrated with PFMPS to a mixture of O_2 and SF_6 in RIE, the silicon underneath the PFMPS was protected from the RIE, whereas the unprotected areas were etched vertically into the silicon substrate (Figure 3.2). The substrate was subsequently sonicated in toluene and nitric acid, to remove the remaining oxidized PFMPS. A silicon substrate patterned with submicron sized and hcp ordered hexagonally shaped pores (Figure 3.4G-I) was obtained without the use of lithographic techniques. The pore size was slightly enlarged to ~300 nm and a thinner wall was observed as compared to Figure 3.4D after etching into the silicon substrate which is attributed to isotropic RIE. The effect of RIE was also observed in the pore shape which was changed slightly from spherical to hexagonal.

An advantage of this method is the ability to control the size of the pores and their periodicity by varying the size of the particles. In Figure 3.5, examples of the patterns fabricated with particle sizes of 60 nm, 300 nm and 500 nm are shown. For the particles of 500 nm (Figure 3.5C), the patterns fabricated in a substrate have a spherical shape rather than hexagonal. When particles of 60 nm were used, the hole patterns were not well ordered as seen in Figure 3.5A. This is attributed to the larger size distribution of the smaller particles.

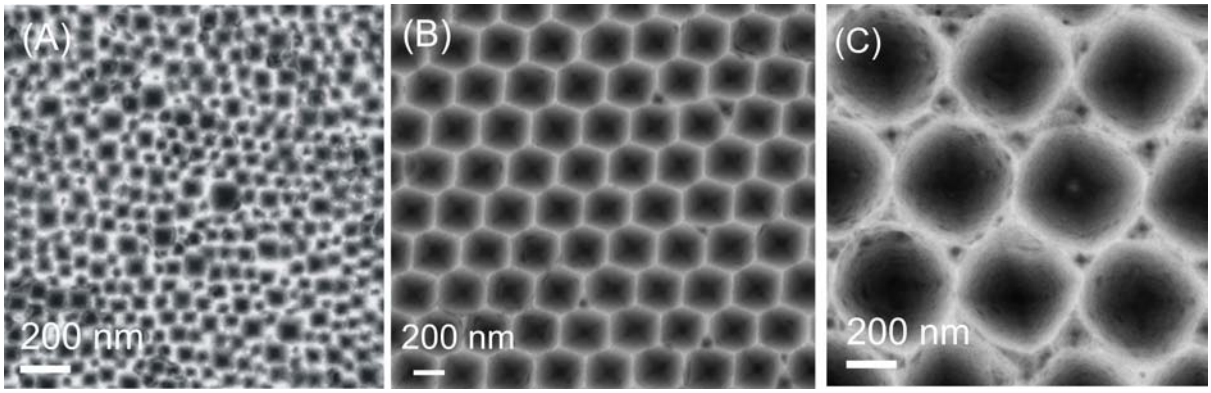

Figure 3.5 Nanosize-patterned silicon substrates prepared by using (A) 60-nm nanoparticles and (B) 300-nm particles and (C) 500-nm particles.

Alternatively, the pore size can be controlled by the RIE etch time used for creating the holes in the Si substrate. Figure 3.6 shows the change in the pattern shape fabricated in a silicon substrate as a function of the etching time using 300 nm particles. By increasing the etching time, the shape of patterns formed in the silicon substrate changed from spherical (Figure 3.6A and B) to hexagonal (Figure 3.6C) due to the underetching of silicon underneath of PFMPS. Figure 3.6D shows the relationship between the hole size and the RIE time, which indicates that the size of the pores can be easily controlled by changing the etching time. The depth of the pores after 1 min of RIE etching was ~ 200 nm.

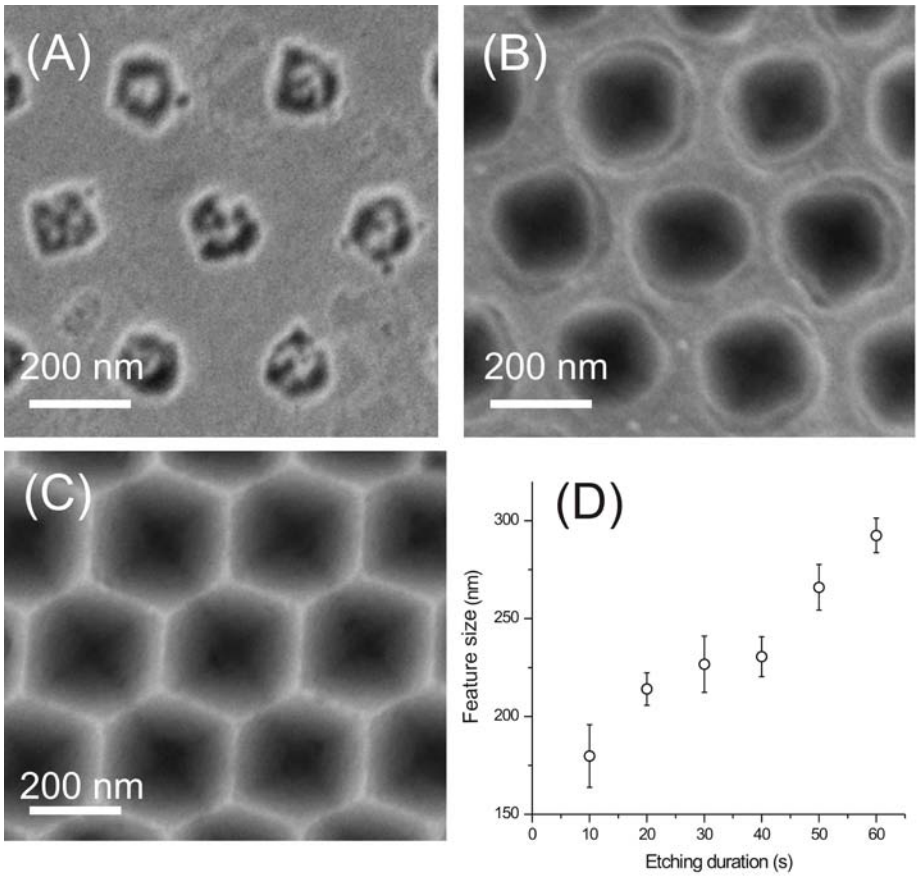

Figure 3.6 SEM images of the features obtained in silicon substrates after etching with SF_6 and O_2 at etching time of (A) 10 s, (B) 30 s, and (C) 60 s. Scale bars indicate 200 nm. (D) The plot of the feature size with respect to variable O_2/SF_6 RIE etching duration.

The patterned silicon substrates were used as molds for nanoimprint lithography (NIL). The mold was first covered with a monolayer of 1*H*,1*H*,2*H*,2*H*-perfluorodecyltriethoxysilane (PFDTS) prior to NIL. The silicon master was pressed against a silicon substrate spin-coated with poly(methyl methacrylate) (PMMA) to yield 3D hemispherical polymer features of ~ 300 nm in size and 200 nm in height (Figure 3.7), which is the positive replica of the original 300-nm nanoparticle array used to fabricate the mold (Figure 3.2). The 3D AFM image (Figure 3.7B) shows that the patterns obtained in PMMA possess a curvature. Such patterns are hard to obtain with commercially available molds. SEM images in Figure 3.7D and E show imprints in PMMA with the masters fabricated using the silica particles with 60 nm, and 500 nm diameter, respectively.

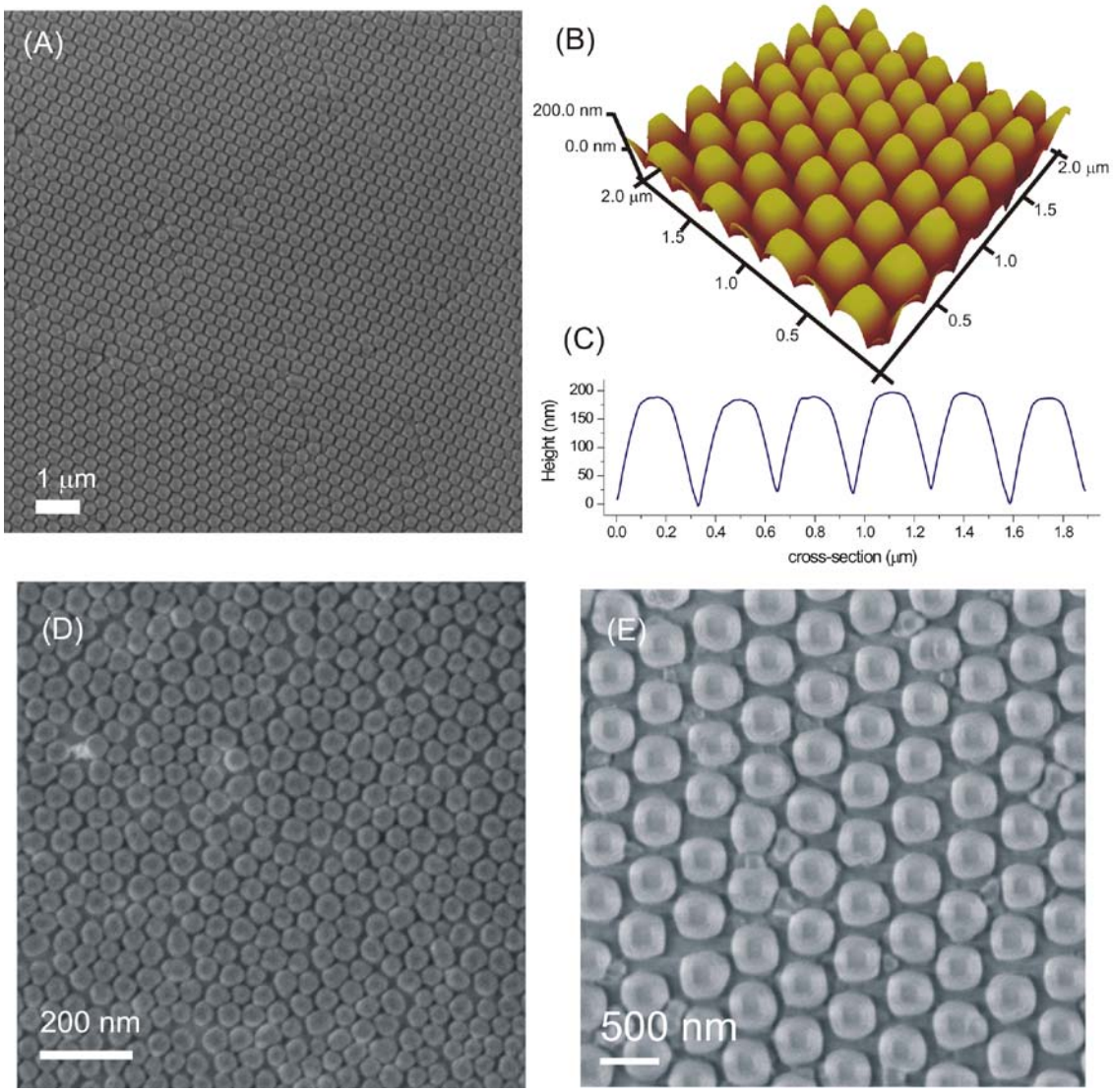

Figure 3.7 SEM (A) and AFM image (B) and height profile (C) of the PMMA nanostructure replicated from the patterned silicon masters fabricated from the 300-nm particles after 1 min of RIE with SF_6/O_2. SEM images of PMMA nanostructures replicated from the patterned silicon masters fabricated using 60 nm (D) and 500 nm (E) particles.

RIE time is very important to obtain patterns with desired shape and height. SEM images in Figure 3.8 show the imprinted structures using molds fabricated from 300-nm particles and etched with SF_6/O_2 plasma for 10, 30 and 60 s. respectively. Figure 3.8D shows the variation in pattern height with the molds employed. Patterns with different height and shapes were replicated depending on the mold used. The silicon substrate etched for 10 s with SF_6 and O_2 showed a pore size of ~170 nm, and the replicated PMMA structures had nearly the same pattern size (Figure 3.8A). Hexagonal patterns in PMMA obtained by using the

mold etched for 1 min (Figure 3.8C) and the height of the PMMA patterns obtained was ~200 nm (Figure 3.8D).

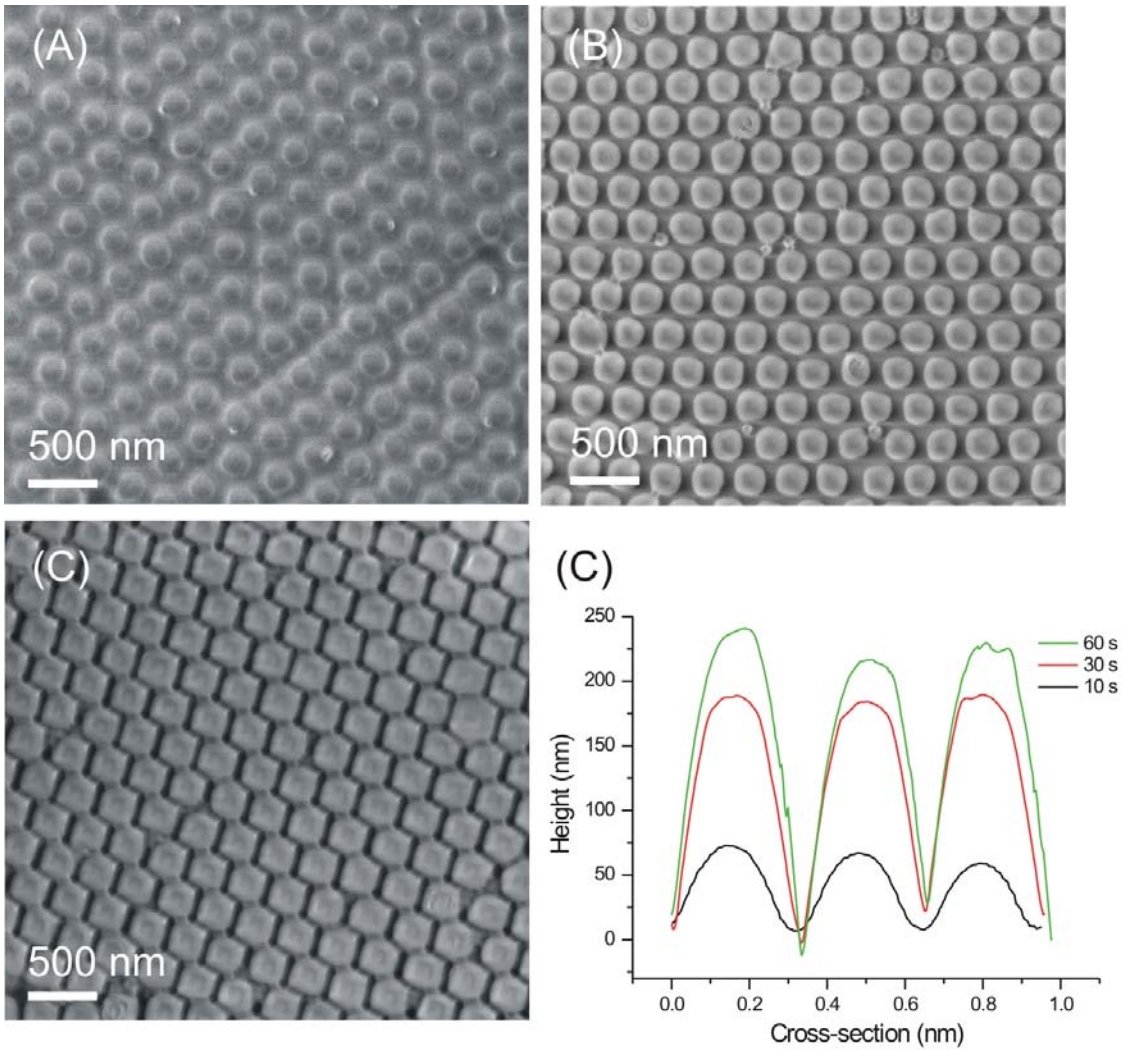

Figure 3.8 Patterns imprinted in PMMA using the molds fabricated with 300 nm silica particles etched with SF_6/O_2 plasma for 10 s (A), 30 s (B) and 60 s. (C). AFM height profiles (D) of the imprinted PMMA structures as a function of RIE time.

3.3 CONCLUSIONS

Pores in silicon substrates with submicron sizes and hcp order were fabricated by nanosphere lithography. Silica nanoparticles of different sizes were used as starting materials and PFMPS as an etch-resistant polymer to produce a negative replica of the nanoparticle array. The patterned silicon substrate was subsequently used as a master to replicate the nanoparticle array by using NIL. By using this method, the size of the pores in silicon substrate can be easily controlled by changing the size of the particles. It is also shown that

the size and shape of the pores can be controlled by changing the etching time. Our approach opens a promising technique to fabricate structures into substrates such as Si, glass as well as into polymers with low cost. These kinds of structures can be used for in the fabrication of micro-optical elements, such as microlenses and microlens arrays.

3.4 EXPERIMENTAL

Silica nanoparticles were purchased from Polysciences Inc. (diameter = 500 nm, 300 nm, 150 nm, standard deviation <10%) as an aqueous suspension, particles of 60 nm were synthesized following a literature procedure.[31] 1*H*,1*H*,2*H*,2*H*-perfluorodecyltriethoxysilane (PFDTS, ABCR) and poly(methyl methacrylate) (PMMA, Mw ~ 35,000, Acros) were used as received.

3.4.1 Polymer synthesis and characterization [1]Methylphenylsilaferrocenophane was prepared as described before.[23, 32] The monomer was purified by several crystallizations from *n*-heptane at –70 °C followed by vacuum sublimation. Transition metal-catalyzed ring-opening polymerization of [1]methylphenylsilaferrocenophane was carried out in the presence of Et_3SiH with the addition of Karstedt's catalyst. The poly(ferrocenylmethylphenylsilane) (PFMPS) was then precipitated in *n*-heptane. The weight average and number average molar masses M_w and M_n of the polymer were determined by gel permeation chromatography (GPC) measurements in THF, using polystyrene calibration, $M_w = 5.5 \times 10^4$ g/mol, $M_n = 5.1 \times 10^4$ g/mol, $M_w/M_n = 1.09$.

3.4.2 Substrate preparation. Silicon substrates were cleaned by immersion in piranha solution (conc. H_2SO_4 and 33% aq H_2O_2 in a 3:1 volume ratio, ***Warning!*** *piranha should be handled with caution; it can detonate unexpectedly*) for 15 min to form a SiO_2 layer on the surface. The substrates were then sonicated in Milli-Q water and ethanol for 1 min, and dried with N_2. A monolayer of silica particles on the silicon substrate was prepared by vertical capillary assisted deposition at a withdrawal speed of 0.5 μm/s.[28] A layer of 80 nm of PFMPS was spin-coated onto the particle layer from a 2 wt % PFMPS solution in toluene. The top layer of PFMPS was etched away by argon plasma sputtering for 25 min (Ion Beam Etcher, 350 V, 6 mA) resulting in exposure of the top of the silica particle arrays. The silica particles were removed by dipping the substrate into a 10 wt% aqueous hydrogen fluoride (HF) solution for 12 h, followed by rinsing with Milli-Q water and drying with N_2. *(**Warning!** HF solution should be handled with caution; it can cause serious health problems).* Reactive ion etching (RIE) experiments were performed in a reactive ion etching

setup, carried out in an Elektrotech PF 340 apparatus (10 mTorr, 20 sccm O_2 and 40 sccm SF_6, 50W). Substrates were dipped in 10 wt% aqueous nitric acid solution to remove oxidized (PFMPS) from the substrate. Subsequently, an anti-sticking layer of PFDTS was applied.

3.4.3 Nanoimprint Lithography. A piranha-cleaned silicon substrate was first spin-coated with a 500 nm thick layer of poly(methyl methacrylate) (PMMA). Stamp and substrate were put in contact and a pressure of 20 bar was applied at a temperature of 200 ºC using a hydraulic press (Specac).

All SEM images were taken with a HR-LEO 1550 FEF SEM. The samples were not coated with a conducting layer. AFM measurements were carried out with a Dimension D3100 using a NanoScope IVa controller equipped with a hybrid 153 scanner (Veeco/Digital Instruments (DI), Santa Barbara, CA) under ambient conditions. Silicon cantilevers from Nanosensors (Nanosensors, Wetzlar, Germany) were used for intermittent contact (tapping) mode operation.

3.5 ACKNOWLEDGMENTS

We thank Mark Smithers for acquiring the SEM images.

3.6 REFERENCES

[1] C. P. Poole, F. J. Owens, *Introduction to Nanotechnology*, Wiley, New Jersey, **2003**.

[2] B. D. Gates, Q. B. Xu, M. Stewart, D. Ryan, C. G. Willson, G. M. Whitesides, *Chem. Rev.* **2005**, *105*, 1171.

[3] Y. N. Xia, G. M. Whitesides, *Ann. Rev. Mater. Sci.* **1998**, *28*, 153.

[4] S. Y. Chou, P. R. Krauss, P. J. Renstrom, *Appl. Phys. Lett.* **1995**, *67*, 3114.

[5] M. D. Austin, H. X. Ge, W. Wu, M. T. Li, Z. N. Yu, D. Wasserman, S. A. Lyon, S. Y. Chou, *Appl. Phys. Lett.* **2004**, *84*, 5299.

[6] P. Jiang, J. F. Bertone, V. L. Colvin, *Science* **2001**, *291*, 453.

[7] X. Chen, Z. M. Chen, N. Fu, G. Lu, B. Yang, *Adv. Mater.* **2003**, *15*, 1413.

[8] U. C. Fischer, H. P. Zingsheim, *J. Vac. Sci. Technol.* **1981**, *19*, 881.

[9] B. T. Holland, C. F. Blanford, A. Stein, *Science* **1998**, *281*, 538.

[10] J. S. Yin, Z. L. Wang, *Adv. Mater.* **1999**, *11*, 469.

[11] P. Jiang, J. Cizeron, J. F. Bertone, V. L. Colvin, *J. Am. Chem. Soc.* **1999**, *121*, 7957.

[12] S. B. Han, A. L. Briseno, X. Y. Shi, D. A. Mah, F. M. Zhou, *J. Phys. Chem. B* **2002**, *106*, 6465.

[13] C. L. Haynes, R. P. Van Duyne, *J. Phys. Chem. B* **2001**, *105*, 5599.

[14] A. A. Zakhidov, R. H. Baughman, Z. Iqbal, C. X. Cui, I. Khayrullin, S. O. Dantas, I. Marti, V. G. Ralchenko, *Science* **1998**, *282*, 897.

[15] A. Valsesia, P. Colpo, M. M. Silvan, T. Meziani, G. Ceccone, F. Rossi, *Nano Lett.* **2004**, *4*, 1047.

[16] M. Olek, J. Ostrander, S. Jurga, H. Mohwald, N. Kotov, K. Kempa, M. Giersig, *Nano Lett.* **2004**, *4*, 1889.

[17] J. Rybczynski, D. Banerjee, A. Kosiorek, M. Giersig, Z. F. Ren, *Nano Lett.* **2004**, *4*, 2037.

[18] B. Fuhrmann, H. S. Leipner, H. R. Hoche, L. Schubert, P. Werner, U. Gosele, *Nano Lett.* **2005**, *5*, 2524.

[19] A. Sinitskii, S. Neumeier, J. Nelles, M. Fischler, U. Simon, *Nanotechnology* **2007**, *18*, 305307.

[20] S. H. Park, Y. N. Xia, *Adv. Mater.* **1998**, *10*, 1045.

[21] B. Gates, Y. D. Yin, Y. N. Xia, *Chem. Mater.* **1999**, *11*, 2827.

[22] S. A. Johnson, P. J. Ollivier, T. E. Mallouk, *Science* **1999**, *283*, 963.

[23] R. Rulkens, A. J. Lough, I. Manners, *J. Am. Chem. Soc.* **1994**, *116*, 797.

[24] D. Foucher, R. Ziembinski, R. Petersen, J. Pudelski, M. Edwards, Y. Z. Ni, J. Massey, C. R. Jaeger, G. J. Vancso, I. Manners, *Macromolecules* **1994**, *27*, 3992.

[25] R. G. H. Lammertink, M. A. Hempenius, J. E. van den Enk, V. Z. H. Chan, E. L. Thomas, G. J. Vancso, *Adv. Mater.* **2000**, *12*, 98.

[26] R. G. H. Lammertink, M. A. Hempenius, V. Z. H. Chan, E. L. Thomas, G. J. Vancso, *Chem. Mater.* **2001**, *13*, 429.

[27] Z. Yuan, D. B. Burckel, P. Atanassov, H. Y. Fan, *J. Mater. Chem.* **2006**, *16*, 4637.

[28] X. Y. Ling, L. Malaquin, D. N. Reinhoudt, H. Wolf, J. Huskens, *Langmuir* **2007**, *23*, 9990.

[29] Y. N. Xia, B. Gates, Y. D. Yin, Y. Lu, *Adv. Mater.* **2000**, *12*, 693.

[30] C. Acikgoz, M. A. Hempenius, G. J. Vancso, J. Huskens, *Nanotechnology* **2009**, *20*, 135304.

[31] X. Y. Ling, D. N. Reinhoudt, J. Huskens, *Langmuir* **2006**, *22*, 8777.

[32] P. Gomez-Elipe, R. Resendes, P. M. Macdonald, I. Manners, *J. Am. Chem. Soc.* **1998**, *120*, 8348.

Chapter 4

Fabrication of Free-standing Nanoporous Polyethersulfone Membranes by Organometallic Polymer Resists Patterned by Nanosphere Lithography

ABSTRACT. A novel method for fabricating free-standing, nanoporous polymer membranes by using colloidal silica particle arrays to obtain patterned poly(ferrocenylsilane) as an etch resist layer for subsequent reactive ion etching (RIE) is reported. The fabrication process starts by spin-coating of a sacrificial cellulose acetate (CA) layer on a silicon wafer followed by spin-coating of polyethersulfone (PES). Silica particles were coated onto the PES layer. RIE resistant poly(ferrocenylmethylphenylsilane) (PFMPS) was used from solution to fill the pores among the tightly packed silica particles. PFMPS acts as an etch resist, and when patterned, it functions as a mask on top of the PES layer to protect it from RIE. During pattern transfer of the silica spheres to the PES, the top layer of PFMPS was removed first exposing unprotected silica spheres. Following removal of the spheres by HF, a negative (hollow) pattern of the colloidal particles was formed in the PFMPS layer resulting in a lateral variation of the thickness of the etch resist. In RIE, the PES film was perforated in unprotected areas corresponding to transfer of the projection pattern of the silica spheres. Subsequent removal of PFMPS in nitric acid resulted in highly uniform, well ordered pores in PES. The preparation of free-standing PES films was completed by dissolving the sacrificial layer CA layer and floating off the free-standing membranes. The PES membranes exhibiting dense, highly ordered pores can serve as a platform for size-selective filtration considering the highly uniform pore size as it was demonstrated by a feasibility filtration experiment using model silica spheres.

This chapter has been published in C. Acikgoz, X. Y. Ling, I. Y. Phang, M. A. Hempenius, D. N. Reinhoudt, J. Huskens and G. J. Vancso, Fabrication of free-standing nanoporous polyethersulfone membranes by organometallic polymer resists patterned by nanosphere lithography, *Adv. Mater*. **2009**, *21*, 2064-2067.

4.1 INTRODUCTION

Membranes are used in many fields such as pharmaceutical, biotechnological and food industries for removal of particles or bacteria, as well as for waste water purification.[1-3] Even though membranes manufactured from silicon, ceramic, or other inorganic materials are gaining importance, the majority of membranes are made of polymers.[4] There are several methods to fabricate membranes, such as track-etching of polymer films[5] or electrochemical etching to form alumina membranes.[6] Alumina membranes have a relatively limited range of pore diameters.[7] Track-etching involves the use of high-energy particles obtained e.g. from a cyclotron, to produce tracks in polymer films that can subsequently be etched to form a pore. The track-etch membranes are commercially available in a variety of pore sizes, but they have low porosities and the pores are randomly distributed.

Alternative approaches for membrane fabrication with controlled pore sizes have recently emerged, employing for instance nanostructures in polymer matrices to produce nanoporous membranes.[8] Block copolymers[9-10] or imprint lithography[11] have also been used to form large arrays of small, cylindrical pores in polymer films. Even though many methods have been developed, the fabrication of porous membranes that have well defined structures and controlled pore sizes is still a challenge. In addition to pore size control, there is a strong recent interest in creating membranes with high surface pore densities to achieve high transport rates.[12-13]

In this chapter, we report on a new method to fabricate free-standing porous polymer membranes using "nanosphere lithography" (NSL)[14-16] with colloidal silica, as a technique which allows the formation of highly ordered, well defined pore size membranes using poly(ferrocenylmethylphenylsilane)[17] (PFMPS) as the etch resist. The versatility of the method is demonstrated by the fabrication of free-standing polymer membranes, obtained by employing cellulose acetate (CA) as a sacrificial layer.

At the heart of our approach is the preparation of a patterned poly(ferrocenylsilane) (PFS) film which exhibits a thickness variation in a given pattern. PFSs consist of polymer main chains featuring ferrocene in their backbone, which renders this organometallic polymer highly useful for applications in optics, semiconductors, nanopatterned catalysis for carbon nanotube growth, electrochemically responsive substrates or media, etc.[18-24] One of the unique applications is their use as resists in "maskless" lithography due to the presence of Fe and Si in the backbone which makes PFSs highly etch resistant in RIE environments in comparison with organic polymers.[25-30] Areas of a substrate covered by PFS are protected against RIE while exposed domains can be etched into substrates such as Si, Si_3Ni_4 and glass.

PFS patterns have been used with success in MIMIC, temperature and solvent assisted lithography and block copolymer lithography (featuring organic-organometallic block copolymers).[31] In this study we used asymmetrically substituted (amorphous) PFMPS to prevent undesired polymer crystallization which could destroy the etch mask.

4.2 RESULTS & DISCUSSION

We followed a multilayer fabrication strategy (Figure 4.1) with the aim of preparing porous polyethersulfone (PES) on silica wafer substrates. PES, a commercially available polymer, is a widely used membrane material. It possesses a high thermal stability, high toughness and an excellent resistance to acids, bases, and to a variety of solvents such as alcohols and aliphatic hydrocarbons.[32] The fabrication process starts by spin-coating a sacrificial CA layer on a silicon substrate followed by spin coating of PES. This was followed by the assembly of silica particles by the convective self-assembly method. The method of convective assembly has been defined as the mechanism of self-assembly of colloidal particle suspensions in thin evaporating films as described in Chapter 3. [33] PFMPS was spin-coated on top of the silica particle layer to fill the pores between the particles, in order to create the etch mask. In contrast to regular NSL, in our case the silica particles are not used as an etch mask, but rather as an inversion mask.

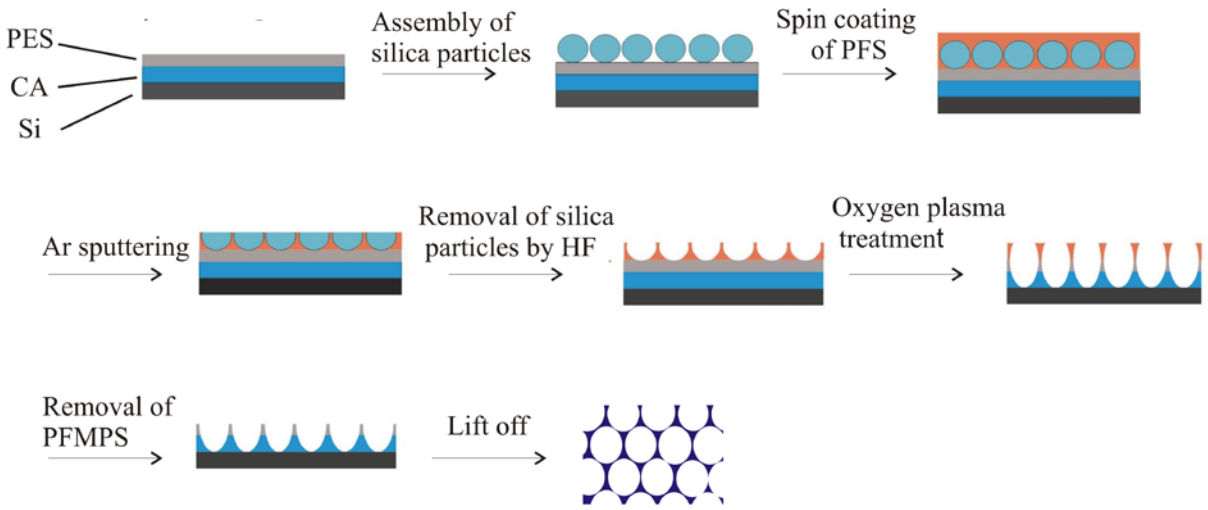

Figure 4.1 Fabrication of free-standing PES membranes.

First we present and discuss the patterns obtained during the fabrication process shown in Figure 4.1. Figure 4.2a displays an Atomic Force Microscopy (AFM) image of the silica colloidal particle array (particle diameter 300 nm), which was ordered in a close-packed arrangement and Figure 4.2d depicts the corresponding three dimensional AFM image. The spin-coated PFMPS inherited the structure of the array (Figure 4.2b) and a three dimensional (3D) AFM image (Figure 4.2e) shows tightly packed silica particles with smooth surfaces. The height of the particle array was about 60 nm as seen in Figure 4.2g. After infiltration with an 80 nm PFMPS layer, the height variation on top of the particle array decreased to 40 nm (Figure 4.2h), proving that PFMPS occupies the triangular voids between the neighboring spheres.

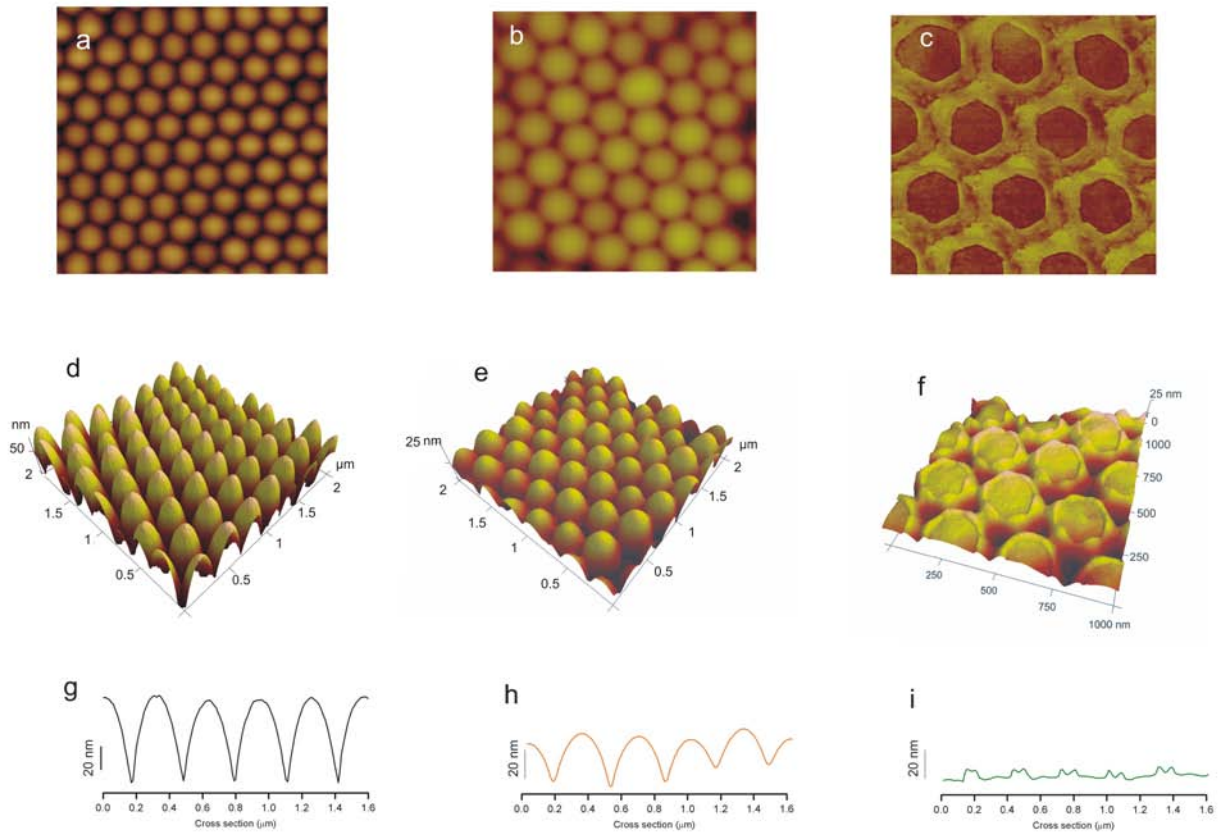

Figure 4.2 (a) AFM height image of a 300 nm particle array as assembled, (b) AFM height image of a 300 nm particle array infiltrated with PFMPS, (c) AFM phase image of particles treated with argon ion sputtering, and corresponding 3D AFM images (d, e, f) with corresponding height profiles (g, h, i), respectively.

Subsequently, exposure of the silica particles was achieved by argon ion sputtering. By Ar sputtering, the top layer of PFMPS was removed, thus exposing the surface of the silica nanoparticles as shown in Figure 4.2 (c, f) and Figure 4.3a (SEM image). The argon sputtering process resulted in circle-shaped silica spheres which were connected with PFMPS as seen in the top view AFM image (Figure 4.2c). The radius of these particles became smaller compared to the initial size of the spheres due to the sputtering rate of silica particles (Figure 4.2i). The height profile revealed a cross-sectional hour-glass shape PFMPS membrane separating the pores with a PFMPS wall of at least 60 nm width remained at the top.

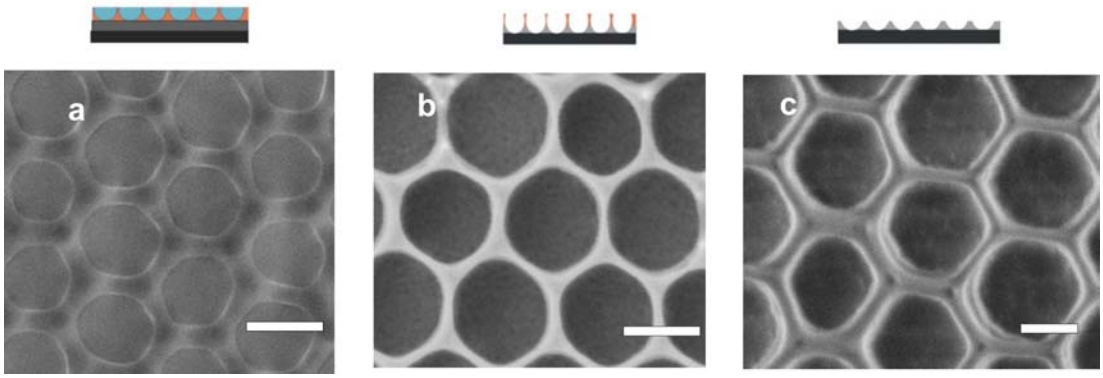

Figure 4.3 SEM images of films (a) after 25 min argon ion sputtering, (b) followed by oxygen plasma etching and (c) after removal of PFMPS in nitric acid. The scale bars indicate 200 nm.

Figure 4.3 shows SEM images captured after the argon sputtering step (a), the oxygen plasma treatment (b) and after subsequent treatment with nitric acid (c). Figure 4.3b shows the pores left in place of the particles after removal of particles with hydrofluoric acid followed by oxygen plasma treatment, representing a negative replica of the original colloidal crystal array. Figure 4.3c displays the highly ordered porous PES network after subsequent removal of PFMPS by ultrasonication in 5% nitric acid.

The CA sacrificial layer was dissolved in acetone in order to obtain free-standing PES films. Keeping the samples for a few minutes in acetone was adequate for detaching the membrane from the silicon substrate. A representative SEM image exhibiting a $20 \times 15\ \mu m^2$ area is shown in Figure 4.4a with an inset showing the structure captured by SEM at a higher magnification, revealing the details of the highly ordered PES membrane which has a thickness of 500 nm. The pore size of the membrane is about 230 nm which is less than the

size of the particles used due to the difference in sputtering rate of PFMPS and silica nanoparticles in a stream of Ar^+ ions. With a thickness of 500 nm, the membrane was strong enough to be peeled off and handled with tweezers. The PES films that peeled off in acetone were readily transferred onto a substrate without any damage to the membrane (Figure 4.4b and c), which proved the mechanical stability of the porous films. The lateral dimensions of the membranes are in principle only limited by the size of the substrate used.

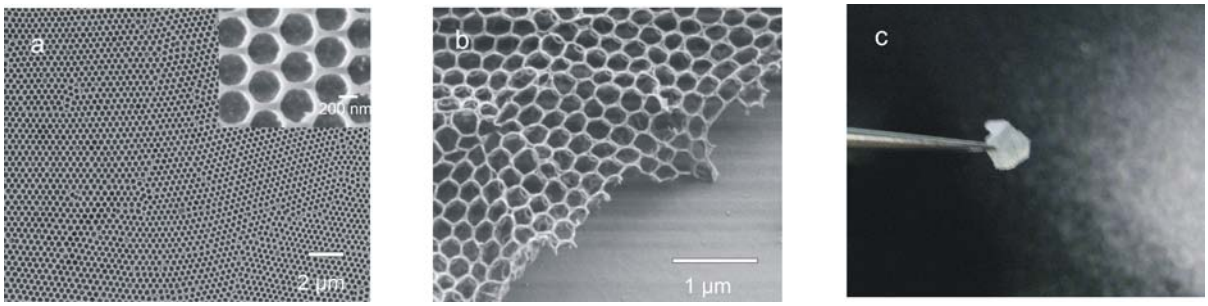

Figure 4.4 (a) SEM images of a PES membrane after removing the sacrificial cellulose acetate layer in acetone, (b) SEM image of the membrane after being peeled off and transferred to a substrate (c) optical photograph of a piece of a PES membrane (picked up by tweezers) after floating off from the substrate.

The pore size can be simply controlled by changing the size of the silica particles used. We here varied the size of the silica particles to show the fabrication of membranes with different pore sizes. Figure 4.5 shows SEM images of membranes made from silica particle sizes of 150 nm, 300 nm and 500 nm. Figure 4.5d shows a membrane fabricated from a mixture of particles with sizes of 150 nm and 500 nm. Since the voids between the particles are larger when using a mixture of particles, more material fills the voids which resulted in wider membrane walls.

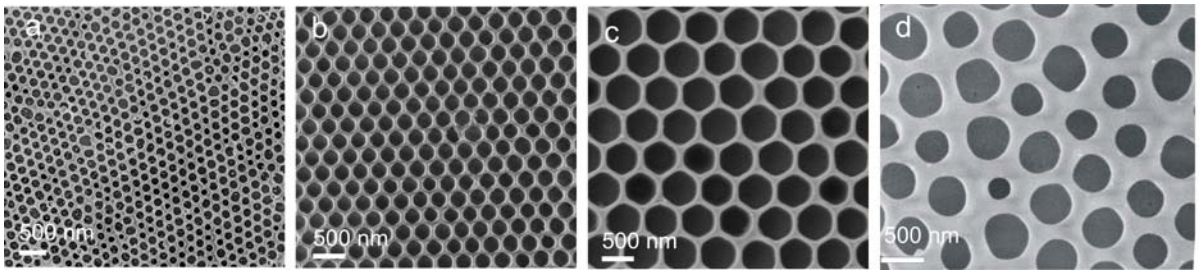

Figure 4.5 PES membranes made from (a) 150-nm, (b) 300-nm, (c) 500-nm particles, and (d) mixed 150-nm and 500-nm particles employing the fabrication sequence in Figure 4.1.

The use of a vertical deposition technique allows one to control the thickness of the layers formed. Monolayer or multilayer of silica particles prepared in this way serves as a template to generate porous PFS structures. Figure 4.6 shows SEM images of porous PFS fabricated from multilayer of particles following the same procedure explained in Figure 4.1.

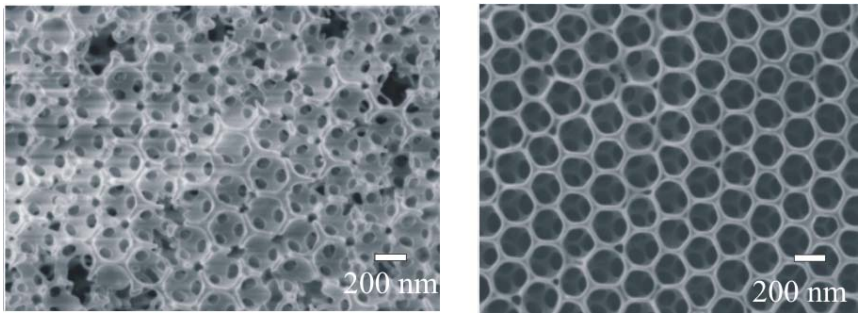

Figure 4.6 SEM images of porous PFS fabricated from multilayer assembly of particles.

Figure 4.7 shows SEM images of 60 nm and 300 nm silica particles filtered using the PES membrane fabricated with a pore size of 300 nm. Filtering was performed into a substrate well (see Experimental part) by the help of capillary forces. Particles of 60 nm were filtered through whereas 300 nm particles stayed on top of the membrane surface. The particles of 60 nm were collected in the substrate well as seen in Figure 4.7b.

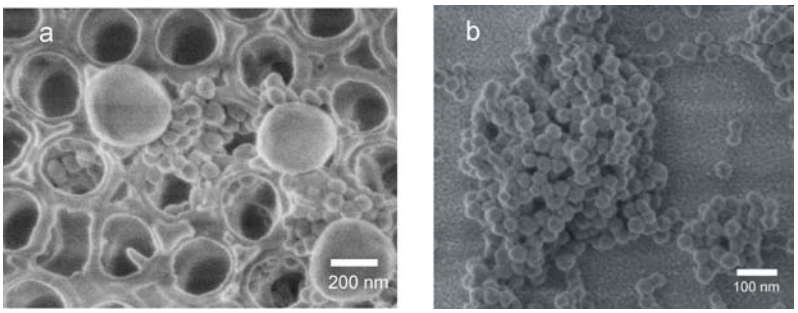

Figure 4.7 (a) SEM image of particles stayed on top of the membrane during filtration. (B) SEM images of particles of 60 nm collected on a substrate well after filtration.

4.3 CONCLUSIONS

In this chapter, we have demonstrated a novel process to obtain free-standing PES films exhibiting regular arrays of circular holes with a high porosity. The combination of NSL lithography and a mask transfer technique used in this process allowed the fabrication of these uniform, nanoporous PES membranes. The etch mask material PFMPS filled the gaps between the particles and served as a protecting layer in RIE after removal of the silica

spheres. Pores were generated in the PES layer during RIE. Detachment of the PES membrane from the substrate was achieved by dissolving the sacrificial CA layer in acetone. A free-standing PES film was obtained, which was used to perform feasibility filtration experiments. Silica particles were successfully separated by size. Since the size of the silica particles can be varied, membranes with a range of pore sizes down to 150 nm were fabricated using this process.

4.4 EXPERIMENTAL

Silica nanoparticles were purchased from Polysciences Inc. (diameter = 300 nm, standard deviation <10%) as an aqueous suspension, particles of 60 nm were synthesized following a literature procedure.[34] Polyethersulfone (PES) (UDEL P-1700) was obtained from Solvay Advanced Polymers and cellulose acetate (CA) was purchased from Acros Organics. *N,N,N′,N′*,-Tetramethylethylenediamine (TMEDA), ferrocene, dichloromethylphenylsilane, Karstedt's catalyst and Et_3SiH were purchased from Aldrich and were used as obtained.

[1]Methylphenylsilaferrocenophane was prepared as described earlier.[17,26] The monomer was purified by several crystallization steps from *n*-heptane at –70 °C followed by vacuum sublimation. Transition-metal-catalyzed ring opening polymerization was carried out in the presence of Et_3SiH with the addition of Karstedt's catalyst. The polymer obtained was precipitated in *n*-heptane. The weight average and number average molar masses M_w and M_n of the polymer were determined by gel permeation chromatography (GPC) measurements in THF, using polystyrene calibration, M_w = 5.5 x 10^4 g/mol, M_n = 5.1 x 10^4 g/mol, M_w/M_n = 1.09.

Silicon substrates were cleaned by immersion in piranha solution, conc. H_2SO_4 and 33% H_2O_2 in a 3:1 volume ratio *(**Warning!** piranha should be handled with caution; it can detonate unexpectedly)* for 15 min to form a clean SiO_2 layer at the surface. The substrates were then sonicated in Milli-Q water and ethanol for 1 min, and dried with N_2. CA layers of 150 nm were obtained by spin coating in a cleanroom environment from toluene solution. Subsequently, a PES film of 500 nm was spin-coated from chloroform onto the CA film. The PES film was exposed to oxygen plasma for 30 sec for mild oxidation in a reactive-ion eching (O_2-RIE) setup, carried out in an Elektrotech PF 340 apparatus (10 mTorr, 20 sccm O_2, 10 W). Mild oxidation of PES resulted in a hydrophilic surface which allowed the assembly of silica particles. A monolayer of silica colloidal particles on the PES substrate

was prepared by capillary assisted deposition at a speed of 0.5 μm/s.[33] A layer of 80 nm PFS was spin-coated onto the particle layer from 2 wt % PFS solution in toluene. The top layer of PFS was etched away by argon plasma sputtering for 25 min (Ion Beam Etcher, 350 V, 6 mA) resulting in exposure of the top of the silica particles. The silica particles were removed by dipping the substrate into a 10 wt% aqueous hydrogen fluoride (HF) solution for 12 h, subsequently rinsing with Milli-Q water and drying with N_2. *(**Warning!** HF solution should be handled with caution; it can cause serious health problems)*

Oxygen plasma etching experiments, for the removal of PES in unprotected areas, were performed in a reactive-ion etching (O_2-RIE) setup, carried out in an Elektrotech PF 340 apparatus (10 mTorr, 20 sccm O_2, 50 W) for 5 min. The substrate was sonicated with 10 wt% aqueous nitric acid solution in a Branson 8510 ultrasonic bath to remove PFMPS. Free standing membranes were obtained by dipping the etched substrates in acetone to dissolve the CA sacrificial layer.

In order to gauge membrane performance, a simple filtration experiment was carried out by filtering silica particles with different diameters onto a substrate exhibiting 'wells' which were fabricated by Focused Ion Beam (FIB). The wells displayed a depth of 10 μm and a diameter of 10 μm to provide capillary forces for particles to be filtrated. The PES membrane was placed on top of the well, and a droplet of an aqueous solution containing a mixture of 300 nm and 60 nm silica particles was placed on top of the membrane.

All SEM images were taken with a HR-LEO 1550 FEF SEM. The samples were not coated with a conducting layer. AFM measurements were carried out with a Dimension D3100 using a NanoScope IVa controller equipped with a hybrid 153 scanner (Veeco/Digital Instruments (DI), Santa Barbara, CA) under ambient conditions. Silicon cantilevers from Nanosensors (Nanosensors, Wetzlar, Germany) were used for intermittent contact (tapping) mode operation.

4.5 ACKNOWLEDGEMENTS

We thank Mr. Mark Smithers for the SEM images and Mr. Clemens Padberg for the technical support.

4.6 REFERENCES

[1] L. J. Zeman, A. L. Zyndey, *Microfiltration and Ultrafiltration Principles and Applications*, Marcel Dekker Inc., New York **1996.**

[2] M. Cheryan, *Ultrafiltration and Microfiltration Handbook*, Technomic Publishing Company, Lanchester, PA **1998**.

[3] J. Mallevialle, P. E. Odendaal, M. R. Wiesner, *Water Treatment Membrane Processes*, McGraw-Hill, New York **1996**.

[4] M. Ulbricht, *Polymer* **2006**, *47*, 2217.

[5] R. L. Fleischer, P. B. Price, R. M. Walker *Nuclear Tracks in Solids*. University of California Press, Berkeley, CA **1975.**

[6] R. C. Furneaux, W. R. Rigby, A. P. Davidson, *Nature* **1989**, *337*, 147.

[7] C. R. Martin, *Science* **1994**, *266*, 1961.

[8] C. Jiang, V. V. Tsukruk, *Soft Matter* **2005**, *1*, 334.

[9] G. J. Liu, J. F. Ding, T. Hashimoto, K. Saijo, F. M. Winnik, S. Nigam, *Chem. Mater*. **1999**, *11*, 2233.

[10] A. S. Zalusky, R. Olayo-Valles, C. J. Taylor, M. A. Hillmeyer, *J. Am. Chem. Soc.* **2001**, *123*, 1519.

[11] S. Y. Chou, *MRS Bull*. **2001**, 26, 512.

[12] D. Zimnitsky, V. V. Shevchenko, V. V. Tsukruk, *Langmuir* **2008**, *24*, 5996

[13] B. Gates, Y. Yin, Y. Xia, *Chem. Mater.* **1999,** *11*, 2827.

[14] P. Jiang, J. F. Bertone, V.L. Colvin, *Science* **2001**, *291*, 453.

[15] X. Chen, Z. Chen, N. Fu, G. Lu, B. Yang, *Adv. Mater.* **2003**, *15*, 1413.

[16] U. C. Fischer, H. P. Zingsheim, *J. Vac. Sci. Technol. B.* **1981**, *19*, 881.

[17] D. A. Foucher, B. Z. Tang, I. Manners, *J. Am. Chem. Soc.* **1992,** *114*, 6246.

[18] I. Manners, *Synthetic Metal-Containing Polymer*, Wiley-VCH, Weinheim, Germany **2004**.

[19] K. Kulbaba, I. Manners, *Macromol. Rapid Commun.* **2001**, *22*, 711.

[20] C. Hinderling, Y. Keles, T. Stöckli, H. F. Knapp, T. De Los Arcos, P. Oelhafen, I. Korczagin, M. A. Hempenius, G. J. Vancso, R. Pugin, H. Heinzelmann, *Adv. Mater.* **2004**, *16*, 876.

[21] J. Q. Lu, T. E. Kopley, N. Moll, D. Roitman, D. Chamberlin, Q. Fu, J. Liu, T. P. Russell, D. A. Rider, I. Manners, M. A. Winnik, *Chem. Mater*. **2005**, *17*, 2227.

[22] R. G. H. Lammertink, M. A. Hempenius, J. E. Van den Enk, V. Z.-H. Chan, E. L Thomas, G. J. Vancso, *Adv. Mater.* **2000**, *12*, 98.

[23] A. C. Arsenault, H. Míguez, V. Kitaev, G. A. Ozin, I. Manners, *Adv. Mater.* **2003**, *15*, 503.

[24] M. Péter, R. G. H. Lammertink, M. A. Hempenius, G. J. Vancso, *Langmuir **2005**, 21, 5115.*

[25] I. Korczagin, R. G. H. Lammertink, M. A. Hempenius, S. Golze, G. J. Vancso, *Adv. Polym. Sci.* **2006**, *200*, 91.

[26] I. Korczagin, S. Golze, M. A. Hempenius, G. J. Vancso, *Chem. Mater.* **2003**, *15*, 3663.

[27] M. A. Hempenius, R. G. H. Lammertink, M. Péter, G. J. Vancso, *Macromol. Symp.* **2003**, *196*, 45.

[28] J. Y. Cheng, C. A. Ross, V. Z. H. Chan, E. L. Thomas, R. G. H. Lammertink, G. J. Vancso, *Adv. Mater.* **2001,** *13*, 1174.

[29] R. G. H. Lammertink, M. A. Hempenius, V. Z. Chan, E. L. Thomas, G. J. Vancso *Chem. Mater*. **2001**, *13***,** 429.

[30] J. Lu, D. Chamberlin, D. A. Rider, M. Liu, I. Manners, T. P. Russell, *Nanotechnology* **2006**, *17,* 5792.

[31] K. Temple, J. A. Massey, Z. H. Chen, N. Vaidya, A. Berenbaum, D. M. Foster, I. Manners, *J. Inorg. Organomet. Polym.* **1999**, *9*, 189.

[32] (a) Z. Fan, Z. Wang, N. Sun, J. Wang, S. Wang, *J. Membr. Sci.* **2008**, *320*, 363. (b) D. S. Wavhal, E. R. Fisher, *J. Polym. Sci. Part B: Polym. Phys.* **2002**, *40*, 2473.

[33] X. Y. Ling, L. Malaquin, D. N. Reinhoudt, H. Wolf, J. Huskens, *Langmuir* **2007**, *23*, 9990.

[34] X. Y. Ling, D. N. Reinhoudt, J. Huskens, *Langmuir* **2006**, *22*, 8777.

Chapter 5

Direct Surface Structuring of Organometallic Resists Using Nanoimprint Lithography

ABSTRACT. The availability of suitable resist materials is essential for nanoimprint lithography (NIL). In this chapter, the application of poly(ferrocenylmethylphenylsilane) (PFMPS) as a new type of imprint resist is reported. As PFMPS contains iron and silicon in the main chain, it possesses a very high resistance to reactive ion etching. Polymer patterns formed after imprinting were transferred into silicon substrates owing to the high etch resistivity of PFMPS. The parameters for imprinting such as polymer molar mass and initial film thickness were investigated. A decrease in the initial film thickness facilitated the residual layer removal, as well as the pattern transfer. Only upon complete removal of the residual layer with argon plasma, pattern transfer resulted in aspect ratios up to 4:1 and lower surface roughness.

This work has been published in C. Acikgoz, M.A. Hempenius, G. J. Vancso, J. Huskens, Direct surface structuring of organometallic resists using nanoimprint lithography, *Nanotechnology* **2009**, *20*, 135304.

5.1 INTRODUCTION

Imprint lithography[1, 2] has become an enabling platform to fabricate micro and nanostructures for a wide variety of applications, for example in electronics[3, 4] and in bio-nanotechnology.[5, 6] Among the imprint-based lithographic techniques, thermal nanoimprint lithography (NIL)[1, 2] is one of the most versatile methods, capable of fabricating patterns from less than ten nanometers to a few microns on a large area, at a low cost with a high throughput. Multiple copies of the pattern can be produced once the stamp is available. A hard stamp is used to replicate patterns by NIL, distinguishing it from microcontact printing (μCP), which uses a soft and flexible PDMS stamp. The hard features on NIL molds can enable imprinting of features with sizes down to below 10 nm, which can not be achieved by μCP using a soft stamp.[2] In order to create the patterns, a stamp is pressed into a thin layer of polymer resist, followed by heating at a temperature approximately 80 $^{\circ}$C above the glass transition temperature (T_g) of the polymer. Polymer and stamp are cooled to below the T_g of the polymer followed by demolding of the stamp, leaving the desired patterns in the polymer film.[3] Pattern transfer is enabled by anisotropic etching such as reactive ion etching.[7]

This technology has found widespread use, however, the resist material is generally regarded as one of the challenges of this technique.[8] There are some requirements for materials to be employed as a NIL resist such as modest imprint temperature and pressure, proper mold release and etch selectivity.[8] Poly(methyl methacrylate) and polystyrene are most widely used as NIL resists and they work well in many processes. Nevertheless, they have in some occasions be subject to mold-sticking and fracture defects during mold release.[9, 10] High imprint temperatures can also cause thermal stress and degradation in the polymer film and increase the processing time.[11] The use of imprinted patterns as an etch mask is necessary if patterns are to be transferred into the substrate using plasma etching. PMMA breaks down easily when exposed to reactive species in RIE processing, i.e. it does not show a high etch resistivity in plasma processing, which prevents pattern transfer into silicon and similar substrates. Anisotropic etching of submicron trenches in silicon has been achieved by using a non-standard SF_6 and $C_2Cl_3F_3$ plasma with a Si/PMMA etch selectivity of about 10:1.[12] The fabrication of high-aspect-ratio patterns can be achieved by implementing an additional metal evaporation and lift-off process, which can increase the selectivity up to 40:1. This approach, however, introduces additional problems such as granularity of the metal and concomitant edge roughness.[13]

Poly(ferrocenylsilane) (PFS),[14-18] containing iron and silicon atoms in the main chain, is a class of organometallic polymers which show very diverse and interesting

properties. PFSs can be prepared by thermal ring-opening polymerization of the corresponding ferrocenophanes,[15] by anionic polymerization and other types of chemistries. Pattern transfer into various substrates by using these organometallic homopolymers as inks in soft lithography owing to their etch resistance has been demonstrated already.[19-21] The high etch resistance of PFS compared to silicon substrates has enabled the fabrication of structures with aspect ratios of 10. An etch rate contrast of 600:1 (silicon to PFS) was established after using PFS as a mask material.[22] In a recent paper, pattern transfer fidelity in capillary force lithography using PFS plasma etch resists was studied. An optimal viscosity range was established with respect to molar masses and processing temperatures. In the optimal processing window polymers possess enough mobility to allow for fast surface pattern fromation, yet they are not too mobile thus patterns preserve shapes when quenched to below T_g prior to serving as etch masks.[23]

In this chapter, the use of poly(ferrocenylmethylphenylsilane) (PFMPS) as a NIL resist is described. As shown earlier,[15] this polymer has a low T_g, it forms homogeneous films and has a high etch resistivity. In the current study, thermal imprinting of PFMPS is demonstrated and the patterns are transferred into silicon substrates by applying different compositions of gases in plasma etching. The residual layer is removed by treatment with argon plasma sputtering prior to transfer into the substrate. Imprint parameters such as initial film thickness and polymer molar mass are investigated. Employing PFMPS as an etch mask reduces the number of process steps by eliminating the need for metal evaporation and lift-off, which implies faster and easier fabrication of nanostructured surfaces.

5.2 RESULTS & DISCUSSION

5.2.1 Synthesis and Characterization of Poly(ferrocenylmethylphenylsilane)

Poly(ferrocenylmethylphenylsilane) (PFMPS) is an amorphous polymer due to atactic substitution on the silicon atom in the main chain, and has a glass transition temperature suitable for thermal imprinting. Since crystallization may destruct patterns, it was essential to choose a non-crystalline polymer. PFMPS forms homogeneous films and has a T_g above room temperature which is important to preserve the shape of the structures after removal of the stamp. The extrapolated value of the T_g for PFMPS to infinite molecular weight was reported to be 92 ^{o}C.[19] The synthesis and characterization of PFMPS were carried out according to a literature procedure (Figure 5.1).[14, 24]

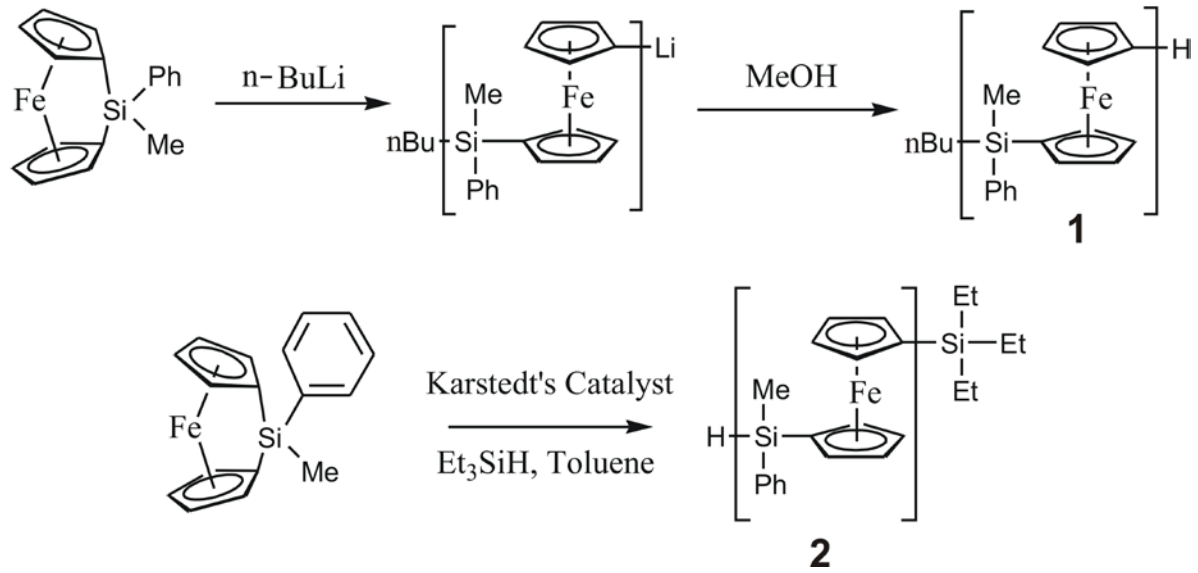

Figure 5.1 Synthesis of PFMPSs **1** and **2** by anionic ring-opening polymerization (top) and by transition metal-catalyzed polymerization (bottom), respectively.

The anionic ring-opening polymerization of [1]methylphenylsilaferrocenophane in THF initiated by *n*–butyllithium resulted in PFMPS **1** with a molar mass of M_n = 2.9 × 10^3 g/mol.[16] To achieve a higher molar mass, transition metal-catalyzed polymerization was performed in the presence of Et_3SiH and Karstedt's catalyst. It was shown that the addition of varying amounts of Et_3SiH to the Pt(0)-catalyzed reaction permits chain length control.[25] Addition of Karstedt's catalyst to a toluene solution of monomer and Et_3SiH resulted in PFMPS **2**. GPC analysis revealed that the molar mass of the polymer was M_n = 5.1 × 10^4 g/mol. Table 5.1 summarizes the molecular and thermal characteristics of the synthesized polymers. These data show the dependence of T_g on the molar mass of the polymer.

Table 5.1. Molecular and Thermal Characteristics of Poly(ferrocenylmethylphenylsilane)s **1** and **2**.

Polymer	M_n (g/mol) x 10^3	M_w/M_n [a]	T_g (^oC) [b]
1	2.9	1.10	77
2	51	1.09	85

[a] Measured by GPC in THF, relative to polystyrene standards. [b] Obtained by DSC at a scan rate of 10 K/min.

5.2.2 Thermal Nanoimprinting of PFMPS

PFMPS **1** and **2**, having different molar masses, were used as resists in NIL. Thin polymer films were spin-coated on silicon oxide substrates from toluene solutions, followed by softbaking at 120 ^{o}C to evaporate the remaining solvent and to improve the resist-substrate adhesion. By the spin-coating process, it was possible to control the thickness of the polymer layer and to prepare uniformly coated silicon substrates.[26] The resulting polymer films were homogeneous, which is essential for imprinting. Following spin-coating, the sample and the stamp were heated to 150 ºC and pressure of 80 bar was applied.

In the case of the low molar mass PFMPS **1,** the stamp features were transferred into the polymer, but incomplete filling and dewetting were observed (Figure 5.2a). These problems are attributed to the low molar mass of the polymer, which favors dewetting. In contrast, in the case of the high molar mass polymer **2**, no dewetting was observed. Figure 5.2 (b and c) shows imprinted lines with a width of 1 µm and a 5 µm period and of 100 nm wide lines with a 1 µm period, respectively, imprinted into 120 nm of PFMPS **2** at a temperature of 150 °C at 80 bar for 1 min. The features of the stamps were successfully transferred into PFMPS **2** after demolding at a temperature of 75 ºC. Therefore, all subsequent experiments were performed with PFMPS **2.**

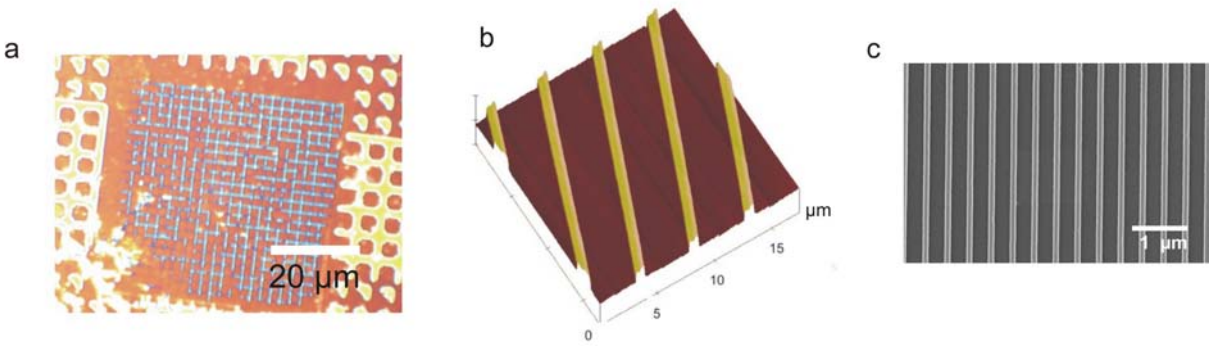

Figure 5.2 (a) Optical micrograph of imprint into PFMPS **1**. (b) AFM image of imprinted lines with a width of 1 µm and a 5 µm period and (c) SEM image of imprinted lines of 200 nm wide with a 500 nm period obtained after NIL in PFMPS **2**.

The flow behavior of polymers at elevated temperatures is a crucial issue in NIL. Polymers at temperatures above their glass transition temperature are liquids, but with a very high viscosity. As the temperature increases, the viscosity of polymer decreases and the mobility of flow increases. Therefore, the viscosity of PFMPS **2** was determined. Viscosity measurements were performed in a parallel plate configuration using oscillatory shear flow experiments at different temperatures. At every measurement point, viscosity was calculated as a ratio of shear stress and shear rate. The zero-shear-rate viscosity was determined by extrapolation of the viscosity values as a function of shear rate. The zero-shear-rate viscosity of PFMPS **2** was found to be 334 Pa.s at 150 °C (the imprint temperature), which is appropriate for NIL since good-quality patterns can typically be generated with polymers having viscosities in the range of 50 to 1500 Pa.s.[23]

Thermal NIL typically results in the formation of a residual resist layer in the imprinted regions. The thickness and the uniformity of the residual layer is thus critical as an additional etching step is required to remove this residual layer before the patterns can be transferred to the substrate. Oxygen and oxygen-containing plasmas are most commonly employed to remove a residual layer. The imprinted PFMPS **2** films were exposed to oxygen reactive ion etching (O_2-RIE) in order to remove the residual layer.

Figure 5.3a demonstrates the influence of oxide layer formation upon oxygen plasma treatment of PFMPS. The residual layer was not removed by this process while the roughness (compared to Figure 5.2b) became more pronounced. This was confirmed by AFM roughness measurements which showed that the roughness before oxygen plasma treatment was 1.0 nm whereas it increased to 3.4 nm after O_2 plasma. Upon exposure to oxygen plasma, a Si/Fe oxide layer is formed at the surface of PFMPS since inorganic components are converted into nonvolatile oxides as witnessed by earlier.[27] After addition of CHF_3 gas to the plasma, the residual polymer layer was removed. This was confirmed by the observation that further etching into the silicon substrate, which was achieved by an O_2/SF_6 plasma and led to an increased feature height of ~ 400 nm (Figure 5.3b). However, considerable roughness was still observed in the regions between the lines (Figure 5.3b and c). This roughness is attributed to traces of residual PFMPS, which, when converted into Si/Fe oxide, acts as an etch barrier.

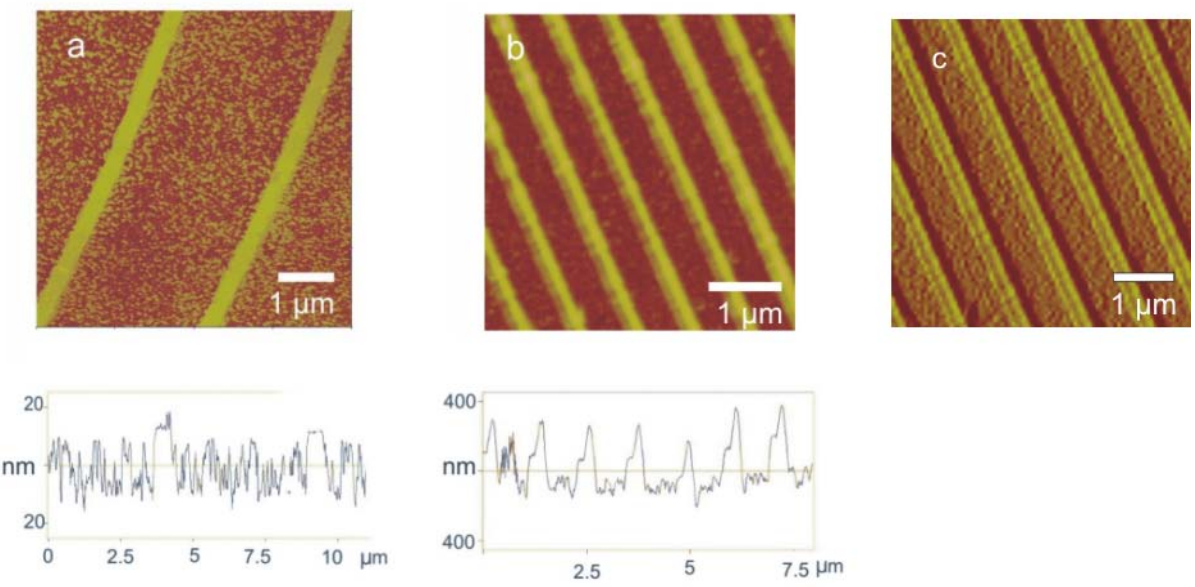

Figure 5.3 (a) AFM height image of a thermal imprint into PFMPS **2** upon exposure to oxygen plasma. AFM height (b) and phase (c) images acquired after residual layer removal by O_2 and CHF_3 plasma followed by etching into the substrate by applying an O_2/SF_6 plasma.

In conclusion, upon treatment of PFMPS resist with oxygen plasma, coverage of the whole surface with an oxide layer hindered the removal of the residual layer. A proper selection of gases from which the plasma is generated could decrease the formation of this oxide layer and thus enhance etching. However, the surface became rough during the initial steps of etching, and this roughness was transferred to the substrate after applying SF_6 and O_2 plasma (Figure 5.3c). Therefore, this oxide layer between the lines limits the etch contrast and prevents the fabrication of high-aspect-ratio patterns.

Optimization of the RIE process conditions requires quantification and control of the residual layer thickness. Achieving a minimal residual layer thickness is advantageous for most imprint applications as this minimizes loss of dimensional accuracy during the plasma etching process. By tuning the initial film thickness, we tried to obtain a thin residual layer. Polymer **2** was spin-coated onto a silicon surface to thicknesses of 120, 70 and 40 nm, respectively. The thickness of the residual layer after imprinting was around 80 nm for the 120 nm initial film thickness, as was measured by AFM after scratching. After decreasing the initial thickness of the polymer layer to 70 nm, the thickness of the residual layer was determined to be 50 nm.

The cross-section SEM images given in Figure 5.4 show the residual layer thicknesses. When the initial film thickness was 70 nm, the thickness of the residual layer was found to be 40 to 50 nm (Figure 5.4a) Decreasing the initial film thickness to 40 nm resulted in a residual layer of 20 to 30 nm as seen in Figure 5.4b. When calculating the residual layer thickness from the observed, partially filled, feature heights, similar values are obtained: the height of 300 nm observed for the 100 nm wide lines at 1 µm period (Figure 5.4a) corresponds to a residual layer of 45 nm, while the height of 140 nm observed for 1 µm lines at 5 µm period (Figure 5.4b) corresponds to a residual layer thickness of about 20 nm.

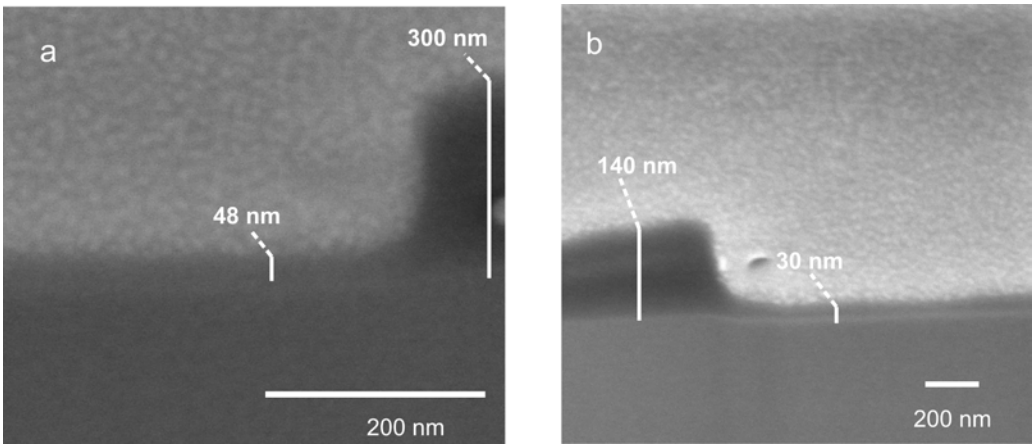

Figure 5.4 Cross-section SEM images of structures imprinted into (a) 70 nm and (b) 40 nm initial layer thickness of PFMPS **2.**

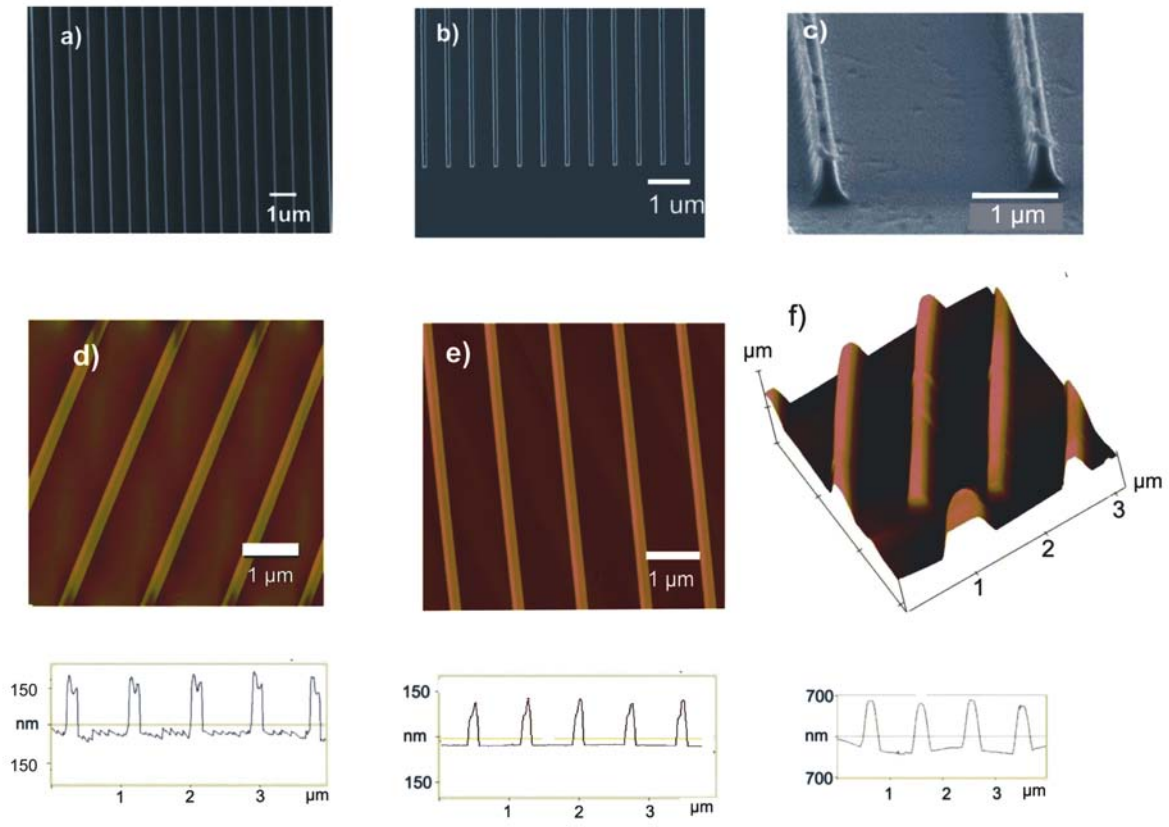

Figure 5.5 SEM (a,b,c) and AFM images and height profiles (d,e,f) of 100 nm lines imprinted into 70 nm thick resist film (a, d), folllowed by 35 min of Ar sputtering (b,e), and subsequent etching with CHF_3 /SF_6/O_2 plasma (c, f).

Figure 5.5a and 5.5d demonstrate the lines imprinted into a 70 nm thick film. Figure 5.5d shows the height variation on top of the lines. Imprinting into polymer layers that are thin compared to the structure height usually results in partial filling of the cavities.[11] Another reason for the filling problem could be an inadequate flow of material when the film thickness is decreased. The top of the polymer patterns did not take the shape of the stamp since the cavities were not filled completely (Figure 5.5d). However, a thin residual layer which is around 50 nm remained present after imprinting under conditions of partial cavity filling (Figure 5.4a). The cavities were even less filled when the initial film thickness was decreased to 40 nm because of insufficient supply of polymer. The application of the same etching conditions as described above to the imprinted structures with a thin residual layer yielded 1:1 aspect ratio patterns as was achieved earlier with thicker residual layers.

5.2.3 Pattern Transfer into the Silicon Substrate

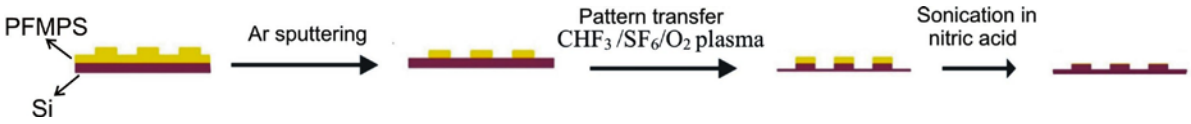

Figure 5.6 Etching process applied to completely remove the residual layer and to etch into the substrate.

Figure 5.6 illustrates the procedure applied to eliminate the residual layer problem. RIE is a combination of chemical and physical etching.[28] The formation of a nonvolatile oxide layer at the surface of PFMPS is due to chemical etching. Physical etching becomes less pronounced during RIE since the oxide layer acts as a very strong mask preventing further etching into the substrate. Argon sputtering, which is a purely physical etching process, is expected to prevent the formation of nonvolatile oxide since the layer is physically bombarded with high energy ions and is removed by the corresponding sputtering effect. Therefore, physical etching was performed with sputtering using high energy Ar ions to remove the residual layer. The etch rate of PFMPS **2** was determined to be 1.5 nm/min after exposure to argon plasma. Taking into account this value, the imprinted sample was exposed to argon plasma for 35 min to ensure that the residual layer was removed completely.

The height difference before (Figure 5.5a, d) and after Ar plasma (Figure 5.5b, e) treatment revealed the complete removal of PFMPS in the recessed regions. Exposure of PFMPS to Ar plasma resulted in a high initial roughness (data not shown). This roughness was not observed after complete removal of PFMPS from recessed regions by sputtering as can be seen in Figure 5.5e. Keeping the film thickness as thin as possible significantly reduces the required time of treatment with Ar plasma. Further etching into the substrate also proved that no residual layer remained (Figure 5.5c, f). Reactive ion etching with a mixture of CHF_3 (20 sccm), O_2 (20 sccm) and SF_6 (50 sccm) was performed to transfer these lines into the substrate[29] (Figure 5.5c). An aspect ratio of 4:1 was achieved after a 2 min treatment with the plasma containing these gases. Using this process we obtained etch rates of 400 nm/min into Si and around 1 nm/min in PFMPS layer resulting in an etch rate contrast of approximately 400. The height profile in Figure 5.5f shows that the sidewalls are not completely vertical after etching into the substrate.

It was observed that changes in pattern size influenced the etching characteristics of the patterns. More vertical sidewalls were obtained for 1 µm wide lines (Figure 5.7a). The

roughness on the recessed regions was also diminished after Ar plasma, which facilitated etching into the substrate. Defect-free patterns were thus reproducibly obtained over large areas (Figure 5.7b).

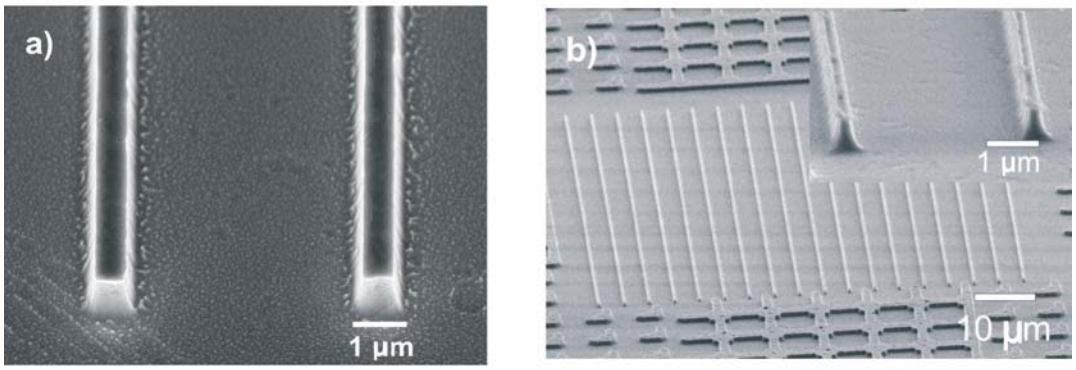

Figure 5.7 (a) SEM image of sidewalls obtained after etching into the substrate for 1 µm wide lines. (b) Large area SEM image of etched sample with a $CHF_3/SF_6/O_2$ plasma.

5.3 CONCLUSIONS

We have described the application of PFMPS as a resist in nanoimprint lithography. Stable, homogeneous high molar mass PFMPS films obtained by spin coating were imprinted and the resulting patterns were further transferred into the substrate by reactive ion etching. Decreasing the initial film thickness and tuning the reactive ion etching conditions facilitated the residual layer removal and improved the pattern transfer. In order to obtain high aspect ratios, the residual layer was completely removed by Ar sputtering since direct etching without removal of the residual layer gave rise to oxide layer formation, which prevented further pattern transfer. A drawback of this process is the relatively long sputtering time needed. This can be further improved by (i) increase of the sputter rate, (ii) further reduction of the residual layer, and/or (iii) use of processes that circumvent the formation of a residual layer altogether.[30] Overall, it was shown that PFMPS, because of its excellent etch contrast vs Si, can be used as a single step resist since there is no need for metal lift-off, which renders this approach a low-cost and potentially high-throughput process

5. 4 EXPERIMENTAL

5.4.1 Polymer Synthesis and Characterization

N,*N*,*N'*,*N'*,-Tetramethylethylenediamine (TMEDA), ferrocene, dichloromethylphenylsilane, Karstedt's catalyst, Et_3SiH and *n*-butyllithium were purchased from Aldrich.

[1]Methylphenylsilaferrocenophane was prepared as described earlier.[15, 24] This monomer was purified by several crystallizations from *n*-heptane at –70 °C followed by vacuum sublimation. Polymerizations were carried out in THF in a glovebox purged with prepurified nitrogen. *n*-Butyllithium was used as initiator for anionic polymerization and the reaction was terminated after 2 h by adding a few drops of degassed methanol. The polymer was precipitated in methanol and dried. Transition metal-catalyzed ring opening polymerization of [1]methylphenylsilaferrocenophane was carried out in the presence of Et_3SiH with the addition of Karstedt's catalyst. The polymer was then precipitated in *n*-heptane. For resists with low/moderate molar masses, anionic polymerisation was employed, while higher molar masses were achieved using transition metal-catalyzed polymerisation. Molar mass characteristics of the polymer were determined by gel permeation chromatography (GPC) measurements in THF, using polystyrene calibration. A Perkin-Elmer Pyris 1 differential scanning calorimeter was used for the determination of glass transition temperatures (T_g) at a scan rate of 10 K/min.

Viscosity measurements were performed on a Physica UDS 200 rheometer using a parallel plate configuration. The gap between the plates was 0.5 mm and a shear strain of 1 % was applied. The viscosity was measured at frequencies from 0.01 to 50 Hz as a function of temperature between 80 ºC and 150 ºC. Zero-shear-rate viscosity was calculated by extrapolation of the viscosity values using an exponential function model for an isothermal scan at 150 ºC.

5.4.2 Pattern Fabrication

The Si stamp was fabricated by electron beam lithography followed by reactive ion etching. The stamp has dimensions of 2×2 cm^2 and contains 80×40μm ^{2} patterned regions with features of 1 μm lines at 5 μm period, 500 nm lines at 5 μm period, 200 nm lines at 1 μm period, 200 nm lines at 500 nm spacings, 100 nm lines at 1 μm period, and all at a height of 500 nm. *1H,1H,2H,2H*-Perfluorodecyltrichlorosilane was used as an anti-adhesion layer to facilitate demolding. Cleaning of the substrates and coating of the films were carried out in a cleanroom. Film thicknesses of 120, 70, and 40 nm were applied, as measured by ellipsometry. Stamp and substrate were put in contact and a pressure of 80 bar was applied at a temperature of 150 ^{o}C using a hydraulic press (Specac).

After imprinting, the residual layer was removed by argon plasma sputtering applied for 35 min (Ion Beam Etcher, 350 V, 6 mA). Further etching into the substrate was accomplished by RIE performed in an Elektrotech PF 340 apparatus. During oxygen plasma RIE, the pressure inside the etching chamber was 10 mTorr, the substrate temperature was 10

^{o}C and an oxygen flow rate of 20 sccm was maintained. The second etch step was performed with a mixture of 50% CHF_3 and 50% O_2 at a pressure of 8 mTorr, with a substrate temperature of 10 ^{o}C. The power was kept at 50 V. The final etch step was enabled with a mixture of 20 sccm of CHF_3 and 20 sccm of O_2 and 50 sccm of SF_6 at a pressure of 10 mTorr. The resist was stripped following sonication for 1 h in 10% nitric acid solution. AFM analysis were carried out with a Nanoscope III multimode AFM (Veeco Co., Santa Barbara, CA) by using a J scanner. SEM characterization was done with a HR-LEO 1550 FEF SEM. A FEI Focus Ion Beam apparatus was used to generate the cross sections in order to determine the exact residual layer thickness.

5.5 ACKNOWLEDGEMENTS

We thank the EC-funded project NAPA that provided the stamp and Mark Smithers for the SEM images.

5. 6 REFERENCES

[1] S. Y. Chou, P. R. Krauss, P. J. Renstrom, *Appl. Phys. Lett.* **1995**, *67*, 3114.

[2] L. J. Guo, *J. Phys. D: Appl. Phys.* **2004**, *37*, R123.

[3] M. Beck, F. Persson, P. Carlberg, M. Graczyk, I. Maximov, T. G. I. Ling, L. Montelius, *Microelectron. Eng.* **2004**, *73-4*, 837.

[4] S. Y. Chou, P. R. Krauss, W. Zhang, L. J. Guo, L. Zhuang, *J. Vac. Sci. Technol. B* **1997**, *15*, 2897.

[5] F. Johansson, P. Carlberg, N. Danielsen, L. Montelius, M. Kanje, *Biomaterials* **2006**, *27*, 1251.

[6] V. N. Truskett, M. P. C. Watts, *Trends Biotechnol.* **2006**, *24*, 312.

[7] S. Y. Chou, P. R. Krauss, P. J. Renstrom, *Science* **1996**, *272*, 85.

[8] P. Choi, P. F. Fu, L. J. Guo, *Adv. Funct. Mater.* **2007**, *17*, 65.

[9] M. D. Chen Y, Boyd E, Moran D, Thayne I, Thomas S *J. Vac. Sci. Technol. B* **2002**, *20*, 2887.

[10] Y. Hirai, S. Yoshida, N. Takagi, *J. Vac. Sci. Technol. B* **2003**, *21*, 2765.

[11] K. Pfeiffer, F. Reuther, M. Fink, G. Gruetzner, P. Carlberg, I. Maximov, L. Montelius, J. Seekamp, S. Zankovych, C. M. Sotomayor-Torres, H. Schulz, H. C. Scheer, *Microelectron. Eng.* **2003**, *67-8*, 266.

[12] V. A. Yunkin, D. Fischer, E. Voges, *Microelectron. Eng.* **1995**, *27*, 463.

[13] N. Bogdanski, M. Wissen, S. Mollenbeck, H. C. Scheer, *J. Vac. Sci. Technol. B* **2006**, *24*, 2998.

[14] D. Foucher, R. Ziembinski, R. Petersen, J. Pudelski, M. Edwards, Y. Z. Ni, J. Massey, C. R. Jaeger, G. J. Vancso, I. Manners, *Macromolecules* **1994**, *27*, 3992.

[15] D. A. Foucher, B. Z. Tang, I. Manners, *J. Am. Chem. Soc.* **1992**, *114*, 6246.

[16] R. Rulkens, Y. Z. Ni, I. Manners, *J. Am. Chem. Soc.* **1994**, *116*, 12121.

[17] K. Kulbaba, I. Manners, *Macromol. Rapid Commun.* **2001**, *22*, 711.

[18] I. Manners, *Synthetic Metal-Containing Polymers* Wiley-VCH, Weinheim, Germany, **2004**.

[19] I. Korczagin, S. Golze, M. A. Hempenius, G. J. Vancso, *Chem. Mater.* **2003**, *15*, 3663.

[20] M. A. Hempenius, R. G. H. Lammertink, M. Peter, G. J. Vancso, *Macromol. Symp.* **2003**, *196*, 45.

[21] J. Y. Cheng, C. A. Ross, E. L. Thomas, H. I. Smith, G. J. Vancso, *Adv. Mater.* **2003**, *15*, 1599.

[22] G. J. Vancso, S. Golze, M. A. Hempenius, H. Hillborg, I. Korczagin, R. G. H. Lammertink, *Polym. Prep.* **2003**, *44*, 197.

[23] I. Korczagin, H. Xu, M. A. Hempenius, G. J. Vancso, *Eur. Polym. J.* **2008**, *44*, 2523.

[24] K. Temple, J. A. Massey, Z. H. Chen, N. Vaidya, A. Berenbaum, M. D. Foster, I. Manners, *J. Inorg. Organomet. Polym.* **1999**, *9*, 189.

[25] K. Temple, F. Jakle, J. B. Sheridan, I. Manners, *J. Am. Chem. Soc.* **2001**, *123*, 1355.

[26] C. B. Walsh, E. I. Franses, *Thin Solid Films* **2003**, *429*, 71.

[27] R. G. H. Lammertink, M. A. Hempenius, V. Z. H. Chan, E. L. Thomas, G. J. Vancso, *Chem. Mater.* **2001**, *13*, 429.

[28] D. M. Manos, D. L. Flamm, *Plasma Etching, An Introduction* Academic Press, San Diego, **1988**.

[29] H. Jansen, M. de Boer, J. Burger, R. Legtenberg, M. Elwenspoek, *Microelectron. Eng.* **1995**, *27*, 475.

[30] Y. S. Chou, Q. Xia, *Nature Nanotechnol.* **2008**, *3*, 295.

Chapter 6

Nanoscale Patterning by UV Nanoimprint lithography Using an Organometallic Resist

ABSTRACT. This chapter presents the fabrication of poly(ferrocenylmethylphenylsilane) (PFMPS) patterns by step-and-flash imprint lithography for use as high-contrast etch masks in dry etch processes. PFMPS was spin-coated onto a resist template made by UV nanoimprint lithography to create a reactive ion etch resist layer with a thickness variation corresponding to the imprinted pattern. Etching back the excess of PFMPS by argon sputtering revealed the imprinted organic resist material, which was subsequently removed by oxygen plasma. PFMPS lines down to 30 nm were obtained after removal of organic resist by oxygen plasma. Because PFMPS contains iron and silicon atoms in its main chain, it possesses a high resistance to oxygen reactive ion etching and e.g., CHF_3/O_2 or SF_6/O_2 reactive ion etch processes. PFMPS patterns formed after imprinting were subsequently transferred into the underlying silicon substrate, and etch rates of 300 nm/min into Si and around 1 nm/min into the PFMPS layer were achieved, resulting in an etch contrast of approximately 300.

This work has been published in C. Acikgoz, B. Vratzov, M. A. Hempenius, G. J. Vancso, J. Huskens, Nanoscale Patterning by UV Nanoimprint lithography Using an Organometallic Resist in ACS Appl. Mater. Inter. 2009, 1, 2645.

6.1 INTRODUCTION

Nanoimprint lithography (NIL) is an emerging nanopatterning technology that allows the fabrication of nanostructures with high resolution and complements an alternative to traditional photolithography. Among the imprint-based lithographic technologies, thermal NIL[1, 2] and UV-light-assisted NIL (UV-NIL)[3, 4] are the two techniques capable of replicating sub-10-nm features in a low-cost and high-throughput manner. The basic principle of these imprint-based techniques is that a rigid template or mold with prefabricated topographic features is used to replicate patterns within a resist layer, which can be subsequently employed as an etch mask for further pattern transfer. In thermal NIL, mold patterns are replicated into a thermoplastic material by heating the polymer above its glass transition temperature and applying pressure on the mold. The necessary but time-consuming temperature cycling gives rise to differences in the thermal expansion of resist, substrate, and template, leading to decreased throughput and improper overlay of the device layers and features.[5] UV-NIL differs from thermal NIL as it is performed at room temperature and low pressure using low-viscosity, photocurable resists and a transparent, rigid template.[6] This method does not require temperature cycling, leading to higher throughput than that in thermal NIL, and the transparency of the template offers the possibility for easy optical and high-precision alignment. UV-NIL uses a low-viscosity resist, which also beneficially influences the imprint force and compression time.

The major components of UV imprint resist materials are an organic acrylate, a cross-linker, and a photoinitiator. The resist may function as an etch mask for pattern transfer into the underlying substrate material.[7] The availability of an appropriate UV-curing resist material is an important issue because the material has to fulfill several requirements such as low viscosity, low adhesion to the mold, good adhesion to the substrate, fast curing times, and high etch resistance to allow pattern transfer into the substrate.[8] There are some commercially available UV-curable imprinting materials but their characteristics and properties are still under study.[9] The development of new resist materials for UV-NIL, therefore, remains crucial for enhancing the performance and scope of the technique.

Poly(ferrocenylsilane)s (PFSs),[10-12] containing iron and silicon atoms in the main chain, show very diverse and interesting properties. PFSs can be prepared by thermal ring-opening polymerization (ROP) of the corresponding silicon-bridged ferrocenophanes,[13] by transition-metal-catalyzed ROP[14] and also by anionic polymerization.[15] Especially the latter technique allows one to produce PFS homopolymers with controlled molar mass and low polydispersities. In addition, because of the living character of this polymerization, well-

defined PFS containing block copolymers can be obtained with regular anionically polymerizable blocks such as polystyrene, polyisoprene, and many others.[16, 17] Because of the presence of iron and silicon atoms in the main chain, PFSs show a very high resistance to reactive ion etching (RIE).[18, 19] Oxygen plasma treatments lead to the formation of iron-silicon oxide layer domains in PFS-covered areas, which prevents further removal of PFS in oxygen RIE, while the high resistance to fluorocarbon and SF_6 RIE allows pattern transfer into silicon, silicon oxide, and silicon nitride substrates.[20]

Methods for PFS-based lithography where generated patterns were transferred into various substrates include soft lithography, involving the use of PFS homopolymers as inks,[21, 22] and block copolymer lithography where self-assembly of hybrid organic-organometallic block copolymers followed by etching led to nanoperiodic structures with feature sizes down to 20 nm in silicon substrates[20] and even in thin metal films.[23] The use of poly(ferrocenylmethylphenylsilane) (PFMPS) as a thermal NIL resist was recently demonstrated by us.[24] Polymer patterns formed after thermal imprinting were directly transferred into silicon substrates. In order to obtain high aspect ratios, the residual layer was completely removed by argon sputtering because direct etching without removal of the residual layer gave rise to oxide layer formation, which prevented further pattern transfer. Although the direct thermal imprinting process into PFMPS enabled us to transfer the patterns into the substrate, shortcomings were observed when the feature sizes became smaller. Small features below 100 nm were not transferred faithfully into the substrate because they were damaged during argon sputtering. Additional benefits of UV-NIL such as higher throughput and elimination of thermal cycling, as discussed above, make the development of a UV-NIL process based on PFSs desirable.

In this chapter, patterns of PFMPS were created on a template made by step-and-flash imprint lithography (SFIL) using a UV-curable resist.[25] This approach is an example of a bilayer-type SFIL process because two different materials are used with different etch selectivities[26] and PFMPS is used as the top resist. The choice of the top resist is critical for successful dry etching into silicon substrates because the masking layer that is to be etched should have a distinctly different etch selectivity over the underlying UV-curable resist. After patterning of the UV-curable resist, PFMPS is spin-coated onto the imprinted structures to form bilayer structures and subsequent treatment with argon and oxygen plasma provides patterns of PFMPS with good reproducibility because of the high etch contrast between the two polymers. The process prevents the formation of a residual layer of PFMPS and thus its cumbersome removal,[24] which thus constitutes an advantage over the direct hot embossing

of PFMPS. The technique allows the possibility of creating etch-resistant patterns of PFMPS with sizes down to the nanometer range. Moreover, using PFMPS in this process allows control of the critical dimensions. Because it is a bilayer process, the final pattern size is not defined by imprinting alone but also by subsequent etch processes, which makes the role of PFMPS highly important. It provides a very high selectivity over UV-curable resist due to its high iron and silicon content which is difficult to obtain with other imprint materials.

6.2 RESULTS & DISCUSSION

Poly(ferrocenylmethylphenylsilane) (PFMPS) was chosen as a resist, because it is an amorphous polymer due to the unsymmetric substitution on the silicon atom in the main chain. The use of an amorphous polymer is essential since crystallization may destroy the imprinted patterns. Also, PFMPS forms homogeneous films. Figure 6.1 summarizes the bilayer-type SFIL process which consists of the fabrication of patterns of a UV-curable monomer, deposition of PFMPS on this template, and the etch sequence steps for transferring the patterns into the substrate. The imprint material was dispensed onto the transfer layer-coated substrates and the template was brought into contact with the still liquid imprint material. The transfer layer provided a good adhesion of the imprint material to the substrate. After exposure and curing of the imprint material, the template was demolded from the substrate, leaving its negative 3D image. The PFMPS was spin coated on top of the imprinted structures, creating an organometallic layer with a corresponding thickness variation. Argon plasma treatment was performed to homogeneously etch down the polymer in order to expose the organic imprint material. Subsequent treatment with oxygen plasma led to removal of the exposed organic imprint material and the PFMPS lines were transferred into the substrate, leading to pattern inversion.

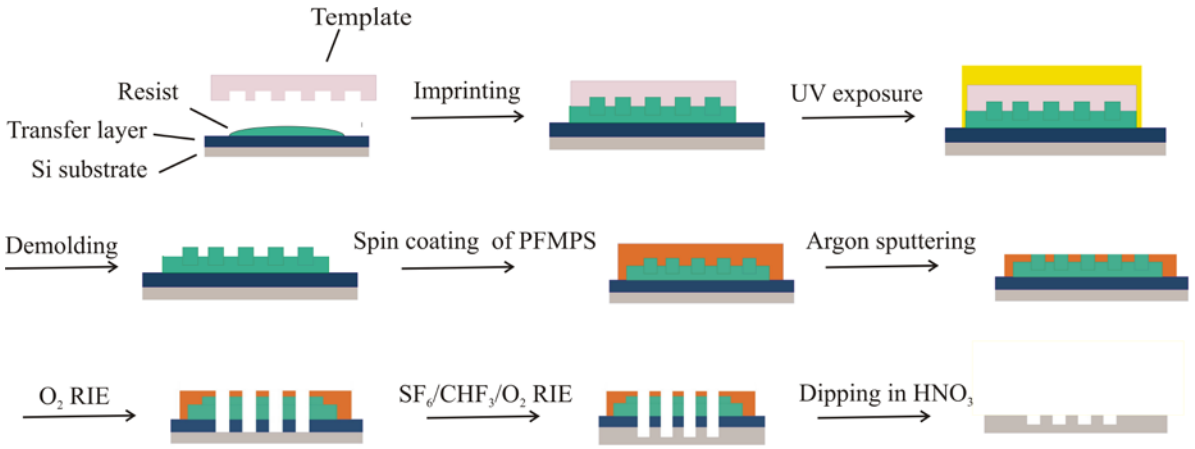

Figure 6.1 Fabrication process for creating PFMPS RIE resist patterns and subsequent pattern transfer into the underlying substrate.

The S-FIL™ method[25] used to create patterns on a substrate, consisting of lines of 100 nm wide with pitches of 1:1, 1:2 and 1:3 and with a height of 100 nm, is shown in Figure 6.2. Figure 6.3 shows a cross-section image of the imprinted lines after spin-coating PFMPS onto the imprinted structures. As seen in the cross section SEM image in Figure 6.3, the thickness of the transfer layer was 60 nm and the residual UV-curable resist layer after imprinting was about 40-50 nm. The dispensing conditions were optimized to obtain such thin residual layers after imprinting. Since the dispensed monomer was crosslinked upon UV-curing, spin coating of a solution of PFMPS in toluene did not affect the resist patterns. The thickness of the PFMPS polymer between the resist lines after spin-coating was determined to be 120 nm, while on top of the UV-imprinted structures it was about 60 nm. It is crucial to adjust the layer thickness to planarize the features. The PFMPS thickness applied here appeared to be sufficient for covering the nanometer and micrometer features completely with sufficient planarization (see also Figure 6.4, below). The PFMPS provided good wetting and adhesion performance to the imprint material which is important for subsequent processing.

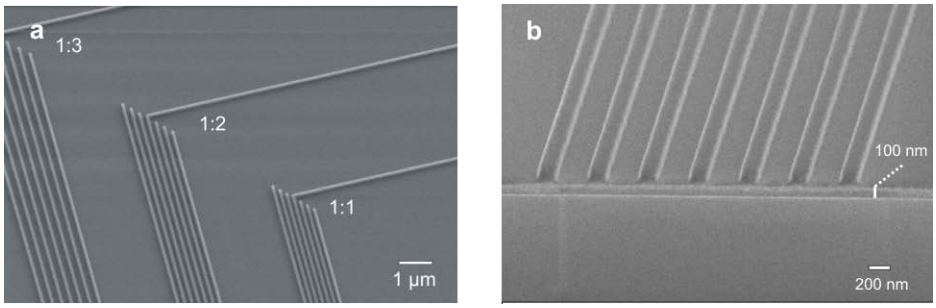

Figure 6.2 SEM images of UV-imprinted structures of (a) lines of 100 nm wide with pitches of 1:1, 1:2 and 1:3 and with a height of 100 nm (b) lines of 100 nm height showing the total thickness of the residual UV-curable resist layer and the transfer layer.

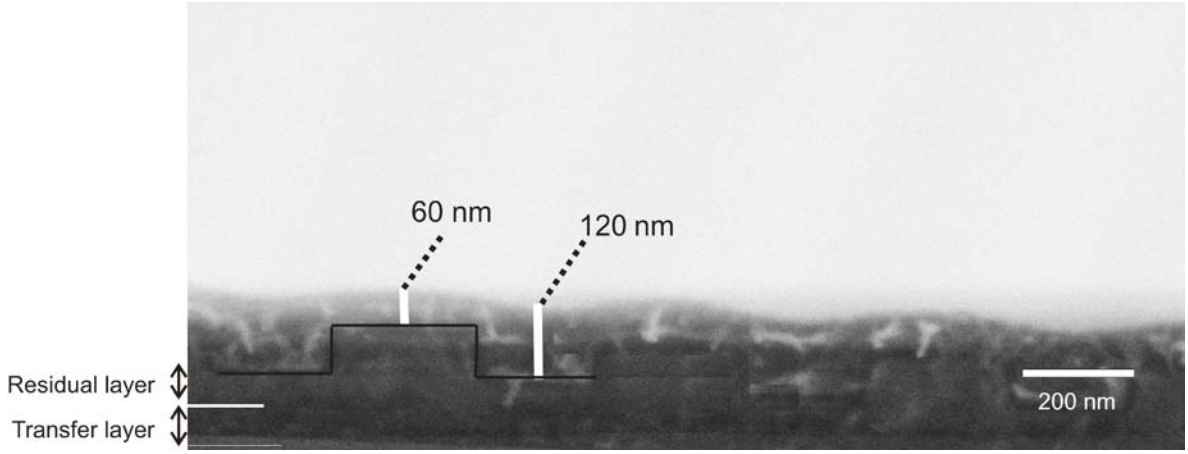

Figure 6.3 SEM image of a PFMPS layer spin coated on top of imprinted resist lines.

The PFMPS layer was etched back homogeneously in an argon plasma to reveal the top of the imprinted structures (Figure 6.4). The etch rate of PFMPS upon argon sputtering was determined to be 1.5 nm min^{-1}. Taking this etch rate into consideration, the time of the argon sputtering treatment was varied from 15 to 25 min. A time of 15 min proved to be insufficient for exposing the resist lines (Figure 6.4a), whereas after 25 min the PFMPS layer was removed, while the resist line shapes were not affected adversely (Figure 6.4b, c). Opening of the imprinted areas could only be achieved by argon sputtering since oxygen plasma results in highly etch resistant oxide formation, as mentioned before.[24]

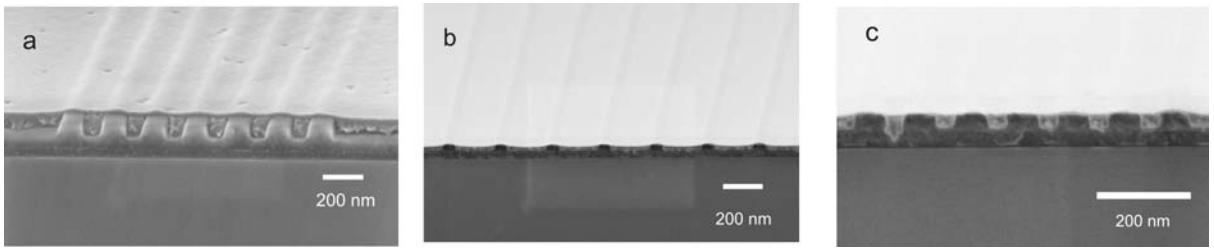

Figure 6.4 SEM images of PFMPS structures after argon plasma treatment to expose the imprinted lines (a) for 15 min, and (b, c) for 25 min. Prior to argon sputtering, PFMPS was spin coated on top of the UV-imprinted resist lines.

The argon sputtering step was followed by O_2 RIE during which the exposed organic imprint layer and the transfer layer material underneath were selectively etched through. During this treatment, the PFMPS was oxidized to form a hard Fe/Si oxide layer which allowed further pattern transfer into the substrate.[18] The O_2 RIE etch rates of PFMPS and the organic imprint material were found to be 1 and 60 nm/min, respectively, which results in an etch selectivity of 60. Two minutes of treatment with oxygen plasma was sufficient to remove the imprint material down to the substrate as shown in Figures 6.5a and 6.5b for features of 80 and 30 nm lines, respectively. PFMPS lines down to 30 nm were obtained after oxygen plasma treatment as shown in Figure 6.5b. The PFMPS lines revealed a linewidth roughness of about 5 nm (for the thinner lines, Figure 6.5b), which is similar to the edge roughness of the lines on the template used during imprinting. The imprint and sputtering processes apparently did not add additional linewidth roughness to the PFMPS features.

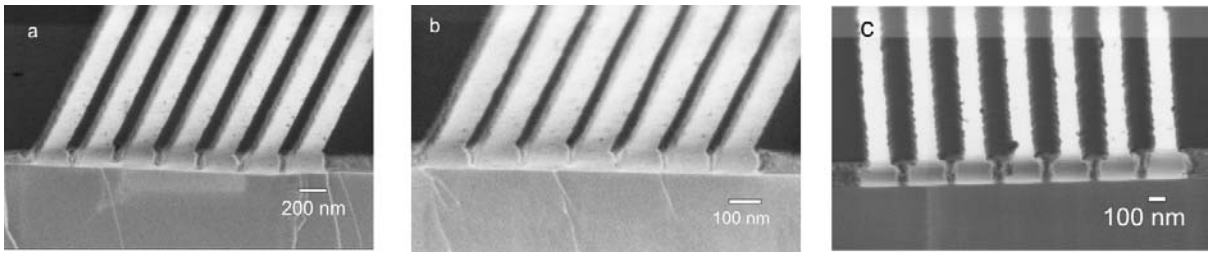

Figure 6.5 SEM images of lines fabricated after O_2 RIE of (a) 80 nm PFMPS lines and (b) 30 nm PFMPS lines after 2 min of treatment. (c) 100 nm PFMPS lines after a 2.5 min treatment. Prior to O_2 RIE, the samples were coated with PFMPS and then etched back for 25 min by argon sputtering. The dark stripes in the images correspond to PFMPS lines.

Figure 6.5a and 6.5b show the occurence of some degree of undercutting upon extension of the O_2 plasma treatment. Figure 6.5c demonstrates the undercut profile obtained

upon increasing the oxygen plasma treatment to 2.5 minutes. Nevertheless, the material in between the PFMPS lines was completely removed while the width of the PFMPS areas remained intact, which are required for transferring these lines into the underlying substrate.

Upon pattern transfer into the underlying Si substrate, RIE with CHF_3 and SF_6 was tested. The thickness of the PFMPS etch mask remained almost the same upon exposure to CHF_3 and SF_6 plasmas. Etch rates of 300 nm/min into Si and around 1 nm/min into the PFMPS layer were found, resulting in an etch contrast of approximately 300. Different etch profiles were obtained by tuning the composition of the gas mixture in the plasma. Figure 6.6a shows the lines etched with a mixture of CHF_3 (25 sccm), O_2 (20 sccm) and SF_6 (30 sccm) for 1 min.[27] Figure 6.6b shows the etching profile attained after decreasing the amount of CHF_3 and SF_6 in the plasma while keeping the amount of oxygen constant. The profile has a rounded shape for the mixture of CHF_3 (20 sccm) and SF_6 (24 sccm). A decrease in CHF_3 (18 sccm) and SF_6 (20 sccm) resulted in profiles which were tapered with an aspect ratio of 3 in case of 2 min of etching (Figure 6.6c). The profile became more vertical with a flat surface at the bottom after a 10 % decrease in the amount of CHF_3 and SF_6 (Figure 6.6d).

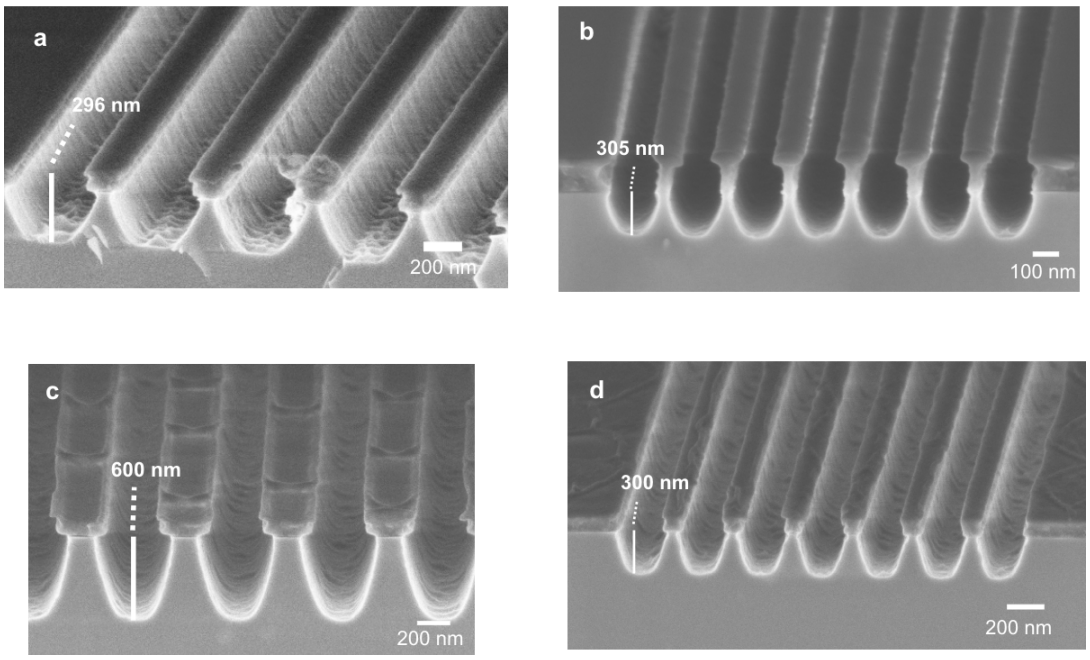

Figure 6.6. SEM images of samples etched with $CHF_3/O_2/SF_6$ (gas flow rates in sccm) (a) (25/20/30) for 1 min for 200 nm lines. (b) 20/20/ 24 for 1 min for 100 nm lines (c) 18/20/20 for 2 min for 200 nm lines (d) 16/ 20/18 for 1 min for 100 nm lines. Organometallic resist material is still present on top of the lines.

The different profiles obtained can be correlated to the oxygen content in the plasma. Increase in the relative oxygen content likely enhances passivation of the vertical silicon surfaces with an SiO_xF_y layer and therefore enables the process to become more anisotropic.[28] It was also observed that changes in pattern dimensions can influence the etching characteristics. In Figure 6.7a, the walls obtained were more vertical than the line patterns in Figure 6.7b, even though they were treated under the same plasma conditions.

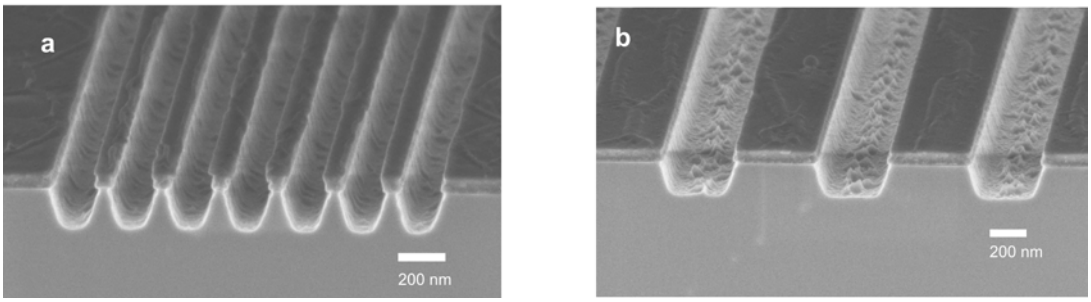

Figure 6.7 Profile obtained after treatment with $CHF_3/O_2/SF_6$ (in sccm) 16/20/18 during 1 min (a) for 100 nm lines (b) for 500 nm lines.

Figure 6.7 exemplifies the stability of the PFMPS resist after exposure to an O_2 containing plasma. Even though the resist is very stable, it could be easily removed in dilute nitric acid followed by sonication in toluene. Figure 6.8a demonstrates grooves fabricated in Si with an aspect ratio of 3 after 3 min of wet etching and Figure 6.8b shows 500 nm lines with an aspect ratio of 1 after 1 min of etching followed by removal of the resist material.

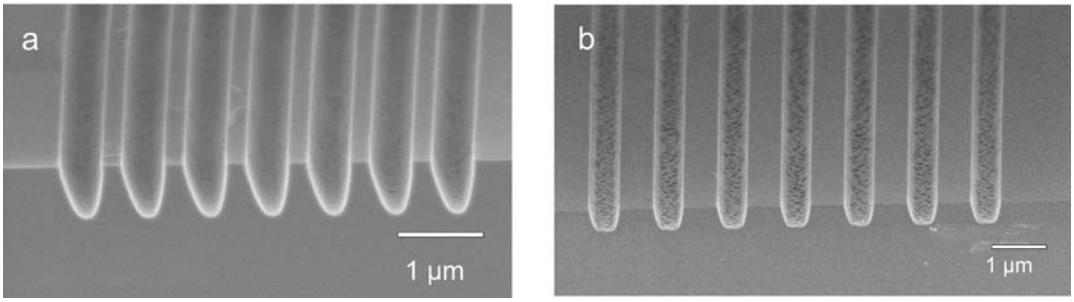

Figure 6.8 SEM images of fabricated lines after removal of resist material, imprint material and transfer layer in dilute nitric acid and toluene (a) after etching with a mixture of CHF_3 (18 sccm), O_2 (20 sccm) and SF_6 (20 sccm) for 500 nm lines for 2 min and (b) after etching with a mixture of CHF_3 (16 sccm), O_2 (20 sccm) and SF_6 (18 sccm) for 1 µm lines for 1 min.

6.3 CONCLUSIONS

We have shown the fabrication of polymeric structures with lateral dimensions down to 30 nm and aspect ratios of up to 3 in a bilayer-type UV-NIL process. The organometallic polymer PFMPS was spin-coated onto a UV-NIL patterned substrate, followed by an argon plasma treatment to expose the imprint material. Removal of the imprint material with oxygen plasma gave rise to PFMPS patterns forming a negative replica of the template employed. Pattern transfer into silicon sustrates was accomplished by the use of a $CHF_3/SF_6/O_2$ plasma. Variations of the plasma composition led to different etch profiles. This process offers the possibility for combining the advantages of UV-NIL with the high etch resistance of poly(ferrocenylsilanes) to produce features sizes down to the sub-100 nm range, and may be of use in areas such as data storage, microelectronics and bioelectronics.

6.4 EXPERIMENTAL

6.4.1 Polymer Synthesis

[1]Methylphenylsilaferrocenophane was prepared as described earlier.[16, 29] The monomer was purified by several crystallizations from n-heptane at –70 °C followed by vacuum sublimation. Transition metal-catalyzed ring opening polymerization of [1]methylphenylsilaferrocenophane was carried out in the presence of Et_3SiH with the addition of Karstedt's catalyst (14). The polymer was then precipitated in n-heptane. Molar mass characteristics of the polymer were determined by gel permeation chromatography (GPC) measurements in THF using polystyrene calibration. M_w = 49501 g/mol, M_n = 44643 g/mol, and M_w/M_n = 1.109.

6.4.2 Pattern Fabrication

Patterns were generated using UV-based nanoimprint technology. All the imprints were carried out on an Imprio 55 from Molecular Imprints Inc., using their S-FIL process (25). As a substrate, double side polished Si wafers were used, which were also coated with a thin transfer layer applied by spin coating and hot baking in order to achieve a good adhesion of the imprint material to the substrate. DUV 30J was used as the transfer layer. The quartz template employed for the imprints consisted of lines with feature sizes from tens of µm down to sub-50 nm. Prior to imprinting, the template was treated with a release layer in order to prevent sticking of the imprint material to the template. The release layer used was perfluoro-1,1,2,2-tetrahydrooctyltrichlorosilane which is used to modify the template surface energy. The surface treatment procedure used in this process started with the cleaning of the

template with a piranha solution (conc. H_2SO_4 and 33% aq H_2O_2 in a 3:1 volume ratio, ***Warning!*** *piranha should be handled with caution; it can detonate unexpectedly*) for 30 min to remove any surface organic contaminants. After the piranha treatment, the substrates were blown dry with N_2 and reacted with the alkyltrichlorosilane (6). Imprinting was performed using a low-viscosity acrylate-based organic SFIL resist. (Monomat, Molecular Imprints Inc.) The imprint material was deposited by direct dispensing, where the volume was locally adjusted to the pattern definition. After dispensing, the template was pressed into the still liquid imprint material and held for 20 s under a pressure of 50 mbar to fill all the features. Thereafter, the imprint material was cured by UV light irradiation through the transparent template, followed by demolding.

6.4.3 Pattern Transfer

The synthesized PFMPS was spin coated on top of the imprinted resist. Argon plasma sputtering was applied for 20-25 min (Ion Beam Etcher, 350 V, 6 mA) in order to expose the organic imprint material. The imprinted resist features were subsequently etched with oxygen plasma to expose the PFMPS lines. Oxygen reactive ion etching to remove the imprinted resist was performed in an Elektrotech PF 340 apparatus (8 mTorr, 50 W, 20 sccm O_2). Etching into the substrate using the PFMPS lines as a template was enabled with different mixtures of CHF_3, O_2 and SF_6 at a pressure of 10 mTorr. The resist was stripped off by sonication for 1 h in 10% nitric acid solution followed by sonication in toluene.

SEM characterization was performed with a HR-LEO 1550 FEF SEM.

6.5 ACKNOWLEDGEMENTS

We thank Mark Smithers for acquiring the SEM images.

6.6 REFERENCES

[1] S. Y. Chou, P. R. Krauss, P. J. Renstrom, *Appl. Phys. Lett.* **1995**, *67*, 3114.

[2] S. Y. Chou, P. R. Krauss, P. J. Renstrom, *Science* **1996**, *272*, 85.

[3] M. Bender, M. Otto, B. Hadam, B. Vratzov, B. Spangenberg, H. Kurz, *Microelectron. Eng.* **2000**, *53*, 233.

[4] S. J. M.Colburn, M. Stewart, S. Dample, T. Bailey, B. Choi, M. Wedlake, T. Michaelson, S. V. Sreenivasan, J. G. Ekerdt, C. G. Willson, *Proc. SPIE* **1999**, 379.

[5] M. D. Stewart, S. C. Johnson, S. V. Sreenivasan, D. J. Resnick, C. G. Willson, *J. Microlithogr. Microfabr. Microsyst.* **2005**, *4*.

[6] T. Bailey, B. J. Choi, M. Colburn, M. Meissl, S. Shaya, J. G. Ekerdt, S. V. Sreenivasan, C. G. Willson, *J. Vac. Sci. Technol. B* **2000**, *18*, 3572.

[7] J. H. Choi, S. W. Lee, D. G. Choi, K. D. Kim, J. H. Jeong, E. S. Lee, *J. Vac. Sci. Technol. B* **2008**, *26*, 1390.

[8] H. Schmitt, L. Frey, H. Ryssel, M. Rommel, C. Lehrer, *J. Vac. Sci. Technol. B* **2007**, *25*, 785.

[9] N. Sakai, J. Taniguchi, K. Kawaguchi, M. Ohtaguchi, T. Hirasawa, *J. Photopolym. Sci. Technol.* **2005**, *18*, 531.

[10] J. C. Eloi, L. Chabanne, G. R. Whittell, I. Manners, *Mater. Today* **2008**, *11*, 28.

[11] K. Kulbaba, I. Manners, *Macromol. Rapid Commun.* **2001**, *22*, 711.

[12] G. R. Whittell, I. Manners, *Adv. Mater.* **2007**, *19*, 3439.

[13] D. A. Foucher, B. Z. Tang, I. Manners, *J. Am. Chem. Soc.* **1992**, *114*, 6246.

[14] P. GomezElipe, P. M. Macdonald, I. Manners, *Angew. Chem. Int. Ed. Engl.* **1997**, *36*, 762.

[15] R. Rulkens, Y. Z. Ni, I. Manners, *J. Am. Chem. Soc.* **1994**, *116*, 12121.

[16] Y. Z. Ni, R. Rulkens, I. Manners, *J. Am. Chem. Soc.* **1996**, *118*, 4102.

[17] C. Kloninger, M. Rehahn, *Macromolecules* **2004**, *37*, 1720.

[18] R. G. H. Lammertink, M. A. Hempenius, V. Z. H. Chan, E. L. Thomas, G. J. Vancso, *Chem. Mater.* **2001**, *13*, 429.

[19] I. Korczagin, R. G. H. Lammertink, M. A. Hempenius, S. Golze, G. J. Vancso, in *Ordered Polymeric Nanostructures at Surfaces, 200*, **2006**, 91.

[20] R. G. H. Lammertink, M. A. Hempenius, J. E. van den Enk, V. Z. H. Chan, E. L. Thomas, G. J. Vancso, *Adv. Mater.* **2000**, *12*, 98.

[21] I. Korczagin, S. Golze, M. A. Hempenius, G. J. Vancso, *Chem. Mater.* **2003**, *15*, 3663.

[22] M. A. Hempenius, R. G. H. Lammertink, M. Peter, G. J. Vancso, *Macromol. Symp.* **2003**, *196*, 45.

[23] J. Y. Cheng, C. A. Ross, V. Z. H. Chan, E. L. Thomas, R. G. H. Lammertink, G. J. Vancso, *Adv. Mater.* **2001**, *13*, 1174.

[24] C. Acikgoz, M. A. Hempenius, G. J. Vancso, J. Huskens, *Nanotechnology* **2009**, *20*, 135304.

[25] S. V. S. D. Resnick, C. G. Willson, *Mater. Today* **2005**, *34*.

[26] I. M. S. V. Sreenivasan, F. Xu, D. Wang, N. Stacey, *Micro Magazine* **2005**.

[27] H. Jansen, M. Deboer, R. Legtenberg, M. Elwenspoek, *J. Micromech. Microeng.* **1995**, *5*, 115.

[28] R. Legtenberg, H. Jansen, M. Deboer, M. Elwenspoek, *J. Electrochem. Soc.* **1995**, *142*, 2020.

[29] K. Temple, J. A. Massey, Z. H. Chen, N. Vaidya, A. Berenbaum, M. D. Foster, I. Manners, *J. Inorg. Organomet. Polym.* **1999**, *9*, 189.

Chapter 7

Exploiting Nanoimprint Lithography for Polymer Brush Engineering and Protein Immobilization

ABSTRACT. In this chapter the combination of step-and-flash imprint lithography and surface initiated polymerization is described to obtain topologically and chemically patterned surfaces. Following fabrication of patterns with lateral dimensions from several microns down to the sub-100-nm range, the residual layer between the imprinted lines was etched down to expose the silicon substrate. Self-assembled monolayers (SAMs) of initiators were anchored to the exposed silicon, and brushes of polystyrene (PS), poly(glycidyl methacrylate) (PGMA), and poly(ethylene glycol methacrylate) (PEGMA) were grown on the initiator-covered areas. PEGMA brush structures were functionalized with succinic anhydride and their swelling properties to different pH were investigated. The variety of the structures enabled us to study the dependence of the size of the patterns on the height of the polymer brush patterns. The functionalized patterned PEGMA layers were used for selective immobilization of proteins. For this purpose, biotin and subsequently streptavidin were immobilized on PEGMA brush layers. Protein patterns were successfully generated and AFM analysis was used to calculate the amount of protein attached on a particular pattern.

7.1 INTRODUCTION

Patterned nanostructures of polymer films have a wide range of applications in biochips, biosensors and photonic crystal materials.[1-5] Stable, covalently bonded polymer films represent a versatile tool to synthesize tunable platforms and allow one to tailor the chemical, mechanical and energetic properties of surfaces. A covalent attachment of the polymers to the surface is desirable especially in biological systems where the patterned surface comes in contact with solvents and with other molecules which might lead to a complete displacement of the polymer film and the loss of the pattern.[6] Different living cationic,[7] anionic,[8] ring opening,[9] nitroxide mediated,[10] and atom transfer radical polymerization[11] (ATRP) reactions have been successfully employed to give surface-grafted polymers under controlled growth conditions providing excellent mechanical stability and functionality and controllable brush length. The formation of dense polymer brushes is possible through a grafting from approach in which covalently attached polymers are grown by surface-initiated polymerization from the substrate (SIP).[12] In SIP, the polymer chains are grown from surface-bound initiators which are self-assembled monolayers [13] of suitably functionalized alkyl-chlorosilanes and alkanethiols. SIP could provide control over the shape, feature dimensions and funtionality of brush architectures when it is combined with other patterning techniques and would allow to fabricate macromolecular sensors, single-protein platforms, antifouling surfaces and nano-fluidic devices with controlled dimensions.[14-16]

Several techniques such as photolithography, microcontact printing,[17, 18] chemical lithography,[19] contact molding,[20] and electron beam lithography[14, 21, 22] have been explored to pattern polymer brushes in combination with a grafting from approach. Of the many patterning techniques studied, imprint lithography shows great promise since it is a low-cost, high-throughput process and larger areas can be patterned simultaneously. Smaller features could be fabricated by thermal imprinting[23, 24] or light-initiated polymerization[25] (UV-NIL) and these techniques have circumvented many limitations of conventional techniques.[26] Step-and-flash imprint lithography (SFIL), a UV-NIL variant, uses a photocurable prepolymer solution as a resist to replicate the topography of a mold.[27] In SFIL, a low viscosity, photocurable liquid or solution is not spin coated but dispensed in the form of small droplets onto the substrate to fill the voids of the quartz mold. The solution contains low molar mass monomer and a photoinitiator. Exposing this solution to UV light cures the photopolymer to make a solidified replica while in contact with the mold. Removing the mold leaves the inverse replica on the substrate. Because of the ability to pattern at room temperature and at low pressure, the template can be stepped to pattern the

whole wafer area as in a stepper lithography tool. Pattern sizes with lateral dimensions from several microns down to the sub-100 nm range could be achieved.[28]

Although detailed aspects of the synthesis and characterization of brushes have been studied, the preparation and the confinement of polymer brush patterns have still to be investigated and new methods for confining polymeric materials in precisely defined positions are needed. Therefore, the development of a fabrication process using a simple, cost-effective, high throughput and large area patterning technique with nanometer resolution is very important for further progress in polymer brush engineering. In the first part of this chapter, we describe a new approach to prepare polymer brush patterns from several microns down to 50 nm with the step-and-flash imprint lithography technique in which brush patterns are created on a template made by SFIL using SIP. The combination of these two techniques (SFIL and SIP) allows the modification of patterned surfaces by means of introducing functional groups on specific positions. Brush line-widths down to 50 nm were obtained thus accomplishing grafting of few tens of polymer chains in between the patterns created by SFIL. In our approach, following patterning of the UV-curable resist, the residual layer between the imprinted lines was etched down by oxygen plasma in order to expose the silicon substrate. Onto these pre-patterned samples, the appropriate initiator molecule was deposited, followed by growing of the polymer brush. Different types of polymer brushes were grown on this pre-patterned substrate such as polystyrene (PS), poly(glycidyl methacrylate) (PGMA), and poly(ethylene glycol methacrylate) (PEGMA). We chose water-soluble monomers such as poly(ethylene glycol methacrylate) and water-methanol soluble glycidyl methacrylate, as well as the water-insoluble monomer styrene to demonstrate the scope of our approach.

Surface initiated ATRP is an effective method for the preparation of brushes with a broad range of chemical and structural properties. The brush obtained could interact with biological macromolecules, supramolecular assemblies and cells.[29-31] Futhermore, patterned brush structures enable selective anchoring of proteins which also minimizes nonspecific adsorption. The non specific adsorption involves relatively weak and reversible interactions thus causing leaching of proteins from the support which results in loss of activity and contamination of surrounding media.[32] For more stable attachment, the formation of covalent bonds is required and these can be formed by coupling the functional group on the brush surface with the functional groups on the protein surface. The use of SFIL allows one to reduce the feature size to the nanoscale to create high density polymer brush patterns, enabling the attachment of individual proteins. In the second part of the chapter, we

demonstrate the use of patterned PEGMA brushes as platforms for immobilization of proteins. To immobilize proteins, the brush patterned substrate was initially passivated with poly(ethylene oxide)-silane monolayers to prevent nonspecific adsorption in the grooves of the brush patterns. Then PEGMA was modified sequentially with succinic anhydride (SA), 1-ethyl-3-(3-dimethylaminopropyl)-carbodiimide (EDC) and *N*-hydroxysuccinimide (NHS), amino-biotin and finally streptavidin. The structure and morphology of the graft-functionalized silicon surfaces were characterized by Fourier transform infrared (FTIR) spectroscopy, and atomic force microscopy (AFM).

7.2 RESULTS & DISCUSSION

7.2.1 Preparation and Characterization of Brushes

Figure 7.1 shows the fabrication scheme of patterned polymer brushes via the combination of SFIL[27] and SIP. In the SFIL process, the acrylate based imprint material was dispensed onto the transfer layer-coated substrates, and the template was brought into contact with the still liquid imprint material. The transfer layer provided a good adhesion of the imprint material to the substrate. After exposure and curing of the imprint material, the template was demolded from the substrate, leaving its negative 3D image. To expose the silicon substrate in the grooves of the imprinted structures, the residual layer was removed by exposure to an oxygen plasma. The wafers were then reacted with an ATRP initiator and polymer brushes were grown from the ATRP initiator-covered regions. After polymerization, the resist lines were removed via sonication. In this process, the imprinted polymeric structures were used as template to grow brushes and the polymer template was removed following the brush synthesis. The removal of the polymer template could be also performed before brush synthesis but since the resist monomer was crosslinked upon UV-curing, the template formed can withstand subsequent polymerization conditions and stay intact during brush synthesis.

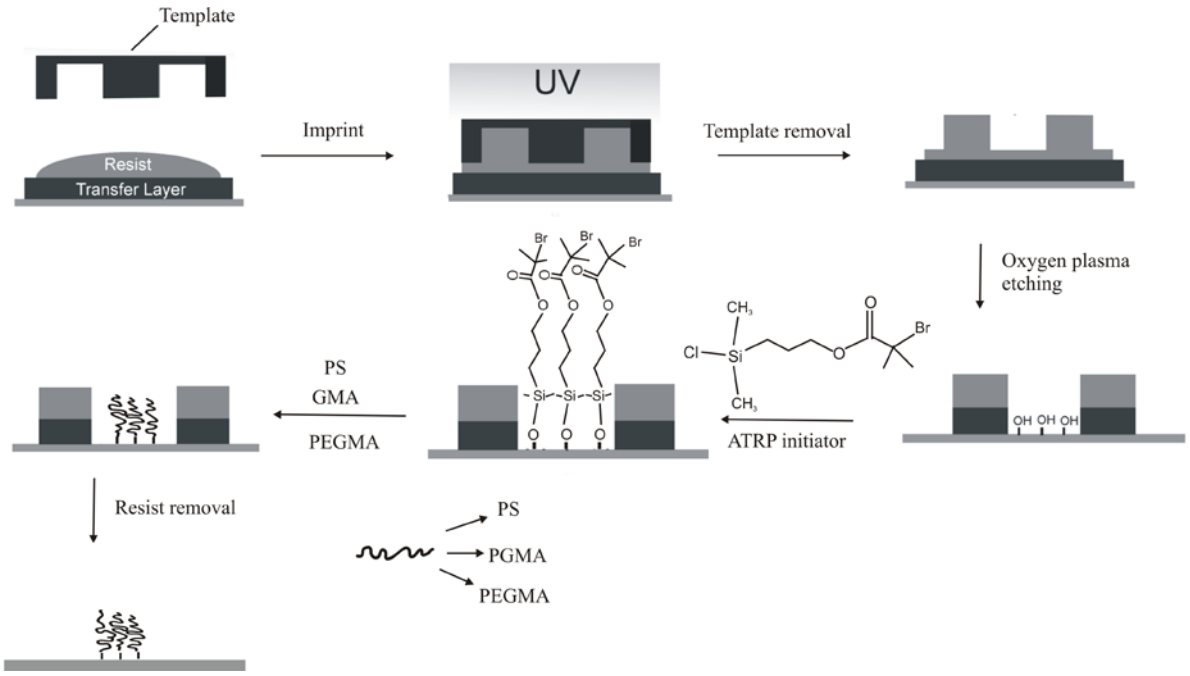

Figure 7.1 Fabrication process for creating polymer brush patterns.

The template used in the S-FIL™ process has patterns consisting of lines of 500 nm to 100 nm wide with pitches of 1:1, 1:2, 1:3, 1:4, 1:5 and with a height of 100 nm. The same template contains pillars and grooves with widths of 70 nm to 200 nm. Figure 7.2a shows the line patterns of 100 nm width onto a substrate with pitches of 1:1, 1:2 and 1:3 created on a substrate with this template. Figure 7.2b shows a cross-section image of the imprinted lines. As seen here, the combined thickness of the transfer layer and residual UV-curable resist layer following imprinting was about 40 nm. This rather thin residual layer thickness was achieved by optimizing the dispensing conditions. Subsequently, the samples were treated with oxygen plasma during which the exposed organic imprint layer and the transfer layer material underneath were removed. A short exposure time to oxygen plasma was sufficient to remove the imprint material down to the substrate as shown in Figure 7.2c. The height of the features of the lines after imprinting was around 100 nm. Following etching the exposed silicon oxide substrate was functionalized with the ATRP initiator which contains a bromoisobutyryl group.

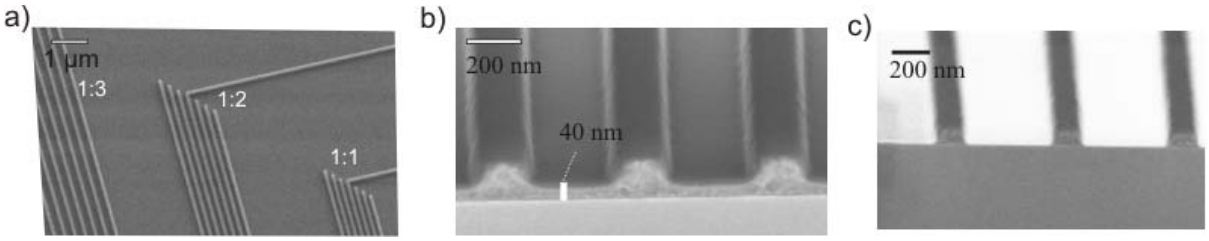

Figure 7.2 SEM images of UV-imprinted structures of (a) lines of 100 nm wide with pitches of 1:1, 1:2 and 1:3 and with a height of 100 nm. (b) SEM images of lines of 200 nm wide showing the total thickness of the residual UV-curable resist layer and the transfer layer. (c) SEM image of lines of 150 nm wide after removal of the residual layer by O_2 RIE.

Growth of dense brushes of PEGMA (Figure 7.3a) on silicon substrates by atom transfer radical polymerization was reported earlier by Xu et al.[33] In our case, using the prepatterned substrate, PEGMA brushes were obtained with the CuCl/$CuBr_2$/bipy catalyst system in aqueous solution at room temperature on prepatterned substrates (Figure 7.3b). The morphology of polymer brushes formed on the surfaces was investigated with tapping mode AFM imaging. Figure 7.3c captures an image of the PEGMA brushes after removal of the resist lines via sonication in acetone. Removal of the imprint material gave rise to PEGMA brush patterns forming a negative replica of the template employed (Figure 7.3c). The height of the brushes after polymerization was around 70 nm after 1 hour of polymerization as determined with AFM analysis (Figure 7.3d).

In order to prove the effective removal of the resist lines between the brush patterns, AFM and SEM analysis were performed. An AFM phase image (Figure 7.4e) shows the clear contrast between the brush (bright areas) and bare silicon surface (dark areas) and confirms the absence of any residual layer. In addition, the SEM image (Figure 7.4f) recorded for the same sample confirms that well-contrasted silicon regions can be recognized in between the brush patterns.

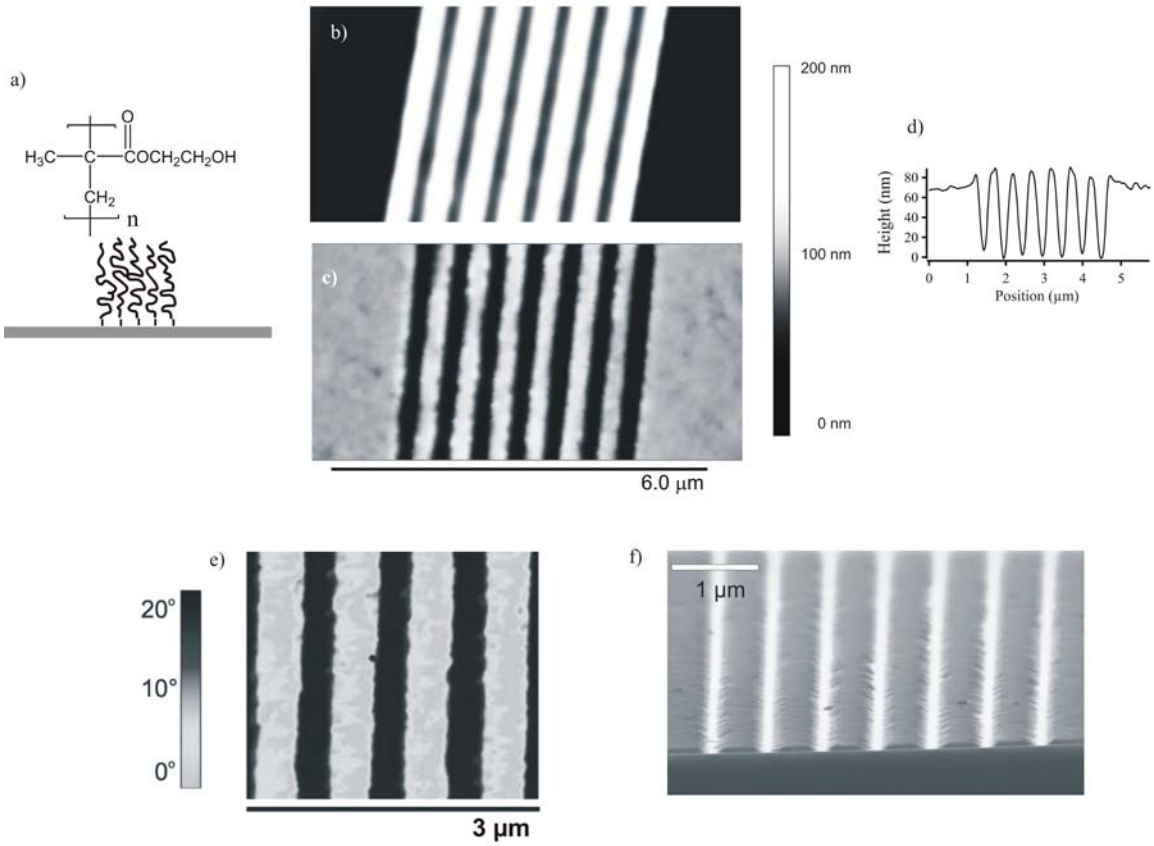

Figure 7.3 (a) Schematic of PEGMA brushes. (b) AFM image of the resist lines of 250 nm with a pitch of 1.2 obtained after etching. (c) AFM image of PEGMA brushes obtained after removal of the resist lines. (d) AFM height profile of the AFM image (c). (e) AFM image of corresponding AFM image (c). (e) SEM image of brush lines after resist removal.

The width of the polymer brushes obtained by using this approach strongly depends on the lateral feature width of the patterns.[34, 35] Figure 7.4a-e shows AFM images of a series of patterns after polymerization with resist patterns and Figure 7.4f-l shows brush patterns after polymerization and subsequent resist removal. The resist patterns used encompasses a series of 100 nm lines with 1:1, 1:2, 1:3, 1:4, 1:5 lateral distances, respectively. A typical imprinted series resulted in brush patterns characterized by average widths ranging from 500 for the 1:5 distance to 80 nm for the 1:1 distance (Figure f and l). Height values varied ranging from 80 to 30 nm (for the widest and narrowest patterns, respectively).

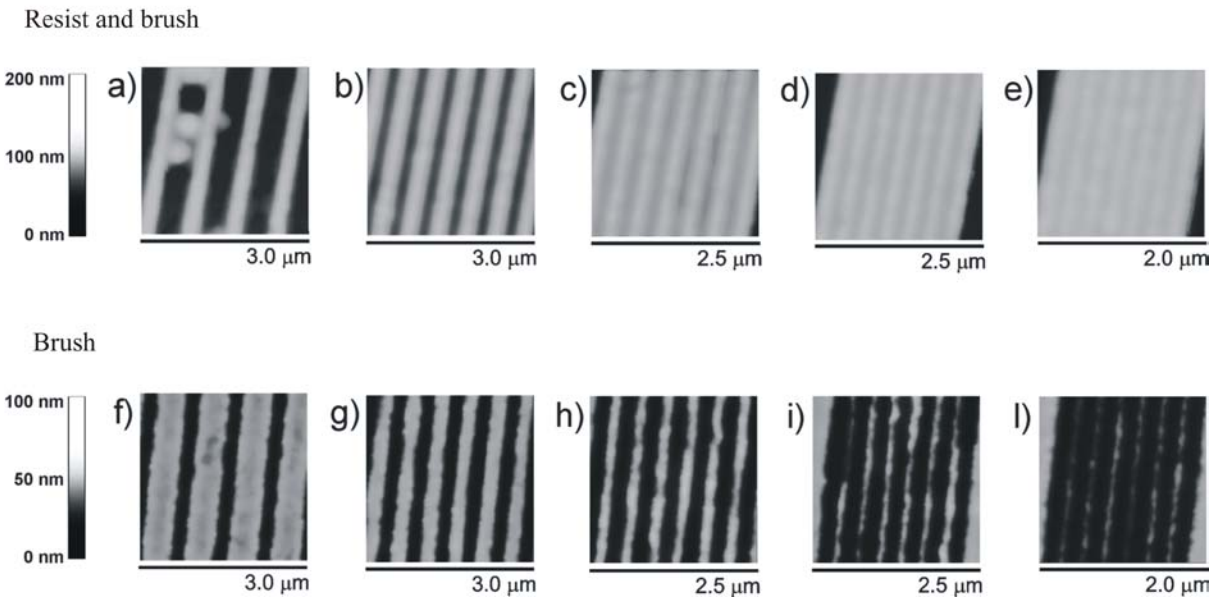

Figure 7.4 AFM images of a series of patterns after polymerization with resist patterns (a-e) and brush patterns after polymerization and subsequent resist removal (f-l).

As the lateral distance between the resist lines gets smaller, size effects becomes more evident and the brush height significantly decreases.[35] The AFM height profiles of the samples are displayed in Figure 7.5A before (grey cross-sections) and following (black cross-sections) removal of the resist lines for AFM imaging (see Figure 7.4a-l). In the graph in Figure 7.5B, the width/height of different brush patterns are plotted as a function of the average line-to-line resist distance. As it is clearly shown in the plot, not only the width of the brush features decreases when the resist lines are closer to each other, but also the height of the features follows a similar trend. When the distance between the resist lines increases, the height of the polymer brushes approaches the value of the thickness of the homogenous polymer film on unpatterned surface as one would anticipate. This behaviour is thought to be related to the density of initiator sites or to a monomer diffusion limitation which become more important when resist lines are more closely spaced. Polymer chains at the domain boundaries extend into the surrounding polymer-free areas resulting in a decrease in the height of the brush which could also explain the observed height decrease.[35]

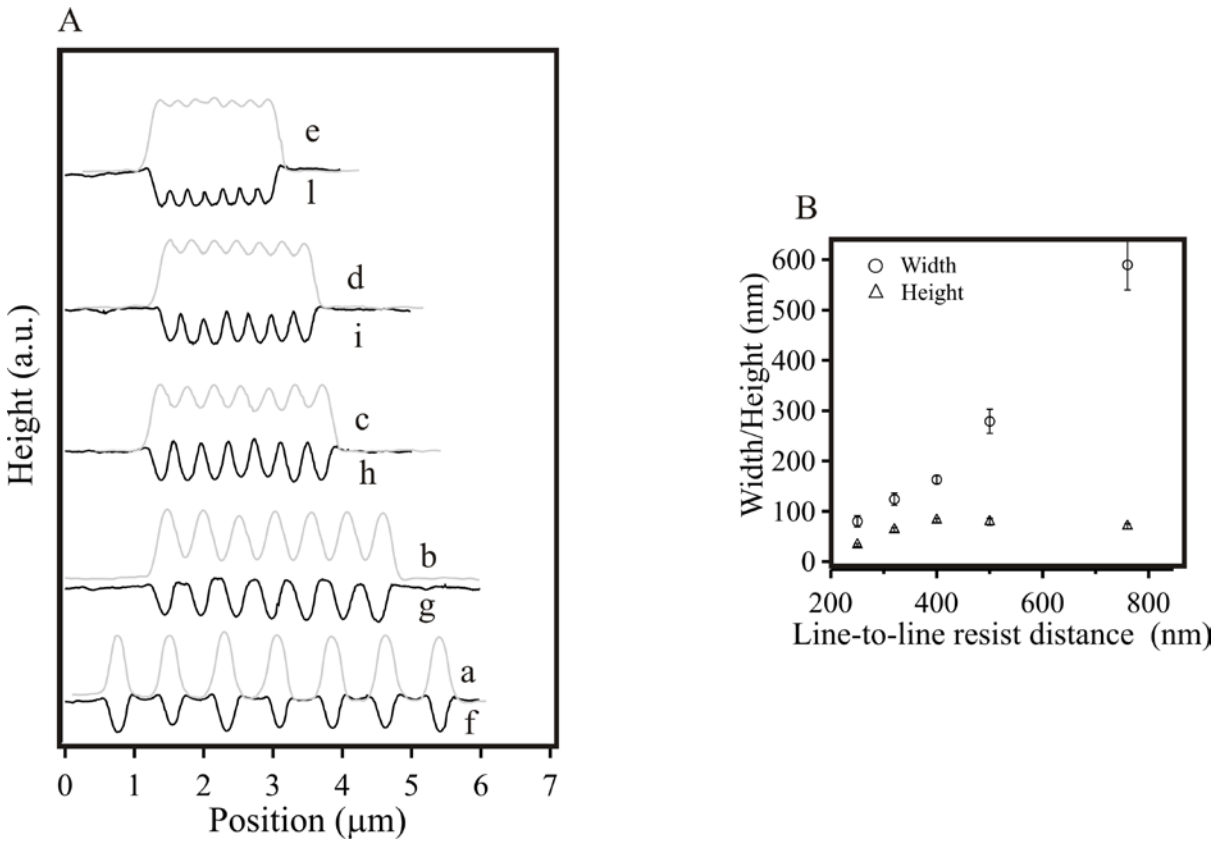

Figure 7.5 (A) Graph showing the height profile before before (grey cross-sections) and following (black cross-sections) removal of the resist lines. (B) Height vs width of brush patterns plotted as a function of the average line-to-line resist distance.

The S-FIL technique in principle allows one to achieve patterning on the nanometer scale which is one of the main advantages of this technique. Employing this method, we demonstrate the fabrication of polymer hedge-brushes of PEGMA having a width of 60 nm and a height of 10 nm (Figure 7.6). According to the lateral width of these features the constituent brush structures are formed by a few tens of grafted macromolecules.

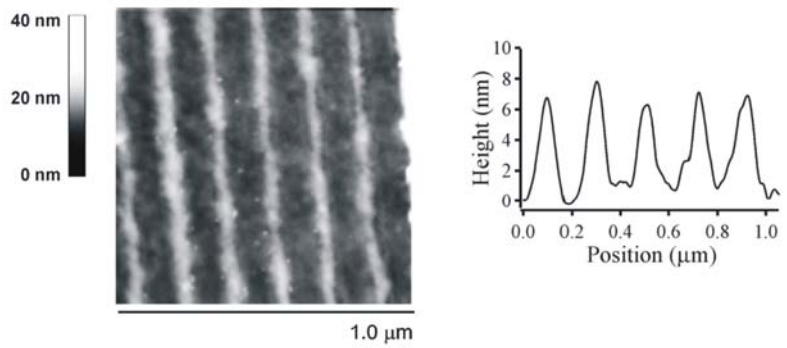

Figure 7.6 AFM image of polymer hedge-brushes of PEGMA obtained with high resolution.

To show the versatility of the approach, PS and PGMA brushes were grown on pre-patterned samples as well. PS brushes were synthesized from initiator-modified silicon substrates by ATRP at 60℃ (as shown in Figure 7.1).[8, 13] The height of the brushes obtained after 12 h of polymerization was 40 nm. The AFM image in Figure 7.7a shows the PS brush patterns with a lateral distance of 100 nm. The pillars (Figure 7.7b) have a width of approximately 40 nm after polymerization and variations in size have been observed. This could be due to swelling behavior of the resist during polymerization since was performed at high T and in bulk. The FTIR spectrum in Figure 7.7c shows the absorption bands corresponding to the symmetric and asymmetric stretching vibration of C–H along the main chain of PS appear between 2800 - 3000 cm^{-1}, whereas those at 3000 - 3200 $cm^{-1}$are assigned to the stretching vibration of the aryl C–H.

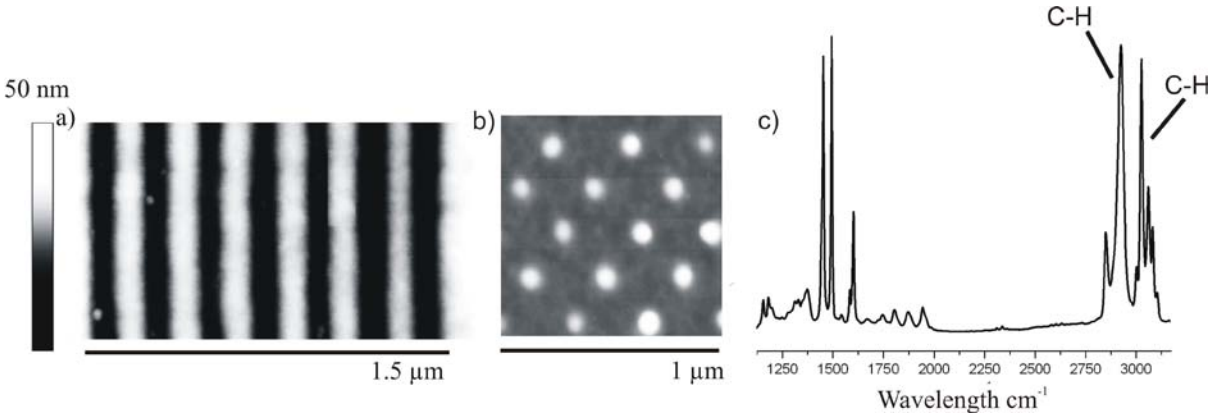

Figure 7.7 AFM images (a, b) and FTIR spectrum (c) of fabricated PS brushes

PGMA brushes may serve as a platform for many applications due to the presence of the epoxide functionalities and thus a chemical functionality which can be further exploited.[18, 36] PGMA brushes were grown by aqueous ATRP as reported earlier.[36] The PGMA structures were analyzed by AFM (Figure 7.8a). The height of the brushes was around 50 nm and they were highly uniform over large areas as seen in Figure 7.8b. FTIR shows the epoxide group peak at around 910 cm^{-1} which is a characteristic fingerprint of this moiety (Figure 7.8c).

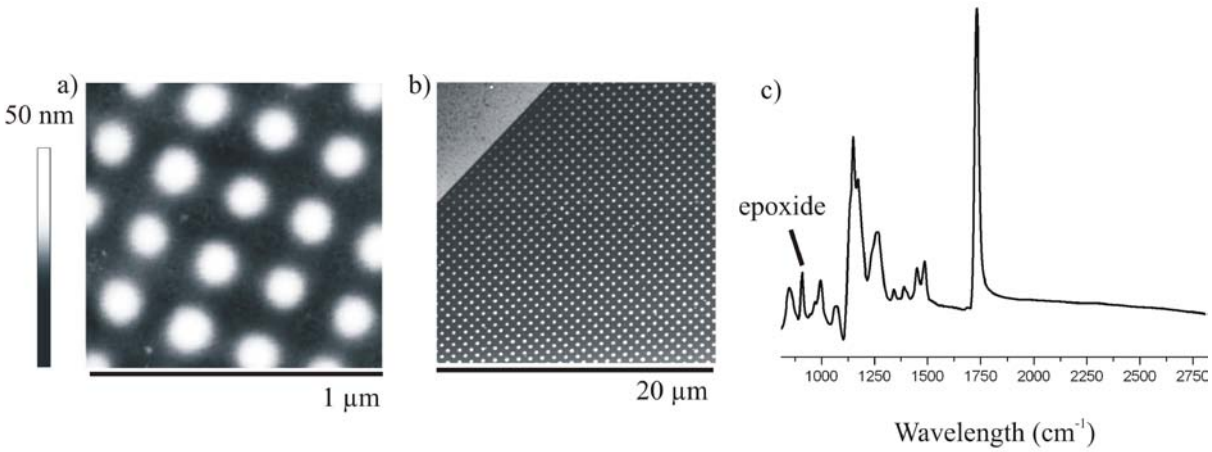

Figure 7.8 AFM images (a, b) and FTIR spectrum (c) of PGMA brushes**.**

7.2.2 PEGMA Brushes as Platforms for Immobilization of Proteins

To be used in biological applications, patterns must fulfill specific requirements, one of which is to create bio-interactive patterns in a non-interactive background. Poly(ethylene glycol)s (PEG)s are commonly used for the preparation of antifouling surfaces. Herein, we covalently couple proteins onto the protein resistant (biologically inert) PEG- based brushes by reacting the hydroxyl group of the PEG brushes via succinic anhydride (SA) and later on by NHS-assisted coupling of the specific biomolecules, thus ensuring a high ratio of specific to non-specific binding.[37] In order to achieve a selective immobilization onto the brush-hedge structures avoiding nonspecific adsorption to the surrounding substrate, the exposed silicon oxide surface was previously passivated via anchoring of PEO-silane species.

Biotin/streptavidin[38, 39] bioconjugates have been used as a model system to study the selective protein immobilization on patterned brushes and brush-hedge structures. Streptavidin with the highly specific interaction to the complementary biotin offers many advantages since the selective and specific interaction between them has been proven while simultaneously all other non-specific binding is being minimized. After binding of streptavidin is optimized with two remaining binding sites facing the aqueous phase, they can be used to bind and organize other functional units like antibodies, their fragments, colloids, oligonucleotides.[39] For immobilization, PEGMA surfaces were first activated and then reacted with biotin-PEG(10)-NH_2 and subsequently with streptavidin in PBS solution (Figure 7.9).

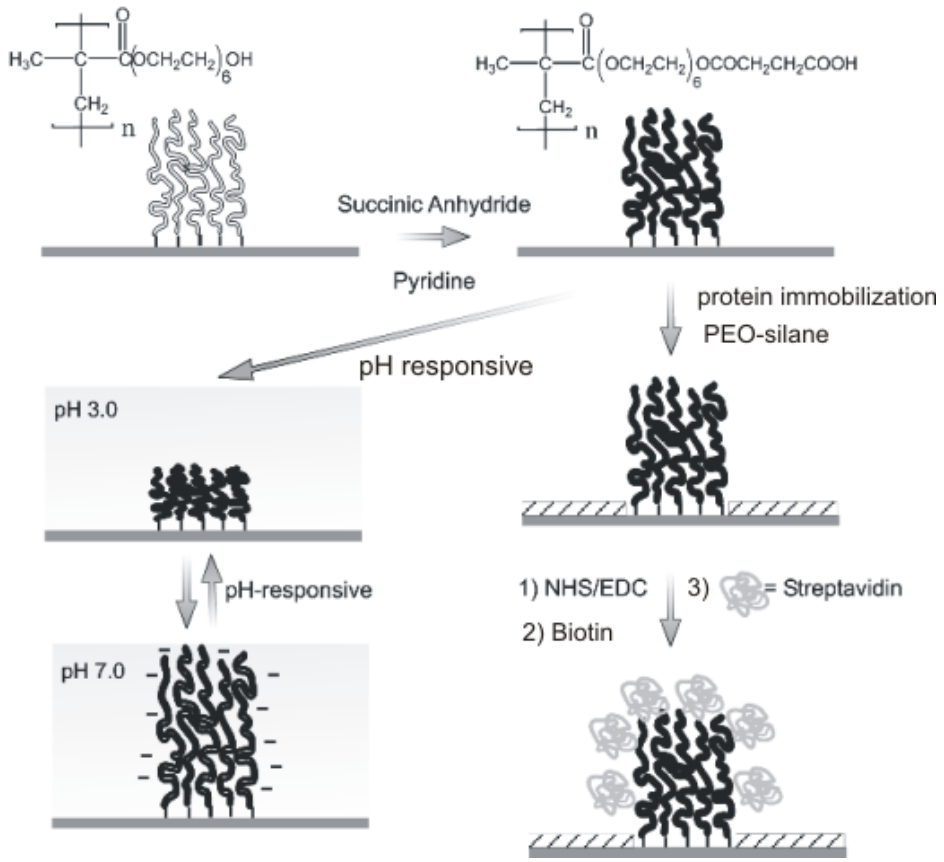

Figure 7.9 Schematics of brush functionalization with proteins and pH-responsive behavior.

PEGMA brush patterns were reacted with succinic anhydride in order to introduce carboxylic acid moieties along the polymer backbones (Figure 7.9). PEGMA samples having a thickness of 70 nm (Figure 7.10a) were incubated for 10 h in a dry pyridine solution of succinic anhydride. Following the reaction, the thickness was measured with AFM and determined to be 80 nm (Figure 7.10b). The increase in the thickness is due to the expected volume increase of the monomer units constituting the brushes (Figure 7.10c). Due to the presence of carboxylic acid moieties in the brush architecture, succinic anhydride functionalized PEGMA brushes display pH-dependent swelling properties. At pH 3.0 the polymer chains are protonated and charge neutral, and they display an average height value of 36 nm and width of 131 nm indistinguishable from the average dry height (Figure 7.11a). When the brush hedges are immersed in a pH 7.0 buffer solution, negative charges accumulate inside the brush structure, thus producing a profused swelling increment (Figure 7.11b). In this case, the average height value increases to 59 nm while the width reaches 140 nm. The graph plotted in Figure 7.11c (height vs pattern) clearly displays the pH-responsive behavior of the brush patterns.

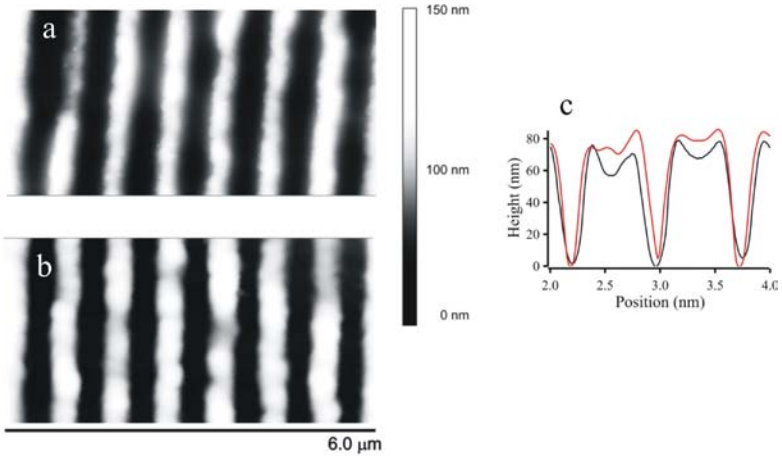

Figure 7.10 (a) AFM height image of PEGMA brush before treatment with SA. (b) AFM image of PEGMA brush after treatment with SA. (c) Cross sectional plot with (a) and (b) showing the height increase after SA treatment.

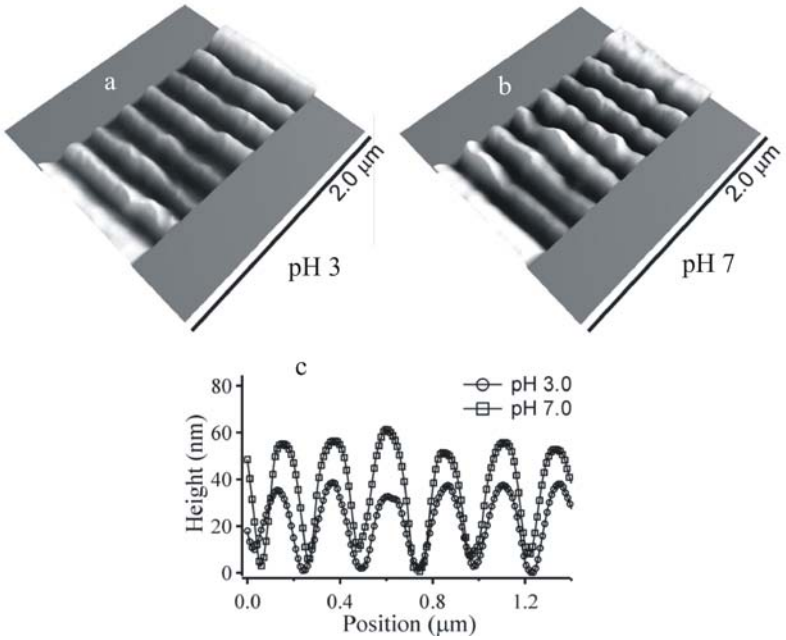

Figure 7.11 pH responsive behavior of PEGMA brushes after treatment with SA (a) at pH 3.0, (b) at pH 7.0. (c) Average brush height plotted as a function of pattern size at pH 3 and at pH 7.0.

FTIR spectra depicted in Figure 7.12 reveal the presence of signals corresponding to the desired functionalities of the polymer brushes discussed earlier. FTIR spectra were taken on continuous brush films which underwent the same treatments with respect to the patterned samples. The FTIR spectrum of the PEGMA surface displays the presence of two major

absorption bands in the 1700 and 1140 cm^{-1} region, arising from the stretching of the ester carbonyl group and the C-O-C group, respectively. As it can be seen in Figure 7.13b, after succinic anhydride functionalization the OH band completely disappeared and the intensity of C=O signal (1700 cm^{-1}) increased as compared to the signal in Figure 7.13a. The increase in height of this peak reflected an increase in C=O content along the PEGMA chain. Each step of the protein immobilization process was monitored by FTIR. Reaction with NHS-EDC resulted in the characteristic peaks shown in Figure 7.13c. The shoulder peaks at 1710 cm^{-1} and 1720 cm^{-1} are assigned to the carbon stretching of NHS. The peak at 1070 cm^{-1} in Figure 7.13c is assigned to the C-N stretching. Reaction with biotin-PEG(10)-NH_2 results in a peak at 1680 cm^{-1} due to the amide stretching vibration of biotin (Figure 7.13d). The FTIR spectrum of the streptavidin functionalized film shows the absorption corresponding to amide I and II bands at 1700-1600 cm^{-1} and 1600-1500 cm^{-1}, respectively (Figure 7.13e).

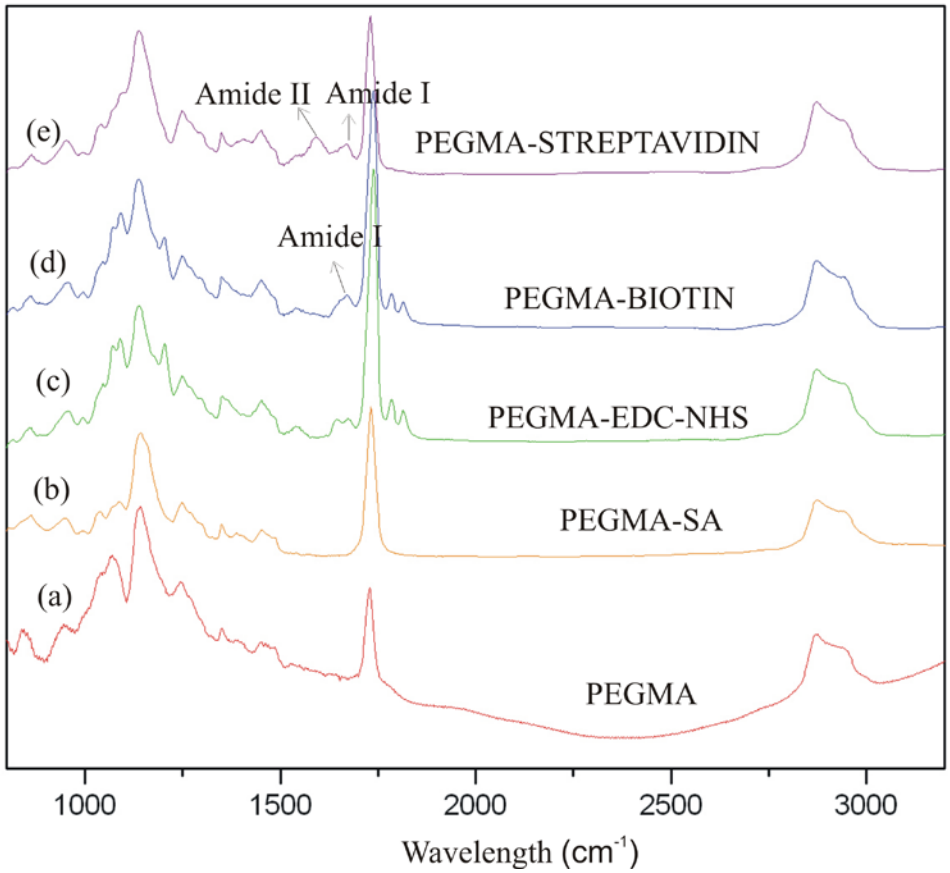

Figure 7.12 FTIR spectra obtained for a) PEGMA brushes, (b) PEGMA reacted with SA, (c) after reaction with NHS-EDC, (d) following amide bond formation with biotin, (e) final reaction with streptavidin.

After introducing carboxylic acid moieties along the PEGMA polymer backbones, the carboxylic acid groups were activated for the protein immobilization, by reacting with *N*-hydroxysuccinimide (NHS) and 1-ethyl-3-(dimethylamino)-propylcarbodiimide (EDC) in water. The activated surface was dried under nitrogen and used immediately for protein immobilization.

The biotin-PEG(10)-NH_2 was attached to the activated PEGMA brushes. The biotin modified brushes were then allowed to react with dye-labeled streptavidin. AFM images in Figure 7.13 demonstrate the change in size and morphology before and after protein immobilization. One can observe that after chemical attachment of biotion/streptavidin, the pillars of 80 nm (in width) have increased in circumference indicating the presence of the protein layer coupled. Protein coupling was further supported by the significant increase of the surface roughness of PEGMA brushes after immobilization from 3.5 nm to 6.3 nm.

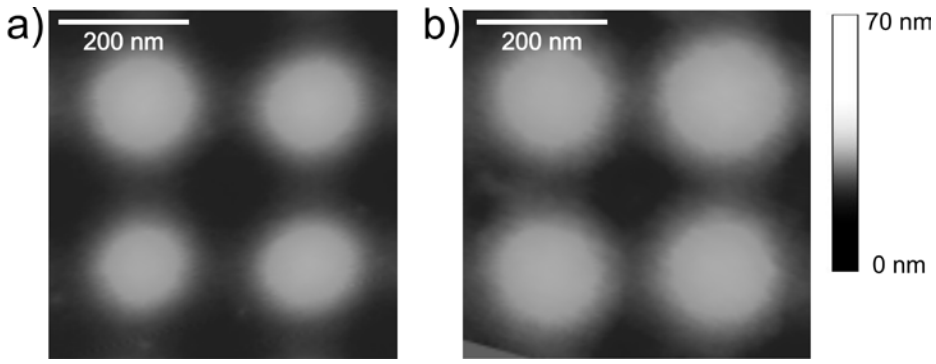

Figure 7.13 AFM images of 80 nm pillars before (a) and after protein immobilization (b).

Next we quantify the number of proteins that could be immobilized on each brush pillar. By reducing the size of the brush-hedge precursor patterns it would be possible to achieve a limited number of proteins. The amount of streptavidin immobilized on the patterned brush surface was determined by bearing analysis of AFM images. The volume change after each preparation step was thus calculated and averaged over a series of 30 pillars in different positions on the same patterned area. The histogram given in Figure 7.14 shows the volume change calculated for each step. After coupling of streptavidin to biotin, the total height change was around 15 nm and the change in width of the pillars was around 40 nm. The dimensions of streptavidin may be considered as 5x5x5 nm^3, i.e. by measuring the volume increase for each brush-pillar it would be possible to estimate how many proteins are immobilized.[40] We found that roughly 60 streptavidin units were immobilized onto one pillar structure.

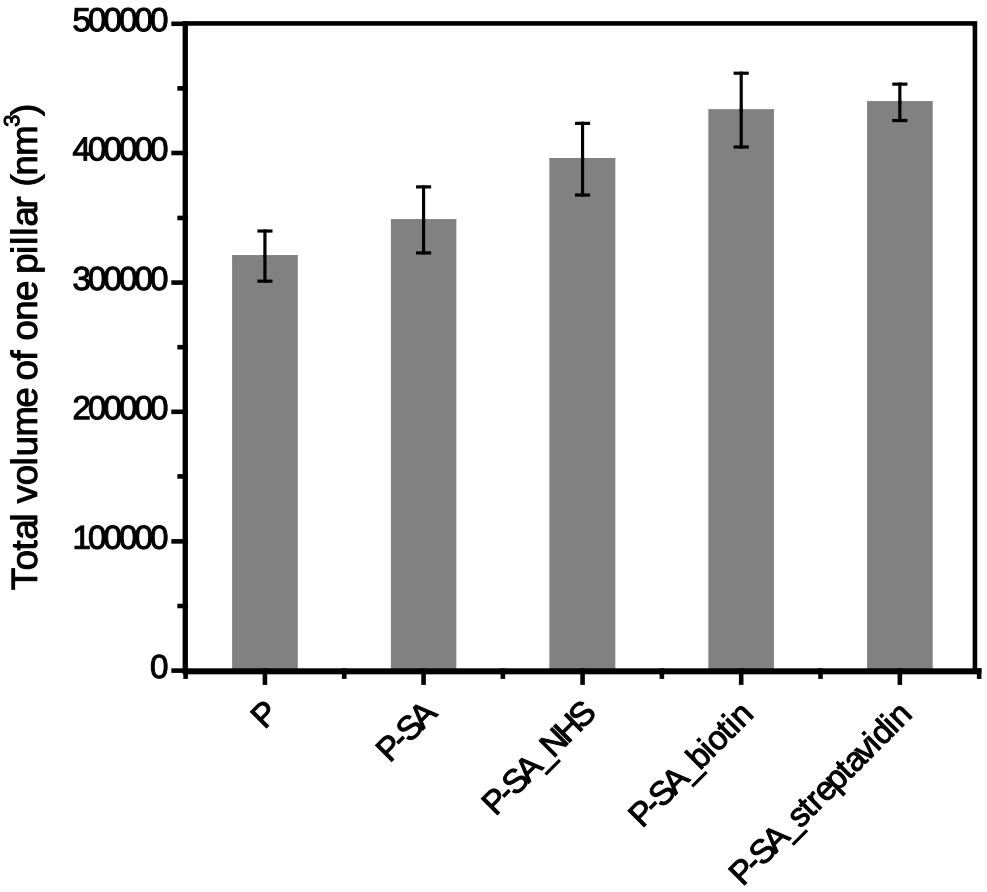

Figure 7.14 Histogram showing the volume of PEGMA brushes, PEGMA brushes were reacted with SA, activated with EDC-NHS, coupled with biotin and finally immobilized with streptavidin(y axis is in nm^3).

Further evidence for the attachament of biotin and streptavidin is provided by fluorescence microscopy (Figure 7.15). The green lines indicate the presence of streptavidin, which coincides with the brush patterns. Binding occurs only to the brush patterns, not to regions in between the brush patterns (dark regions). The results indicate that streptavidin was only bound to the regions where biotin was present on the brush patterns. In addition, the regions between the patterns were successfully passivated and no nonspecific absorption of protein was observed within these regions.

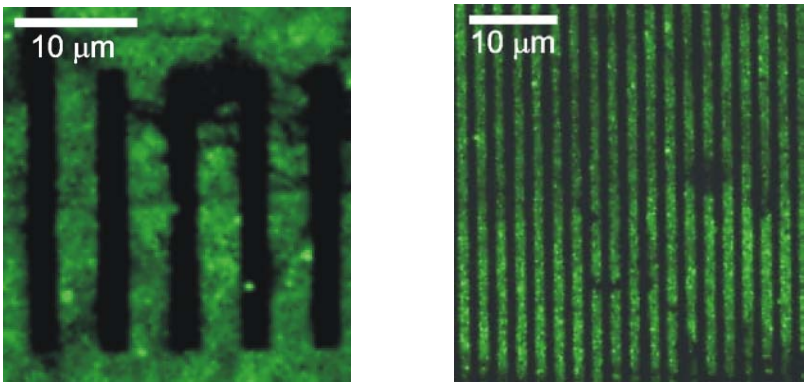

Figure 7.15 Fluorescence microscopy images of patterned PEGMA brushes coupled with biotin/streptavidin.

7.3 CONCLUSIONS

We presented a simple but versatile method to fabricate polymer brush patterns by combining SFIL and SIP. Patterns created by SFIL were further used for anchoring SAM of initiator for performing SIP. The method allowed controlled preparation of brush patterns of PEGMA, PS and PGMA with lateral dimensions ranging from several microns down to 40 nm. Such variations in domain size enabled the study of the dependence of the width of the pattern on the height/width of the brush structures. It was shown that nanosized domains exhibit a significantly reduced height. The functionalization of PEGMA brush patterns was demonstrated. Due to the presence of carboxylic acid moieties in the PEGMA brush architecture, these brushes exhibit controlled swelling at different pH values, which was monitored by AFM. The structurally robust and functional patterned PEGMA polymeric nanostructures obtained enabled protein immobilization. Streptavidin/biotin were selectively coupled on the activated PEGMA brush patterns. This approach is very promising for fabricating protein patterns which could be integrated into microfabricated devices and sensors.

7.4 EXPERIMENTAL

7.4.1 Pattern Fabrication

Patterns were generated using UV-based nanoimprint technology. All imprints were carried out on an Imprio 55 from Molecular Imprints Inc., using the S-FIL process.[28] As a substrate, double side polished Si wafers were used, which were also coated with a thin transfer layer applied by spin coating and hot baking in order to achieve a good adhesion of the imprint material to the substrate. DUV 30J was used as the transfer layer. The quartz

template employed for the imprints consisted of lines, pillars, and groves with feature sizes from tens of µm down to sub-50 nm. Prior to imprinting, the template was treated with a release layer of perfluoro-1,1,2,2-tetrahydrooctyltrichlorosilane in order to prevent sticking of the imprint material to the template. The surface treatment procedure used in this process started with the cleaning of the template with a piranha solution (conc. H_2SO_4 and 33% aq H_2O_2 in a 3:1 volume ratio, ***Warning!*** *Piranha should be handled with caution; it can detonate unexpectedly*) for 30 min to remove any organic contaminants from the surface. Following the piranha treatment, the substrates were blown dry with N_2 and reacted with the alkyltrichlorosilane. Imprinting was performed using a low-viscosity acrylate-based organic SFIL resist. (Monomat, Molecular Imprints Inc.) The imprint material was deposited by direct dispensing, where the volume was locally adjusted to the pattern definition. After dispensing, the template was pressed into the still liquid imprint material and held for 20 s under a pressure of 50 mbar to fill all the features. Thereafter, the imprint material was cured by UV light irradiation through the transparent template, followed by demolding. Oxygen reactive ion etching to remove the residual layer was performed in an Elektrotech PF 340 apparatus (10 mTorr, 10 W, 10 sccm O_2) for 70 sec. As an initiator 3-(chlorodimethylsilyl)proply 2-bromo-2-methylpropionate was used and the synthesis of the initiator was shown before. The initiator was anchored to a surface by gas-phase evaporation in a desiccator under vacuum.

7.4.2 Preparation, Functionalization and Characterization of Brushes

7.4.2.1 Surface-initiated ATRP of PEGMA

$CuBr_2$ was purchased from Aldrich and used as received. CuCl was purified by washing glacial acetic acid and, after filtration by rinsing with ethanol and acetone. Poly(ethylene glycol methacrylate) with an average molecular weight of 360 Da was purchased from Sigma and subsequently purified from inhibitors employing basic alumina column. In a typical ATRP 0.162 g of bipyridine were added to a mixture of 7.5 g of PEGMA 360 and 7.5 g of water. This solution was degassed by three freeze-thaw-pump cycles and later on transferred, via a degassed syringe, to a second flask containing CuCl (41.18 mg), $CuBr_2$ (9.2 mg). The resulting mixture was stirred at ambient temperature for 30 minutes, until complete formation of dark-brown complex. Subsequently, the reaction solution was transferred, via a degassed syringe, into an argon purged flask containing the ATRP initiator functionalized samples. The polymerization was carried out for 1 h at room temperature under nitrogen.

7.4.2.2 Surface-initiated ATRP of PGMA

PGMA was purchased from Aldrich and subsequently purified from inhibitors by employing a basic aluminum oxide column. A solution of glycidyl methacrylate (5 ml, 5.21 g) in methanol and water (1 ml) was degassed by bubbling through argon for 15 min. To this solution added CuCl (36.4 mg), $CuBr_2$ (3.9 mg), and 2,2'-dipyridyl (141 mg). To dissolve all solids, the mixture was stirred for 5 min while degassing continued, giving a dark brown solution. After stirring, the reaction solution was transferred, via a degassed syringe, into an argon purged flask containing the ATRP initiator functionalized samples. The polymerization had been allowed to proceed for 1 hour and then the sample was removed and washed with methanol and water, followed by dichloromethane and dried under a nitrogen stream.

7.4.2.3 Surface-initiated ATRP of PS

Styrene was purchased from Aldrich and subsequently purified from inhibitors employing a basic aluminum oxide column. Polymerization of styrene from the ATRP initiator coated silicon substrates was carried out in bulk conditions (Styrene concentration 8.6 M). The catalyst comprised of Cu(I)Br and ligand, PMDETA, with a molar ratio of 1:1 and a catalyst concentration of 8.6×10^{-2} M. The monomer was degassed by three freeze-pump-thaw cycles and then transferred to the catalyst with maximum precautions to avoid oxygen. After stirring, the reaction solution was transferred, via a degassed syringe , into an argon purged flask containing the ATRP initiator functionalized samples . The polymerization was carried out at 60℃ overnight under an Ar stream.

7.4.2.4 Functionalization of Brushes and pH responsive

Before functionalization the of PEGMA brushes, the samples were immersed in dry toluene solution of 2-[methoxy(polyethyleneoxy)propyl]trimethoxysilane overnight under an Ar stream for passivation.

PEGMA-based brush films were derivatized with succinic anhydride by overnight reaction in 30 mg/ml dry pyridine solution. The pH was adjusted by adding 0.1 M HCl or 0.1 M NaOH to the aqueous solutions.

The derivatized PEGMA brush films were activated by immersion in an aqueous solution of EDC (1 M) and NHS (0.2 M) for 30 min. The samples were then rinsed with Milli-Q water, dried in a stream of nitrogen, and used immediately thereafter.

7.4.2.5 Characterization

Surface morphology images of the fabricated brush films were recorded by tapping mode atomic force microscopy. Contact mode AFM imaging was performed using a liquid

cell setup in order to determine the swelling properties of the brush films at different pH values.

FTIR-spectra (spectral resolution of 8 cm^{-1}, 2048 scans) were obtained using a BIO-RAD FTS575C FTIR spectrometer equipped with a nitrogen-cooled cryogenic cadmium mercury telluride detector. Background spectra were obtained by scanning a clean silicon substrate.

SEM images were taken with a HR-LEO 1550 FEF SEM. No sample surface coating was applied.

7.4.3 Protein Immobilization

Following activation of surfaces with EDC/NHS, the samples were incubated in PBS solution of biotin-PEG (10) NH_2 overnight (1 µM). Biotin functionalized surfaces were immersed PBS solution of streptavidin (1 µM) overnight.

7.5 ACKNOWLEDGEMENT

We thank Mark Smithers for acquiring the SEM images.

7.6 REFERENCES

[1] M. Geissler, Y. N. Xia, *Adv. Mater.* **2004**, *16*, 1249.

[2] H. Tu, C. E. Heitzman, P. V. Braun, *Langmuir* **2004**, *20*, 8313.

[3] C. D. H. Alarcon, T. Farhan, V. L. Osborne, W. T. S. Huck, C. Alexander, *J. Mater. Chem.* **2005**, *15*, 2089.

[4] N. Mahajan, R. B. Lu, S. T. Wu, J. Y. Fang, *Langmuir* **2005**, *21*, 3132.

[5] P. T. Hammond, *Adv. Mater.* **2004**, *16*, 1271.

[6] O. Prucker, J. Habicht, I. J. Park, J. Ruhe, *Mater. Sci. Engin. C* **1999**, *8-9*, 291.

[7] M. D. K. Ingall, C. H. Honeyman, J. V. Mercure, P. A. Bianconi, R. R. Kunz, *J. Am. Chem. Soc.* **1999**, *121*, 3607.

[8] R. Jordan, A. Ulman, J. F. Kang, M. H. Rafailovich, J. Sokolov, *J. Am. Chem. Soc.* **1999**, *121*, 1016.

[9] M. Weck, J. J. Jackiw, R. R. Rossi, P. S. Weiss, R. H. Grubbs, *J. Am. Chem. Soc.* **1999**, *121*, 4088.

[10] M. Husemann, M. Morrison, D. Benoit, K. J. Frommer, C. M. Mate, W. D. Hinsberg, J. L. Hedrick, C. J. Hawker, *J. Am. Chem. Soc.* **2000**, *122*, 1844.

[11] X. Huang, M. J. Wirth, *Macromolecules* **1999**, *32*, 1694.

[12] O. Prucker, J. Ruhe, *Langmuir* **1998**, *14*, 6893.

[13] A. Samadi, S. M. Husson, Y. Liu, I. Luzinov, S. M. Kilbey, *Macromol. Rapid Commun.* **2005**, *26*, 1829.

[14] S. J. Ahn, M. Kaholek, W. K. Lee, B. LaMattina, T. H. LaBean, S. Zauscher, *Adv. Mater.* **2004**, *16*, 2141.

[15] R. C. Bailey, J. T. Hupp, *Anal. Chem.* **2003**, *75*, 2392.

[16] N. Nath, A. Chilkoti, *Adv. Mater.* **2002**, *14*, 1243.

[17] M. Husemann, D. Mecerreyes, C. J. Hawker, J. L. Hedrick, R. Shah, N. L. Abbott, *Angew. Chem. Int. Ed.* **1999**, *38*, 647.

[18] D. M. Jones, W. T. S. Huck, *Adv. Mater.* **2001**, *13*, 1256.

[19] U. Schmelmer, R. Jordan, W. Geyer, W. Eck, A. Golzhauser, M. Grunze, A. Ulman, *Angew. Chem. Int. Ed.* **2003**, *42*, 559.

[20] T. A. von Werne, D. S. Germack, E. C. Hagberg, V. V. Sheares, C. J. Hawker, K. R. Carter, *J. Am. Chem. Soc.* **2003**, *125*, 3831.

[21] U. Schmelmer, A. Paul, A. Kuller, M. Steenackers, A. Ulman, M. Grunze, A. Golzhauser, R. Jordan, *Small* **2007**, *3*, 459.

[22] Y. Tsujii, M. Ejaz, S. Yamamoto, T. Fukuda, K. Shigeto, K. Mibu, T. Shinjo, *Polymer* **2002**, *43*, 3837.

[23] S. Y. Chou, P. R. Krauss, P. J. Renstrom, *J. Vac. Sci. Technol. B* **1996**, *14*, 4129.

[24] S. Y. Chou, P. R. Krauss, P. J. Renstrom, *Science* **1996**, *272*, 85.

[25] M. Bender, M. Otto, B. Hadam, B. Vratzov, B. Spangenberg, H. Kurz, *Microelectron. Eng.* **2000**, *53*, 233.

[26] B. D. Gates, Q. B. Xu, M. Stewart, D. Ryan, C. G. Willson, G. M. Whitesides, *Chem. Rev.* **2005**, *105*, 1171.

[27] D. Resnick, S. V. Sreenivasan, C. G. Willson, *Mater. Today* **2005**, *34*.

[28] S. V. Sreenivasan, I. McMackin, F. Xu, D. Wang, N. Stacey, *Micro Magazine* **2005**.

[29] J. Nicolas, G. Mantovani, D. M. Haddleton, *Macromol. Rapid Commun.* **2007**, *28*, 1083.

[30] S. Zauscher, A. Chilkoti, *Biointerphases* **2009**, *4*, FA1.

[31] R. Dong, S. Krishnan, B. A. Baird, M. Lindau, C. K. Ober, *Biomacromolecules* **2007**, *8*, 3082.

[32] L. S. Wong, F. Khan, J. Micklefield, *Chem. Rev.* **2009**, *109*, 4025.

[33] D. Xu, W. H. Yu, E. T. Kang, K. G. Neoh, *J. Colloid Interface Sci.* **2004**, *279*, 78.

[34] W. K. Lee, M. Patra, P. Linse, S. Zauscher, *Small* **2007**, *3*, 63.

[35] M. Mathieu, A. Friebe, S. Franzka, M. Ulbricht, N. Hartmann, *Langmuir* **2009**, *25*, 12393.

[36] S. Edmondson, W. T. S. Huck, *J. Mater. Chem.* **2004**, *14*, 730.

[37] F. J. Xu, H. Z. Li, J. Li, Y. H. E. Teo, C. X. Zhu, E. T. Kang, K. G. Neoh, *Biosens. Bioelectron.* **2008**, *24*, 773.

[38] Z. L. Ding, R. B. Fong, C. J. Long, P. S. Stayton, A. S. Hoffman, *Nature* **2001**, *411*, 59.

[39] P. Jonkheijm, D. Weinrich, H. Schroder, C. M. Niemeyer, H. Waldmann, *Angew. Chem. Int. Ed.* **2008**, *47*, 9618.

[40] A. Arakaki, S. Hideshima, T. Nakagawa, D. Niwa, T. Tanaka, T. Matsunaga, T. Osaka, *Biotechnol. Bioeng.* **2004**, *88*, 543.

Chapter 8

Size Distribution of Microdomains in Spherical Morphology Polystyrene-polyferrocenyldimethylsilane Block copolymer Thin Films

ABSTRACT. Thin films of organic-organometallic block copolymers have been used in bottom-up lithography because of the high etch selectivity between the two blocks and the etch resistance of the organometallic block. The study in this chapter investigates the effects of volume fraction, molecular weight, and polydispersity index (PDI) on the distribution of the size and spacing of the spherical microdomains of thin films of polystyrene-*block*-polyferrocenyldimethylsilane (PS-*b*-PFS) block copolymers which are comprised of a monolayer of PFS microdomains. Size and spacing distributions depend on volume fraction, but have little dependence on PDI and molecular weight. The minor effects of PDI are attributed to the statistical variation in the number of chain ends per microdomain, which is only 7% of the total number of chain ends per PFS microdomain.

8.1 INTRODUCTION

As the size of electronic and magnetic devices decreases, strategies to accomplish planar processing on the nanoscale have become increasingly important. Patterning is conventionally achieved using top-down lithographic processes such as optical or electron-beam lithography, but the resolution of optical lithography is limited to ~50 nm for 193 nm wavelength, while electron-beam lithography is too slow for manufacturing. Instead, bottom-up methods based on self-assembly have been explored for their potential to create high-throughput nanoscale patterns suitable for nanolithography. Diblock copolymers form a variety of well-ordered morphologies depending on the volume fractions of the two constituents with nanoscale periodicity,[1] and have been widely studied for lithographic patterning.[2-12] The size and the periods of the microdomains are governed by the chain dimensions and are typically on the order of 10 nm. Structures smaller than 10 nm are also obtainable if one chooses appropriate blocks with a high Flory-Huggins interaction parameter[1] and decreases the block lengths. The periodic patterns, including spheres, cylinders or lamella generated by block copolymers, are particularly well suited for applications requiring periodic arrays of nanostructures, for example for the fabrication of high-density patterned magnetic recording media where a 25 nm periodicity would correspond to up to 1 Tb/in^2 of data density.[4, 13] Futhermore, each block of the copolymer can be used for a specific application, and selective removal of one block relative to the other one is possible by use of chemical and physical dissimilarities between the two blocks.

Much work on block copolymer lithography has been carried out using polystyrene-*b*-polymethylmethacrylate (PS-*b*-PMMA), which has excellent etch selectivity between the two blocks, allowing the PMMA to be removed upon plasma treatment.[14, 15] However, the remaining PS microdomains have a low etch resistance, which limits subsequent pattern transfer steps. In order to be used in the lithography process, the block copolymer film also must be compatible with the etch process. To obtain a pattern with higher etch resistance, block copolymers containing both an organic block and an organometallic or Si-containing block, such as polystyrene-*b*-polyferrocenyldimethylsilane[4, 16-19] (PS-*b*-PFDMS) (Figure 8. 1) or polystyrene-*b*-polydimethylsiloxane[20, 21] (PS-*b*-PDMS) have been explored. Typically, the organic block is removed using an oxygen plasma, and the remaining, partly oxidized PFS or PDMS microdomains have a high etch resistance, enabling them to be used as a mask for subsequent etching steps to pattern an underlying material.

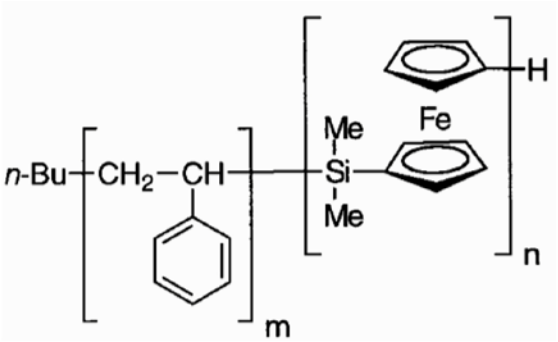

Figure 8.1 The chemical structure of polystyrene-*b*-polyferrocenyldimethylsilane.

Processing and pattern transfer methods of the hybrid block copolymers are now established, but there has been less study of how the uniformity in size and spacing of the microdomains depends on the polymer characteristics and the processing conditions.[22, 23] The uniformity is critical in applications of block copolymers in lithography and it is assumed that a strong segregation of blocks and a narrow molecular weight distribution are necessary to achieve a high degree of ordering. For example, in patterned media fabrication, variability in the placement and size of the magnetic 'bits' leads to jitter which degrades the readback signal.[24] In this chapter, we examine a set of five spherical morphology PS-*b*-PFS block copolymers to study the origins of the size distribution of the spherical PFS microdomains. In this chapter, in particular, we examine the effects of volume fraction, molecular weight, and polydispersity index (PDI) on microdomain size distribution, period and correlation length of thin films of spherical-morphology PS-*b*-PFS block copolymers.

8.2 RESULTS & DISCUSSION

8.2.1 Sequential Anionic Polymerization of Styrene and 1,1'-Dimethylsilyl-ferrocenophane

Poly(styrene-*block*-polyferrocenyldimethylsilane) copolymers were synthesized by sequential anionic polymerization (Table 8.1). Polymerization of styrene in ethylbenzene was initiated by *n*-butyllithium and allowed to proceed for 5 hours. After the styrene block formation was completed, 1,1'-dimethylsilylferrocenophane was added to the solution and stirred for 5 minutes. Since 1,1'-dimethylsilylferrocenophane does not polymerize in ethylbenzene, THF was added to the reaction mixture, allowing the polymerization of the organometallic block to proceed. By using this method the reaction of living polystyryl chains with THF is prevented. After 2 hours, the living chains were terminated by adding a few drops of degassed methanol. The polymers were precipitated and dried under vacuum.

Table 8.1 shows the molecular characteristics of PS-*b*-PFS, obtained by ^{1}H NMR and GPC measurements. The variation in PDI was achieved by adding the required amount of initiator in several portions at different time intervals, rather than at once.

Table 8.1 Molecular characteristics of the five PS/PFS samples studied. Φ indicates volume fraction.

Sample	PDI	Φ PFS (vol%)	MW_{PS} (10^3 kg/mol)	MW_{PFS} (10^3 kg/mol)	Composition fractions
A	1.198	13	42	7.5	$PS_{403}PFS_{31}$
B	1.114	17	39	9.4	$PS_{371}PFS_{39}$
C	1.109	19	43	11.8	$PS_{371}PFS_{39}$
D	1.188	20	40	12	$PS_{378}PFS_{50}$
E	1.123	22	35	11.8	$PS_{337}PFS_{49}$

8.2.2 Film Thickness and Annealing Time Effects

The effect of film thickness on morphology was investigated for polymer C, which has the lowest PDI, 1.109, and the median volume fraction of PFS, 19%. A thickness range of 36.1 to 62.2 nm was selected in order to cover the range over which a monolayer of spheres forms. On oxidized silicon, PFS wets the substrate to form a surface layer of ~10 nm thickness,[19] and the periodicity of the block copolymer is near 30 nm, so a film in the range of 40 nm thick is expected to exhibit a monolayer of spheres.

Polymer C formed a single layer of spheres for films up to 45 nm thick (Figure 8.2a), beyond which a second layer of spheres nucleated (Fig. 8.2b). Figure 8.3 shows the variation of the microdomain area, correlation length, and periodicity with thickness. The mean distance between the PFS microdomains and the mean area of the microdomains are larger in the monolayer samples than in the bilayer samples, and the correlation lengths of the monolayer samples are greater than those of the bilayer samples. Monolayer correlation lengths range from 162 to 195 nm (5.5-6.5 periods), while bilayer correlation lengths range from 138 to 165 nm. Bilayer measurements were made using only the top layer of spheres, which are distinguished due to their greater contrast on SEM images. Based on these results, a thickness of 42 nm was chosen for subsequent measurements. This produced a monolayer of spheres for all five polymers.

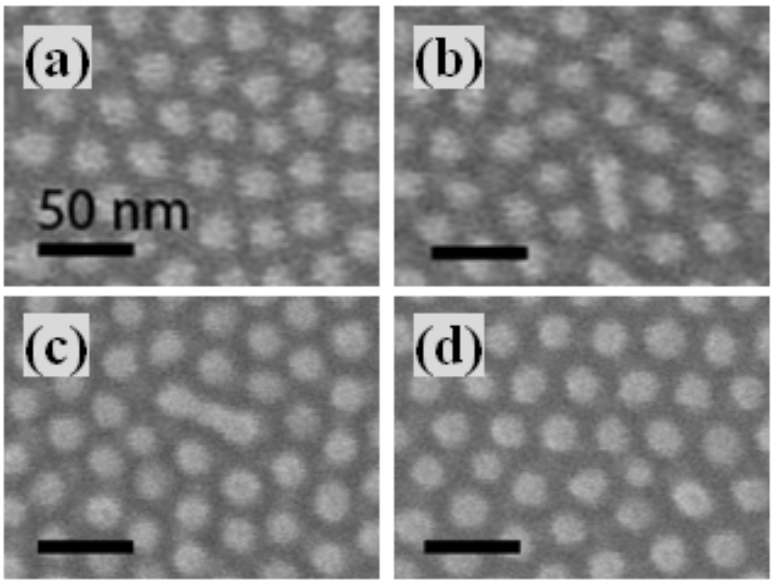

Figure 8.2 The effects of thickness and annealing time on PS-*b*-PFS films of polymer C. (a-b) Films with thickness (a) 45 nm and (b) 62.2 nm, annealed for 30 hours at 140˚C. (c-d) Films with thickness 42 nm annealed at 140°C for (c) 1 day and (d) 7 days.

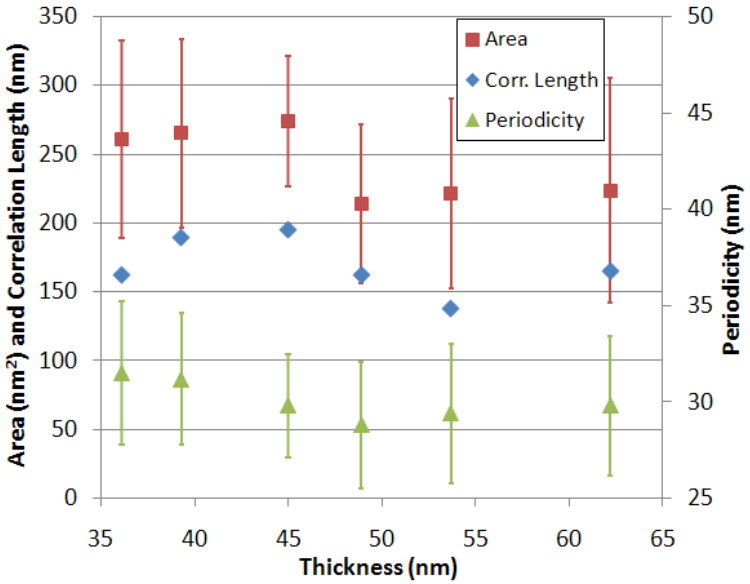

Figure 8.3 Dependence of microdomain area, correlation length, and periodicity as a function of film thickness for polymer C.

The effects of annealing time were investigated for a 42 nm thick film of polymer C. Samples were annealed at 140°C (413 K) for 1, 2, 4, and 7 days. The sample annealed for 1 day contained some PFS cylinders, which converted into spheres as annealing time was increased. The films exhibited greater correlation length and size uniformity as annealing time increased. The standard deviation in microdomain area decreased from 24.9% in the

sample annealed for 1 day to 16.1% in the sample annealed for 7 days, while the standard deviation in the microdomain period decreased from 32.2% to 8.7% and the correlation length increased from 135 to 198 nm. Correlation length has been found to increase slowly with annealing time by a power law $\xi(t) \propto t^{1/4}$ for spherical-morphology PS-*b*-PI under thermal annealing.[25] In our experiment, the correlation length after 2 days of annealing was similar to that after 7 days annealing, so an annealing time of 30 h was chosen for subsequent experiments.

8.2.3 Volume Fraction and Molecular Weight Effects

Figure 8.4 shows the morphology of etched 42 nm thick films of the five polymers after 30 h annealing at 140°C. Although these polymers differ in their PFS volume fraction, PDI and total molecular weight, the morphologies correlate most clearly with volume fraction Φ_{PFS}. At low volume fractions (sample A: Φ_{PFS} = 13%), the PFS microdomains are small and irregular. At mid-range volume fractions (samples B, C: Φ_{PFS} = 17-19%), the PFS microdomains form uniform spheres, but at higher volume fractions (samples D, E: Φ_{PFS} = 20-22%), short PFS cylinders and spheres form simultaneously. The sphere-to-cylinder transition occurring at Φ_{PFS}= 20% is similar to results from previous work.[4, 26] Table 8.2 gives the distributions in microdomain area and period and the correlation length for the five polymers. The microdomain area (and its standard deviation) and period both increase with Φ_{PFS}.

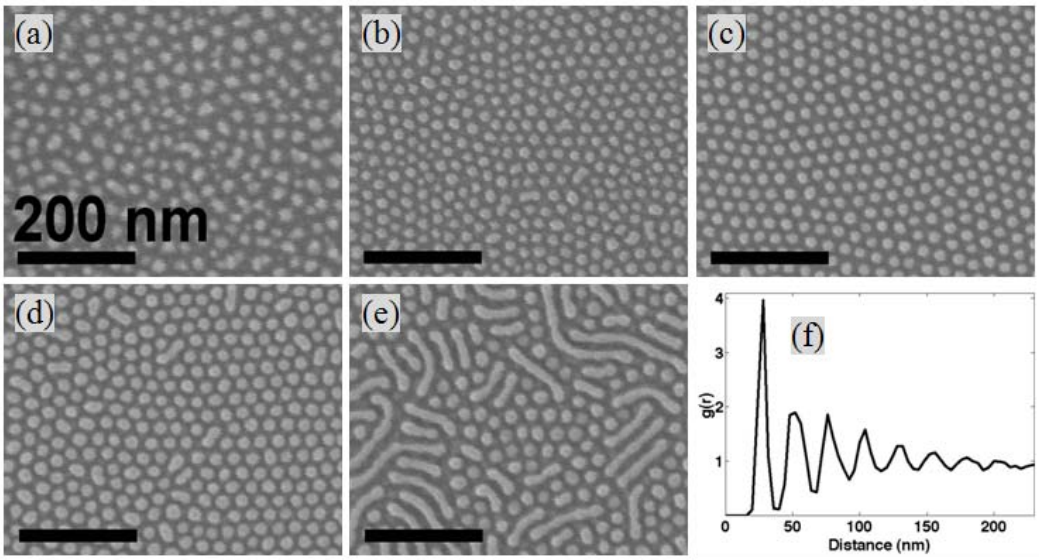

Figure 8.4 (a-e) PS-*b*-PFS films with thickness 42 nm, annealed for 30 hours, from polymers A – E, respectively. (f) A pair density function (PDF) for image C.

Table 8.2 Properties of five PS/PFS films with thickness of 42 nm, annealed for 30 hours.

Sample	Area(nm^2)		Period(nm)		ξ
	Mean	Std. Dev.	Mean	Std. Dev	(nm)
A	117.8	47.3	22.7	4.5	120
B	222.5	47.7	26.4	2.9	141
C	249.8	44.9	29.5	3.1	171
D	290.7	104.9	29.0	3.3	195
E	447.1	381.2	30.3	3.2	135

The sphere-to-cylinder (S/C) and order/disorder (O/D) transitions may be predicted from χN, with N the degree of polymerization and χ the Flory-Huggins interaction parameter. For the PS-*b*-PFS system, χ is given by:

$$\chi_{PS/PFS}(T) = 0.028 + 3.28/T \text{ [27]}$$

At an annealing temperature of 413 K and the average N-value of 419.7, χN = 15.1. The χN vs. Φ phase diagram for the ideal behavior of a polystyrene-polyisoprene block copolymer[1] predicts an O/D transition at Φ = 27% and S/C transition at Φ = 37%. In this experiment, microphase separation clearly occurs for Φ_{PFS} = 13%, with a χN-value of 15.5, and the S/C transition occurs near Φ_{PFS} = 22%, with a χN-value of 13.7. The phase diagram of PS-*b*-PFS diblock-homopolymer blends is shown to be asymmetric which explains the shift in O/D transition.[28]

No clear trends in microdomain area, period and correlation length with molecular weight could be identified in this series of samples because of the overriding effects of volume fraction. An increase in microdomain diameter and period with $M^{2/3}$ is expected in the strong segregation limit.[29] Comparing polymers B (Φ_{PFS} = 17%, M = 48.3 kg/mol) and C (Φ_{PFS} = 19%, M = 54.1 kg/mol), both in the spherical regime without cylinders present, the period increases by 1.12 (with standard deviation 10%), similar to the ratio $(M_C/M_B)^{2/3}$ = 1.08. The ratio of PFS microdomain diameters is 1.06 (standard deviation 18%), but this is at least partly due to the 5% increase in Φ_{PFS}.

8.2.4 Polydispersity Effect (PDI)

The PDI, defined as M_w/M_n, where M_w is the weight average and M_n the number average molecular weight is of particular interest because it may determine the ultimate

monodispersity in microdomain size and period attainable from a well-annealed block copolymer. The PDI in the samples of the present study varied between 1.109 and 1.198, and in these samples, no clear correlation with the thin film properties was observed. A comparison of samples C (Φ_{PFS} = 19%, PDI = 1.109) and D (Φ_{PFS} = 20%, PDI = 1.188) actually showed a slightly higher correlation length for D (195 nm) compared to C (171 nm) despite the presence of a few short cylinders in D. Comparing samples B (Φ_{PFS} = 17%, PDI = 1.114) and E (Φ_{PFS} = 22%, PDI = 1.123) revealed a much larger mean area and standard deviation for E (447.1 nm and 381.2 nm, respectively) than for B (222.5 nm and 47.7 nm), despite their similar values of PDI.

The weak effect of PDI can be explained by considering the number of polymer chains present in each PFS microdomain. For sample C, with a PFS microdomain cross-sectional area of 250 nm^2 and a volume of 2970 nm^3, and with a molecular weight of 11,870 g/mol for the PFS block, of density 1.26 g/cm^3, each microdomain contains on average Z = 190 PFS polymer chains. If the statistical variation in the number of chains Z within a microdomain is taken as $\sqrt{Z}$ = 14, this would correspond to a variability in sphere volume of 7%, or 5% variation in cross-sectional area between spheres, even for a perfectly monodisperse block copolymer with PDI of 1.

Taking the standard deviation of M_n as $\sigma_n = M_n(PDI - 1)^{0.5}$[30] the same polymer with a PDI of 1.1 would have σ_n/M_n = 32%. Assuming a Gaussian distribution of chain lengths and a sphere size of 190 chains, the PDI would introduce a 2.3% variability in sphere volume. This variability is significantly less than the 7% due to statistical variation of a monodisperse block copolymer. For this reason, the small changes in PDI examined in this study do not affect the observed properties of the films.

8.3 CONCLUSIONS

The effects of thickness, annealing time, molecular weight, block volume fraction, and polydispersity on the microdomain size distribution, period and correlation length of thin films of spherical-morphology PS-PFS block copolymers were investigated. For a series of block copolymers of the same thickness, annealed under identical conditions, the volume fraction (13 – 22%) had the greatest effect on PS-PFS morphology, with the microdomain area and its standard deviation, and the period and its standard deviation all increasing with the volume fraction of the PFS. The molecular weight (48 – 54 kg/mol) accounted for small increases in period, while the polydispersity (1.109 – 1.198) had little effect on the size

distribution and period of the microdomains. The minor effects of PDI are attributed to the large number of chains present in each microdomain.

Block copolymers containing an organic and an organometallic block are of interest for self-assembled lithography because of the high etch selectivity between the blocks and the high etch resistance of the organometallic block. The results of this study have implications in the design of block copolymers for lithographic applications, such as the fabrication of patterned magnetic recording media, where variation in the size and spacing of the microdomains would produce a distribution of magnetic bit sizes and positions, leading to increased noise in the readback signal.

8.4 EXPERIMENTAL

Poly(styrene-*block*-ferrocenyldimethylsilane) copolymers were synthesized by sequential anionic polymerization. *N*,*N*,*N'*,*N'*,-Tetramethylethylenediamine (TMEDA), ferrocene, styrene, *n*-butyllithium (1.6 M in hexanes), dibutylmagnesium (1.0 M in heptane) and dichlorodimethylsilane were purchased from Aldrich. [1]Dimethylsilaferrocenophane was prepared as described earlier and was purified by sequential crystallization and vacuum sublimation cycles.[18, 31] Crystallizations was performed at low temperature in *n*-heptane. Solutions of styrene in ethylbenzene were dried on dibutylmagnesium and distilled under vacuum. *n*-Butyllithium was diluted to 0.2 M with *n*-heptane, which was dried over *n*-butyllithium and distilled under vacuum. Tetrahydrofuran (THF) for anionic polymerization was distilled from sodium-benzophenone under argon, degassed in three freeze-pump-thaw cycles, and distilled by vacuum condensation from *n*-butyllithium at low temperature.

Polymer synthesis was carried out in an Mbraun Labmaster 130 glovebox under an atmosphere of prepurified nitrogen (<0.1 ppm of H_2O). Polymerization of styrene in ethylbenzene was initiated by *n*-butyllithium and stirred for 5 hours at room temperature. After the styrene block formation was completed, [1]-dimethylsilaferrocenophane was added to the solution followed by some THF, allowing the formation of the organometallic block. After 2 hours, the living chains were terminated by adding a few drops of degassed methanol. The polymers were precipitated in methanol and dried under vacuum. Five different copolymers were prepared by adding the required amount of initiator in several portions at different time intervals, rather than at once.

The polymers were characterized by gel permeation chromatography (GPC) and ^{1}H NMR spectrometry. GPC measurements were carried out in THF using Waters™ microstyragel columns with pore sizes of 10^5, 10^4, 10^3 Å and a 500 Å guard column (Waters).

The instrument was equipped with a dual detection system consisting of a differential refractometer (Waters model 410) and a viscometer (Viscotek model H502). Molar masses were determined relative to narrow polystyrene standards. ^{1}H NMR spectra were recorded on a Varian Unity Inova (300 MHz) instrument at 300.3 MHz in deuterated chloroform. Block ratios were calculated from ^{1}H NMR peak integrals. The density of poly(ferrocenyldimethylsilane), 1.26 g/cm^3, was obtained using a pycnometer. The properties of the polymers are summarized in Table 8.1.

Solutions of the polymers in toluene (1.5 wt%) were spin coated onto prime silicon to form films with thicknesses between 32 and 63 nm. Samples were annealed in a vacuum furnace at 140 °C (413 K) for 1 to 7 days. The films were then reactive ion etched (RIE) in oxygen for 25 seconds at 90W, which removed the PS and partly oxidized the PFS [27].

Samples were imaged using scanning electron microscopy (SEM) after etching, and the images were analyzed using SigmaScan imaging processing and MATLAB software. The areas and coordinates of the PFS microdomains were recorded, and MATLAB scripts were used to calculate the size distribution and the pair density function (PDF). The PDF, *g(r)*, is a dimensionless measure of the density of objects around a point, and is defined as

$$g(r) = \frac{1}{\rho}\frac{dn(r, r+dr)}{dA(r, r+dr)}$$

where ρ is the areal particle density, *dn* is the number of pairs of particles between a radial distance *r* and *r* + *dr*, and *dA* is the area contained between *r* and *r* + *dr*. The correlation length, ξ, was defined as the distance at which the amplitude of the PDF oscillations fell below 5% of the peak amplitude. Correlation length is a measure of the order in a system.

8.5 ACKNOWLEDGEMENTS

We thank Mr. Clemens Padberg for performing GPC analysis.

8.6 REFERENCES

[1] F. S. Bates, G. H. Fredrickson, *Annu. Rev. Phys. Chem.* **1990**, *41*, 525.

[2] M. Park, C. Harrison, P. M. Chaikin, R. A. Register, D. H. Adamson, *Science* **1997**, *276*, 1401.

[3] K. Asakawa, T. Hiraoka, *Jpn. J. Appl. Phys.* **2002**, *41*, 6112.

[4] J. Y. Cheng, C. A. Ross, V. Z. H. Chan, E. L. Thomas, R. G. H. Lammertink, G. J. Vancso, *Adv. Mater.* **2001**, *13*, 1174.

[5] S. J. Jeong, G. D. Xia, B. H. Kim, D. O. Shin, S. H. Kwon, S. W. Kang, S. O. Kim, *Adv. Mater.* **2008**, *20*, 1898.

[6] C. Park, J. Yoon, E. L. Thomas, *Polymer* **2003**, *44*, 6725.

[7] I. W. Hamley, *Nanotechnology* **2003**, *14*, R39.

[8] G. Krausch, R. Magerle, *Adv. Mater.* **2002**, *14*, 1579.

[9] M. Lazzari, M. A. Lopez-Quintela, *Adv. Mater.* **2003**, *15*, 1583.

[10] R. A. Segalman, *Mater. Sci. Eng. Rep.* **2005**, *48*, 191.

[11] J. Y. Cheng, C. A. Ross, H. I. Smith, E. L. Thomas, *Adv. Mater.* **2006**, *18*, 2505.

[12] S. B. Darling, *Prog. Polymer Sci.* **2007**, *32*, 1152.

[13] K. Naito, H. Hieda, M. Sakurai, Y. Kamata, K. Asakawa, *IEEE Trans. Magn.* **2002**, *38*, 1949.

[14] C. C. Liu, P. F. Nealey, Y. H. Ting, A. E. Wendt, *J. Vac. Sci. Technol. B* **2007**, *25*, 1963.

[15] T. Thurn-Albrecht, J. Schotter, C. A. Kastle, N. Emley, T. Shibauchi, L. Krusin-Elbaum, K. Guarini, C. T. Black, M. T. Tuominen, T. P. Russell, *Science* **2000**, *290*, 2126.

[16] R. G. H. Lammertink, M. A. Hempenius, J. E. van den Enk, V. Z. H. Chan, E. L. Thomas, G. J. Vancso, *Adv. Mater.* **2000**, *12*, 98.

[17] R. G. H. Lammertink, M. A. Hempenius, V. Z. H. Chan, E. L. Thomas, G. J. Vancso, *Chem. Mater.* **2001**, *13*, 429.

[18] Y. Z. Ni, R. Rulkens, I. Manners, *J. Am. Chem. Soc.* **1996**, *118*, 4102.

[19] J. Y. Cheng, C. A. Ross, E. L. Thomas, H. I. Smith, G. J. Vancso, *Adv. Mater.* **2003**, *15*, 1599.

[20] Y. S. Jung, C. A. Ross, *Nano Lett.* **2007**, *7*, 2046.

[21] I. Bita, J. K. W. Yang, Y. S. Jung, C. A. Ross, E. L. Thomas, K. K. Berggren, *Science* **2008**, *321*, 939.

[22] S. G. Xiao, X. M. Yang, *J. Vac. Sci. Technol. B* **2007**, *25*, 1953.

[23] K. W. Guarini, C. T. Black, S. H. I. Yeuing, *Adv. Mater.* **2002**, *14*, 1290.

[24] M. Albrecht, C. T. Rettner, A. Moser, M. E. Best, B. D. Terris, *Appl. Phys. Lett.* **2002**, *81*, 2875.

[25] C. Harrison, D. E. Angelescu, M. Trawick, Z. D. Cheng, D. A. Huse, P. M. Chaikin, D. A. Vega, J. M. Sebastian, R. A. Register, D. H. Adamson, *Europhys. Lett.* **2004**, *67*, 800.

[26] R. G. H. Lammertink, M. A. Hempenius, E. L. Thomas, G. J. Vancso, *J. Poly. Sci. Poly. Phys.* **1999**, *37*, 1009.

[27] H. B. Eitouni, N. P. Balsara, H. Hahn, J. A. Pople, M. A. Hempenius, *Macromolecules* **2002**, *35*, 7765.

[28] R. G. H. Lammertink, M. A. Hempenius, E. L. Thomas, G. J. Vancso, *J. Polym. Sci. Part B, Polym. Phys.* **1999**, *37*, 1009.

[29] T. Hashimoto, M. Shibayama, H. Kawai, *Macromolecules* **1980**, *13*, 1237.

[30] S. S. Rane, P. Choi, *Chem. Mater.* **2005**, *17*, 926.

[31] R. G. H. Lammertink, M. A. Hempenius, E. L. Thomas, G. J. Vancso, *J. Polym. Sci., Polym. Phys. Ed.* **1999**, *37*, 1009.

Summary and Outlook

The main goal pursued in this thesis is to investigate the role of organometallic polymers in bottom-up and top-down nanofabrication techniques to provide patterned platforms. Poly(ferrocenylsilane)s (PFSs) were explored for their use in top-down fabrication since they show a high etch resistance to reactive ion etching (RIE). The PFS polymers synthesized were used as resists in top-down lithographic applications on the micro- and nanometer scales. Phase separation in block copolymers was used to create bottom-up patterns on a nanometer scale. Surface-initiated polymerization (SIP) was performed for the preparation of polymer brush patterns for use in biological applications.

Different lithography techniques such as nanoimprint lithography (NIL), UV-nanoimprint lithography (UV-NIL) and nanosphere lithography (NSL) were employed to fabricate patterns of PFS. The patterns fabricated were further utilized to create structures on various polymer and silicon surfaces at different lengthscales. In addition, nanostructured polymer brushes were grafted from a patterned initiator obtained by the step-and-flash imprint lithography (SFIL) process. Block copolymer self-assembly was also used to generate nanoperiodic PFS patterns. Symmetry, pattern quality and correlation as a function of the primary structure of polystyrene-*block*-poly(ferrocenyldimethylsilane) (PS-*b*-PFS) is discussed.

Chapter 1 provides a general introduction to this thesis. In Chapter 2, a broad overview on existing lithography techniques and materials used in these techniques have been given.

Chapter 3 presents a method to fabricate porous structures on silicon substrates by using colloidal particle arrays as a template and PFS as an etch mask. Pores in silicon substrates with submicron sizes and hcp order were fabricated by nanosphere lithography. Silica nanoparticles of different sizes were used as starting materials and poly(ferrocenylmethylphenylsilane) (PFMPS) as an etch-resistant polymer to produce a negative replica of the nanoparticle array. The patterned silicon substrate was subsequently used as a master to replicate the nanoparticle array by using NIL. The size of the pores in the silicon substrate was controlled by changing the size of the particles. It was also shown that the size and shape of the pores can be controlled by changing the etching time.

Chapter 4 describes a process to obtain free-standing poly(ethersulfone) (PES) films exhibiting regular arrays of circular holes with a high porosity. The combination of NSL lithography and a mask transfer technique used in this process allows the fabrication of uniform, nanoporous PES membranes. RIE resistant poly(ferrocenylmethylphenylsilane) (PFMPS) was used to fill the pores among the tightly packed silica particles. During pattern transfer of the silica spheres to the PES, the top layer of PFMPS was removed first, exposing the unprotected silica spheres. Following removal of the spheres by HF, a negative (hollow) pattern of the colloidal particles was formed in the PFMPS layer. In RIE, the PES film was perforated in unprotected areas corresponding to transfer of the projection pattern of the silica spheres. Detachment of the PES membrane from the substrate was achieved by dissolving the sacrificial CA layer in acetone. The PES membranes exhibiting dense, highly ordered pores can serve as a platform for size-selective filtration of particles.

The application of PFMPS as a resist in nanoimprint lithography is introduced in Chapter 5. Stable, homogeneous high molar mass PFMPS films obtained by spin coating were imprinted and the resulting patterns were further transferred into the substrate by reactive ion etching. Decreasing the initial film thickness and tuning the reactive ion etching conditions facilitated the residual layer removal and improved the pattern transfer. In order to obtain high aspect ratios, the residual layer was completely removed by Ar sputtering since direct etching without removal of the residual layer gave rise to oxide layer formation, which prevented further pattern transfer. Overall, it was shown that PFMPS, because of its excellent etch contrast vs silicon, can be used as a single step resist since there is no need for metal lift-off, which renders this approach a low-cost and potentially high-throughput process.

Chapter 6 describes the development of a UV-NIL process with a bilayer system, one of which is PFMPS. The organometallic polymer PFMPS was spin-coated onto a UV-NIL patterned substrate, followed by an argon plasma treatment to expose the imprint material. Removal of the imprint material with oxygen plasma gave rise to PFMPS patterns forming a negative replica of the template employed. Pattern transfer into silicon substrates was accomplished by the use of a $CHF_3/SF_6/O_2$ plasma. Variations of the plasma composition led to different etch profiles. The fabrication of polymeric structures with lateral dimensions down to 30 nm and aspect ratios of up to 3 was demonstrated. This process offers the possibility for combining the advantages of UV-NIL with the high etch resistance of poly(ferrocenylsilanes) to produce feature sizes down to the sub-100 nm range.

In Chapter 7 the preparation of polymer brush patterns by combining SFIL and SIP techniques is reported. Patterns created by SFIL were further used for anchoring SAMs of an

initiator for performing SIP. The method allowed for the creation of brush patterns of PEGMA, PS and PGMA, with sizes from several microns down to 40 nm. Such variation in domain size enabled the study of the effect of the pattern size on the polymer brush height. It was shown that nanosize domains exhibit a significantly reduced height. Several interesting perspectives of patterned PEGMA brushes were demonstrated. PEGMA hydroxy groups were converted into carboxylic acid groups and the pH response of these functionalized PEGMA layers was analyzed by varying the pH. The fabricated structurally robust and functional patterned PEGMA polymeric nanostructures were used for protein immobilization. Streptavidin/biotin were selectively coupled on the activated PEGMA brush patterns.

Chapter 8 deals with the synthesis and symmetry, pattern quality and correlation as a function of the primary structure of PS-*b*-PFS block copolymers. The effects of thickness, annealing time, molar mass, block volume fraction, and polydispersity on the microdomain size distribution, period and correlation length of thin films of spherical-morphology PS-*b*-PFS block copolymers were investigated. For a series of block copolymer films of the same thickness, annealed under identical conditions, the volume fraction was found to have the greatest effect on PS-*b*-PFS morphology, with the period and its standard deviation all increasing with the volume fraction of the PFS. On the other hand polydispersity had little effect on the size distribution and period of the microdomains.

Organometallic polymers are very attractive materials which could be further explored for other possible applications in lithography. Further research on controlled patterning of PFS block copolymers by means of UV-NIL lithography can be carried out to study the influence of confinement on block copolymer assembly. In addition, PFS block copolymers could be utilized to pattern polymer surfaces down to 20 nm by carefully designing the processes like etching, annealing, and deposition of materials.

The results presented in Chapter 7 illustrate the fabrication of polymeric platforms which were further used for protein immobilization. The same approach could be performed for the covalent attachment of CdSe/ZnS nano-crystals at the brush chain ends. In this case, the confinement and patterning of nano-crystals could be studied.

The results presented in this thesis show that polymers provide a variety of structures and dimensions, when patterned by bottom-up and top-down micro- and nanofabrication techniques. The incorporation of organometallic units into the main chain of polymers improves the properties such as etch resistivity, and thus applicability of these macromolecules. Metal-containing polymers are proven to have high etch-resistant properties when applied in NIL, SFIL and NSL techniques. They appear to be valuable candidates for

developing new resists formulations. The fabricated structures by using these techniques could be employed in areas such as data storage, microelectronics and bioelectronics.

Samenvatting

Het hoofddoel van dit proefschrift is om de rol van organometaalpolymeren in “bottom-up”- en “top-down”-nanofabricagetechnieken voor het vervaardigen van nanogestructureerde platforms te onderzoeken. Het gebruik van poly(ferrocenylsilanen) (PFSs) voor “top-down”-fabricage werd bestudeerd vanwege de hoge weerstand van deze polymeren in “reactive ion etching” (RIE) processen. De gesynthetiseerde PFS-polymeren werden gebruikt als resists in top-down lithografische toepassingen op micrometer- en nanometerschaal. Oppervlakte-geïnitieerde polymerisatie werd uitgevoerd voor de constructie van polymere brush-patronen voor gebruik in biologische toepassingen.

Verschillende lithografische technieken zoals nanoimprint-lithografie (NIL), UV-nanoimprint-lithografie (UV-NIL) en nanodeeltjes-lithografie (NSL) zijn gebruikt om PFS-patronen te genereren. De gefabriceerde patronen zijn gebruikt om structuren op polymeer- en siliciumoppervlakken aan te brengen op verschillende lengteschalen. Nanogestructureerde polymere brushes werden gegroeid vanaf initiatoren, patroonsgewijs aangebracht door middel van “step-and-flash” imprint-lithografie (SFIL). Blokcopolymeer zelf-assemblage werd ook gebruikt voor het verkrijgen van PFS patronen op nanometerschaal. Symmetrie, patroonkwaliteit en correlatielengte als functie van de primaire structuur van polystyreen-*block*-poly(ferrocenyldimethylsilaan)- (PS-*b*-PFS-) blokcopolymeren worden besproken.

Hoofdstuk 1 geeft een algemene inleiding tot het proefschrift. In Hoofdstuk 2 wordt een overzicht van bestaande lithografische technieken en bijbehorende materialen gegeven.

Hoofdstuk 3 beschrijft een methode om poreuze structuren op silicium-substraten te fabriceren door gebruik te maken van geordende monolagen van colloidale deeltjes als mal en PFS als etsmasker. Poriën in silicium-substraten met submicrometer afmetingen en hcp-ordening werden vervaardigd door middel van NSL. Silica nanodeeltjes van verschillende grootte werden gebruikt als uitgangsmateriaal en poly(ferrocenylmethylphenylsilaan) (PFMPS) als etsresistent polymeer, zodat een negatieve replica van de nanodeeltjes-laag werd geproduceerd. Het op deze wijze gestructureerde silicium-substraat werd vervolgens als mal gebruikt om de nanodeeltjes-laag te vermenigvuldigen door middel van NIL. De poriegrootte in de silicium-substraten kon worden gevarieerd door het veranderen van de deeltjesgrootte.

Ook werd aangetoond dat de grootte en vorm van de poriën kan worden gestuurd door het aanpassen van de etstijd.

Hoofdstuk 4 beschrijft een proces om vrijstaande, niet door een substraat gedragen poly(ethersulfon)- (PES-) films met regelmatige structuren van cirkelvormige poriën en een hoge porositeit te vormen. De combinatie van NSL en een patroonoverdrachts-techniek gebruikt in dit proces maakte de fabricage van uniforme, nanoporeuze PES-membranen mogelijk. Het etsbestendige PFMPS werd gebruikt om de poriën tussen de dichtgepakte silica-deeltjes op te vullen. Tijdens de patroonoverdracht van de silica-deeltjes in PES werd de toplaag van PFMPS eerst weggehaald, resulterend in deels onbeschermde silica-deeltjes. Na verwijdering van de silica deeltjes met HF werd een negatief gaten-patroon van de colloidale deeltjes gevormd in de PFMPS-laag. Tijdens RIE werd de PES-film geperforeerd in de onbeschermde gebieden, wat leidde tot overdracht van het projectiepatroon van de silica-deeltjes. Loshalen van het PES-membraan van het onderliggende substraat bleek mogelijk door het oplossen van de tussenliggende cellulose-acetaat laag in aceton. De PES-membranen met hun dichtgepakte, goed gedefiniëerde poriën kunnen worden gebruikt voor de grootte-selectieve filtratie van deeltjes.

De toepassing van PFMPS als resist in nanoimprint-lithografie wordt geïntroduceerd in Hoofdstuk 5. Stabiele, homogene, hoog molecuulgewicht PFMPS-films verkregen door spin-coating werden geperst met NIL en de resulterende patronen werden overgebracht in het substraat door RIE. Het verminderen van de oorspronkelijke filmdikte en het optimaliseren van de RIE-omstandigheden vergemakkelijkten het verwijderen van de resterende resistlaag en verbeterden zo de patroonoverdracht. Om hoge aspect verhoudingen te verkrijgen werd de resterende resistlaag volledig verwijderd door Ar-sputtering omdat direct etsen zonder verwijderen van de resterende resistlaag de vorming van een oxidelaag tot gevolg had waardoor verdere patroonoverdracht werd verhinderd. Aangetoond werd dat PFMPS vanwege het zeer hoge etscontrast met silicium kan worden gebruikt als eenstapsresist omdat zogenaamde “metal lift-off” niet noodzakelijk is, waardoor deze aanpak als een goedkoop en mogelijk hoog-volume-proces kan worden beschouwd.

Hoofdstuk 6 beschrijft de ontwikkeling van een UV-NIL-proces op basis van een bi-laag-systeem, waarvan één laag bestaat uit PFMPS. Het organometaalpolymeer PFMPS werd gespincoat op een door UV-NIL gestructureerd substraat, gevolgd door een argon-plasma-behandeling om de imprintresistlaag bloot te leggen. Verwijdering van de imprintresist door middel van een zuurstofplasma gaf PFMPS-patronen die een negatieve afdruk vormden van de gebruikte mal. Patroonoverdracht in silicium-substraten werd gerealiseerd door gebruik te

maken van een $CHF_3/SF_6/O_2$-plasma. Variaties in de plasmasamenstelling leidde tot verschillende etsprofielen. De fabricage van polymeerstructuren met laterale afmetingen tot 30 nm en aspect verhoudingen tot 3 werd aangetoond. Dit proces biedt de mogelijkhed om de voordelen van UV-NIL te combineren met de hoge etsweerstand van poly(ferrocenylsilanen), om zo structuren met afmetingen tot onder de 100 nm te fabriceren.

In Hoofdstuk 7 wordt de vorming van polymere brush-patronen door het combineren van SFIL en SIP behandeld. Patronen gemaakt met SFIL werden gebruikt voor het hechten van zelf-assemblerende monolagen van een initiator voor SIP. De methode maakte het mogelijk om brush-patronen van PEGMA, PS en PGMA te vormen met afmetingen van enkele micrometers tot 40 nm. Door deze variatie in domeingrootte kon de invloed van patroonafmetingen op de hoogte van de polymeerbrushes worden bestudeerd. Verschillende interessante aspecten van lateraal gestructureerde PEGMA-brushes werden aangetoond. De hydroxy-groepen van de gevormde PEGMA-structuren werden omgezet in carbonzuurgroepen en de pH-respons van deze gefunctionaliseerde PEGMA-structuren werd bestudeerd door het variëren van de pH. De gefabriceerde, robuuste PEGMA-nanostructuren werden gebruikt voor eiwithechting. Streptavidine/biotine werden selectief gekoppeld aan geactiveerde PEGMA-brush-patronen.

Hoofdstuk 8 beschrijft de synthese en symmetrie, patroonkwaliteit en ordening in dunne films als functie van de primaire structuur van PS-*b*-PFS-blokcopolymeren. De invloed van filmdikte, “annealing” omstandigheden (tijd, temperatuur) voor optimale domeinvorming en -ordening door fasescheiding van de PS- en PFS-blokken, moleculaire massa, blok-volumefractie en polydispersiteit op de microdomein-grootteverdeling, -periodiciteit en -correlatielengte van dunne films van PS-*b*-PFS-blokcopolymeren met bolvormige morfologie werd onderzocht. Voor een serie blokcopolymere films van dezelfde dikte, “annealed” onder dezelfde omstandigheden, bleek dat de volumefractie de grootste invloed had op de PS-*b*-PFS-morfologie. De domeinafstand en standaarddeviatie namen toe met toenemende PFS-volumefractie. Polydispersiteit bleek echter weinig invloed te hebben op de grootteverdeling en domeinafstand van de microdomeinen.

Organometaalpolymeren zijn attractieve materialen die verder kunnen worden onderzocht op hun toepasbaarheid in lithografie. Verder onderzoek aan de gecontroleerde structurering van PFS-blokcopolymeren door middel van UV-NIL-lithografie kan worden uitgevoerd om de invloed van ruimtelijke begrenzing op blokcopolymere zelf-assemblage te bestuderen. Bovendien zouden PFS-blokcopolymeren gebruikt kunnen worden om

polymeeroppervlakken te patroneren met structuren tot 20 nm door een zorgvuldige keuze van procesparameters tijdens etsen, “annealing” en depositie van materialen.

De resultaten gepresenteerd in Hoofdstuk 7 illustreren de fabricage van polymeerplatforms die vervolgens werden gebruikt voor eiwithechting. Dezelfde methode zou gevolgd kunnen worden voor de covalente hechting van CdSe/ZnS-nanokristallen aan de uiteinden van de brushes. In dit geval kan de ruimtelijke inperking en laterale structurering van nanokristallen worden bestudeerd.

De resultaten uit dit proefschrift laten zien dat polymeren een reeks van structuren met diverse afmetingen en chemische functionaliteiten op oppervlakken kunnen vormen wanneer ze worden gestructureerd door bottom-up en top-down micro- en nanofabricagetechnieken. Het aanbrengen van organometaaleenheden in de hoofdketen van polymeren verbetert de eigenschappen zoals etsweerstand en daardoor de toepasbaarheid van deze macromoleculen. Metaalbevattende polymeren hebben bewezen te beschikken over een hoge etsweerstand bij hun toepassing in NIL-, SFIL- en NSL-processen. Deze polymeren lijken waardevolle kandidaten te zijn voor de ontwikkeling van nieuwe resists. De door middel van deze technieken gefabriceerde structuren kunnen worden toegepast in gebieden zoals dataopslag, microelectronica en bioelectronica.

Acknowledgements

When I first came to Enschede I had little idea how I would improve myself scientifically, besides how much fun I would have in these four years. I finished my thesis finally, and I would like to thank many people for their help and support in accomplishing this. I am very glad that now it is time for me to write this part of the thesis.

First, I would like to thank one of my promoters and supervisors Prof. Jurriaan Huskens for accepting me as a PhD student. Dear Jurriaan, I always had your support and trust during these four years. You always believed me and you made me feel this when I needed it the most. That is why I did not give up and kept going on. From our biweekly meeting, I have learnt so much from you. You were always patient to me even when I was making the same mistakes while writing a manuscript. You gave me enough freedom to collaborate and try the things that I wanted to do. These helped me to be more independent researcher. I want to thank you for all your help, ideas, guidance, and patience throughout this whole thesis. There are not enough words to explain my gratitude. Thank you very much.

I would like to express my gratitude and appreciation to my second promoter Prof. Julius Vancso. Thanks Julius for the opportunity you gave me to be part of the MTP group which has been a pleasure both scientifically and personally. The scientific discussions we had, especially in the last year, were very instructive and I really learnt a lot. I truly appreciate it. I wish that we had more of these meetings which were very useful for me.

I owe my gratitude to my daily supervisor, Dr. Mark Hempenius. Dear Mark, thanks for all your help in the lab. You taught me how to do synthesis and how to handle the things in the lab. You were very patient and you always had time for me even though you were very busy. I felt very confident to have you always there. I would also like to thank you for translating the summary into Dutch.

I would like to thank Prof. David Reinhoudt for the meetings we had in the first year of my PhD and for the scientific contributions. They were useful with lots of nice ideas. We also had nice talks about life, food, travelling which I really enjoyed.

During these four years I had the chance to collaborate with many people, the results of which are presented in this thesis. I owe my appreciation to Dr. Boris Vratzov for all his help he provided to teach me the SFIL technique. You always had time for me to prepare the samples or for discussions. We had many nice discussions which were very essential to obtain the results presented in Chapters 6 and 7. I would like to thank Prof. Caroline Ross and Joy Perkinson from MIT for their contribution to Chapter 8. I would like to thank Dr. Edmondo Benetti for introducing me to the world

of polymer brushes and for his participation in Chapter 7. Your help and advice during the last period of this thesis were very essential, thank you very much Eddy. I really learnt a lot from you. My appreciation also goes to Xiaofeng Sui for his help with Chapter 7. You are a good chemist Xiaofeng and you are always willing to help. I would like to thank my other collaborators. Dr. Xing Yi Ling and Dr. In Yee Phang for all their help, ideas and support for Chapters 3 and 4. My dear friends, it was pleasure to work with you and without your help I could not have completed this part of the work. A special thanks goes to Dr. Szczepan Zapotoczny for teaching me AFM and for always being very friendly. Christiaan, thanks for helping me in the cleanroom and in the laboratory when I started my PhD.

Dear Clemens, thank you very for all your help during these years. You are an amazing person, always positive. You managed to solve all my problems related to computers, equipment, etc. We had nice, long talks (the topic could be whatever). You were patient to listen me and even you gave me wise advice. I appreciate your friendship. Thanks to Marcel and Richard for their technical support. The secretaries of MnF/SMCT/MTP, Izabel, Gerardine, Genevieve, are also thanked for taking care of all the administrative work. I thank you Pascal for going so carefully through my concept thesis. I also spent some time doing SEM measurements. Dear Mark Smithers, thanks for your help and contribution to the SEM images. I enjoyed our talks about life, family especially music while doing measurements. I would like to thank all the people in the cleanroom and in particular to Hans, Huib, Ite-Jan, Eddy, Rene and Peter for their technical support and patience.

During my PhD, I have had the opportunity to meet a lot of fantastic people. I would like to thank those who made these four years an unforgettable period for me: Denis and Eddy, my dear friends, thanks for being there always to listen me. Even though you find my problems very stupid, I like to share them with you guys. You always managed to cheer me up with your humor Denis. You are my drinking coach. You trained me so much that I could compete with you now (more vodka, only strong alcohol). I really appreciate it. We have been through the stressful thesis writing time, thanks for all the support. Eddy, after sometime, I could get used to your way of living and your way of handling things. You were always around so I never felt alone. I am also very grateful for your scientific help as well. You taught me a lot (brush synthesis and AFM). I really know what tip imaging means now. We really shared a lot during this time. I really enjoyed drinking tea, having dinners, getting drunk, dancing, and watching movies together with you guys. Denis and Eddy, it is nice having you as friends. Dear Xing Yi and In Yee, after our trip to Istanbul we got closer. Since then we had great time together (especially dinners :)) Xing Yi, it was pleasure to talk and to share things with you. In yee, I really miss to have drinks with you and I was amazed how much you could eat and drink. Martina and Slyvain, thanks very much for your hospitality in Bordeaux and all the nice French food. Dear Mirko, I remember with a lot of pleasure our trip to Istanbul (always doner, kebap). Please keep in touch. Henk, you are the best movie editor and director I have ever worked with. It was so much fun to make a movie with you. Nuria, the kid, it was so nice to have you in the group. We

participated in all the Erasmus parties by your initiative. Thanks for keeping the contact and calling me when I needed. Dear Francesca, now you are a doctor and I am very happy about it. We shared too much lately, even the same flat. Thanks for this. I wish to visit you and Riccardo in Rome. Davide (the most relaxed Italian) I had the best time in Lunteren when you were there with us. Carlo (the grandpa), thanks for your hospitality in Munster (bed and breakfast). Kim, the most addictive friend of mine to Turkish food. You are the most relaxed and easy going visitor that I had so far. Sorry that I did not understand your English at the beginning. Do you remember our first weeks writing in the same office but not talking? Now it is much fun to talk with you while taking tea, eating cookies and of course drinking. Victoria, you are a very social person and, we were having lots of fun dancing (non-stop). Nobody could replace you.

I would like to thank Bilge for her unconditional support during the last year of my PhD. Thanks for cooking for me when I was working till late. You made sure that I was eating properly. Thanks for all the good care. I am very happy to have you as a friend and I know that I can always trust you. Another very good Turkish friend of mine, Deniz, thanks for waiting me in the lab when I was working till late. You always have tea, cookies to share and of course tosties. You always tried to cheer me up when I was down. I am sorry if I bothered you too much. I always feel relieved to talk with you. And Oya, my alternative friend, you helped me a lot especially at the beginning when I was very new in the group. During these years you always managed to surprise me (you know what I mean) but I really enjoyed a lot with you especially while traveling (Venice, States, Barcelona). Staying in the same room was always fun with you even though you were smoking. Cem, always willing to help without asking anything back. Thanks for helping me when I was moving. You did not complain at all (amazing). Erhan-Arzu, thanks for being there when I needed (especially for maintenance of my bike and moving my stuff even twice). I wish that we had spent more time together. I would also like to thank some people in TUSAT community; Kamil, Aysegul, Hasan, Selim, Emre, Feridun, Anil (my dear japanish-turkish friend), Berk, Murat, Can (my dear dancing and drinking friend), Burak (my ex-neighbor; thanks for everything during these years), Ayse, Ozlem, Mustafa and Zeynep-Aytac.

With many people from outside of my groups I spent great times and we have nice memories. Raffaella, Mauritzo, Giulia, Pietro, Nick, Stefano, Bob, Can, Laura, Anil, Cem, Bilge, David (the great salsa-dancer, thank you for teaching me salsa), Roald (thanks for your advice for my future), Burak, Lorenzo and Valeria. My dear friend Valeria, my best Italian flatmate ever. We shared the same flat for two years without having any problem. I enjoyed having Turkish breakfast with you. We had great time together. Even, you never complained about Denis and Eddy being there. You are a very special person and I miss you a lot.

I would like to thank some people who left the group but I still keep in touch. Monique, you were very friendly since the beginning. You were part of the PFS team. Thanks for helping me with the synthesis and for all the lab work. Another member of PFS team: Thomas. It has been always

pleasure to go out with you (too much dancing). Thanks for visiting me in Istanbul and thanks for the hospitality in Barcelona. Dear Marina and Melba, you were like my sisters. I appreciate your guidance and support during your staying here. Miguel- Marina, thanks for everything when we visited you in Barcelona. Enschede has never been the same after you left. Bas, Janina, Olga, Alessio, Fernando, Lourdes, Riccardo and Olga (Turkish one) are also thanked for all the good times.

It is time to thank people from MTP/MnF and SMCT. Joost, I always enjoyed our conversations about work, life, and relations. Lately, I even like your humor. You are very nice and polite to help me with many paper work and with AFM related problems. Jealemy, you are a good friend to have, I had a lot of fun doing our girly things. I don't remember how many times we partied lately. I will always remember the party in Atak (with many Russians). A special thanks to Albert for being a great actor. Jing, my dear office-mate, thanks for listening to my complaints in the mornings. You were always very patient with me even to my never ending AFM related questions. I hope I can visit you in Singapore. Please don't work there that much. Dear Jordi, you are a very sweet and nice person. Please try to be happier and more positive. I know how hard it is here but you will manage. Yiping, I enjoyed our talk in the cleanroom and you were always ready to help me when I needed. Thanks for this. I would also like to thank to Shu-Han, Pieter, Duan, Carlo, Mudassir (thanks calling me paradise), Lanti, Alberto, Melanie, Raluca, Vijay, Chien-Ching Wu, Dae June, Oktay, Edit, Anika, Qi, Wilma, Gabriella, Mathijs, Nayeli, Gerwin, Anna, Maryana (always nice to see you in the lab or in the cleanroom) and Mine. Dear Mine, we shared the same flat for a while. You were very supportive and very nice to me. I really enjoyed our talks about work, people, and life.

All the people I mentioned here have contributed to make the time I spent in Enschede an unforgettable time of my life. But most importantly, I owe my deepest gratitude to my family; my parents, my two sisters and my brother for all the support they give me. Canim annecim ve babacim, bana her zaman cok destek oldunuz. Her zaman ne istediysem yapmama izin verdiniz ve bana hep guvendiniz. Maddi ve manevi tum desteginiz icin cok tesekkur ederim, sizi cok seviyorum. Canim ablam Keti, sen her zaman, her seyimle ilgilendin. En ufak sorunuma yetistin. Cok saol ablacim, iyi ki varsin. Krisim, bi tanem, biz seninle hep ikiz gibiydik. Her seyimizi paylastik, Beni en iyi taniyan kisi de sensin, her zaman beni anladin. Bunca yil uzakta kalmis olsak da, hic kopmadik ve kopmayalim. Biricik erkek kardesim Nasirim, sensiz bir yasam dusunemiyorum. Cok komiksin, cok tatlisin ama biraz daha buyumen lazim. Canlarim siz benim herseyimsiniz.

Canet Acikgoz

About the Author

Canet Acikgoz was born in 10th January, 1980 in Iskenderun, Turkey. She obtained her bachelor degree of chemistry from Middle East Technical University (METU) in the year of 2003. She continued her master education in the same university and joined the group of Prof. Dr. Metin Zora at METU. She received her master degree of Chemistry in August 2005, with the research project entitled “The use of Fischer carbenes in the synthesis of cycloheptadienones incorporating ferrocenyl moiety”. During these two years, she also worked as a teaching assistant at Atilim University in Ankara. From January 2006, she has been a PhD student under the supervision of Prof. Dr. Jurriaan Huskens and Prof. Dr. Julius Vancso, in the Molecular Nanofabrication (MNF) and Material Science and Technology of Polymers (MTP) groups at the University of Twente, on the use of polymers in bottom-up and top-down micro-and nanofabrication techniques. The results of this research work are described in this thesis